TECHNISCHE UNIVERSITÄT MÜNCHEN

FAKULTÄT FÜR CHEMIE

Cryo-EM structure of CUL5-ARIH2 E3-E3 Ligase complex reveals novel allosteric NEDD8 mechanism

Sebastian Kostrhon

Vollständiger Abdruck der von der Fakultät für Chemie der Technischen Universität München zur Erlangung eines

Doktors der Naturwissenschaften (Dr. rer. nat.)

genehmigten Dissertation.

Vorsitzender: Prof. Dr. Johannes Buchner

Prüfer der Dissertation:

1. Hon.-Prof. Brenda Schulman, Ph.D
2. Prof. Dr. Matthias Feige

Die Dissertation wurde am 17.01.2022 bei der Technischen Universität München eingereicht und durch die Fakultät für Chemie am 22.03.2022 angenommen.

„No sacrifice, no victory!“
-Archibald Witwicky

TABLE OF CONTENT

SUMMARY

Eukaryotic signaling has been likened to a code, written and read by modules catalyzing and binding post-translational modifications, respectively. The information transferred by this code ultimately determines the fate of virtually all cellular processes, from cell cycle regulation to metabolic pathways. Homologous modules often mediate signaling by parallel structural mechanisms.

However, we discovered that structurally unique super-assemblies are formed between related but distinct modification targets (NEDD8-modified cullin-RING ligase E3s, CRLs) and their homologous readers (ARIH-family RBR E3s), which are ubiquitin writers for CRL-bound substrates.

Modification of CUL5-RBX2 with the ubiquitin-like protein NEDD8 and "reading" by the ubiquitin writer ARIH2, was genetically-validated for its importance in pathological hijacking of CUL5 by HIV-1[1]. HIV-1 replication in host cells depends on usurping cellular UB-dependent proteasomal degradation pathways to degrade host immune proteins. HIV-1 virion infectivity factor (Vif), acting together with its conscripted host protein CBFβ, act as CRL5 substrate receptors mediating ubiquitylation of APOBEC3 family restriction factors[2-4]. Surprisingly, studies found that the level of APOBEC3G and HIV-1 infectivity further depends on the presence of the RBR E3 ARIH2 and on the activation of CRL5 by NEDD8. These findings are consistent with results from previous studies where CRLs and ARIH E3 ligases have to work together to ubiquitylate substrates[1,5,6]

Here, our structures and biochemistry reveal distinctive autoinhibition and activation mechanisms of the ARIH RBR E3 ligase ARIH2. It is activated upon super-assembly into an E3-E3 ubiquitin ligase complex with HIV-1 Vif-hijacked neddylated CUL5-RBX2 and APOBEC3-family substrates. Comparison of neddylated CUL1-RBX1 super-assemblies with ARIH1 shows NEDD8 uniquely contacts with its covalently-linked CUL5. While ARIH1 is directly recruited to the CUL1-linked NEDD8, CUL5-linked NEDD8 forms no direct contacts with ARIH2 but instead elicits large-scale structural rearrangements in CUL5 that expose cryptic ARIH2 binding sites. Our data reveal that

5

a UBL modification is read indirectly through allostery, which may offer routes for specifically targeting related UBL pathways including those hijacked by viruses.

ZUMSAMMENFASSUNG

Eukaryotische Signalwege sind vergleichbar mit einem Code, bei dem posttranslationale Modifikationen durch Proteinmodule „geschrieben" und „abgelesen" werden. Die Information, die durch diesen Code weitergeleitet wird, bestimmt am Ende das Schicksal aller zellulären Prozesse, angefangen von der Regulation des Zellzykluses bis hin zu Stoffwechselvorgängen. Homologe Module führen dabei die Signalweiterleitung durch ähnliche strukturelle Mechanismen aus.

Allerdings haben wir strukturell einzigarte Superkomplexe entdeckt, die zwischen verwandten aber dennoch einzigartigen Modifizierungszielen (NEDD8-modifizierten Cullin-RING E3 Ligasen, CRLs) und ihren homologen „Lesern" (Mitglieder der ARIH-Familie der RBR E3 Ligasen) geformt werden. Diese Komplexe sind dabei „Schreiber" der Ubiquitin Modifikation auf CRL-gebundenen Substraten.

Die Modifikation von CUL5-RBX2 mit dem Ubiquitin-ählichen Protein NEDD8 und das „Lesen" dieser Modifikation durch den Ubiquitin „Schreiber" ARIH2, wurde bereits in seiner Bedeutung durch genetische Experimente bestätigt. CUL5 wird dabei während einer Infektion mit HIV-1 übernommen und umfunktioniert. Die Vermehrung von HIV-1 in Wirtszellen hängt von der Übernahme des zellulären Ubiquitin-Proteasom Systems ab um sich damit Proteinen des Immunsystems zu entledigen. Der HIV-1 virion infectivity factor (Vif) arbeitet bei diesem Vorgang mit dem einberufenen Wirtsprotein CBFβ zusammen und dient als eine Art Substratrezeptor für CRL5. Die beiden Proteine binden den Restriktionsfaktor APOBEC was zu dessen Ubiquitinylierung führt. Interessanterweise wurde nachgewiesen, dass das Level an APOBEC3G und die Infektiosität von HIV von der Anwesenheit der RBR Ligase ARIH2 und der Aktivierung von CRL5 durch NEDD8 abhängen. Diese Ergebnisse stehen im Einklang mit ähnlichen Studien in denen nachgewiesen wurde, dass CRL und ARIH E3 Ligasen zusammenarbeiten um Substrate zu ubiquitinylieren.

In dieser Studie zeigen unsere Strukturen und biochemischen Analysen, dass ARIH2 in einem autoinhibitorischen Zustand vorliegt und durch bestimmte Mechanismen aktiviert werden muss. Es wird durch die Assemblierung in den E3-E3 Superkomplex mit dem Vif-übernommenen und neddylierten CUL5-RBX2 aktiviert um Substrate der

APOBEC Familie zu ubiquitinylieren. Vergleiche mit dem NEDD8–CRL1-ARIH1 Superkomplex zeigen, dass einzigartige Kontakte zwischen CUL5 und NEDD8 gebildet werden. Während ARIH1 von CUL1-gebundenem NEDD8 direkt rekrutiert wird, formt CUL5-gebundenes NEDD8 keine Kontakte mit ARIH2. Stattdessen löst NEDD8 großflächige strukturelle Veränderungen in CUL5 aus und offenbart versteckte ARIH2 Bindestellen. Unsere Daten zeigen, dass diese Ubiquitin-ähnlichen Modifikation durch allosterische Mechanismen „gelesen" wird, was vielleicht neue Wege eröffnet, um Ubiquitin-ähnliche Signalwege (unter ihnen auch solche, die von Viren genutzt werden) in spezifischen Therapien gezielt zu erreichen.

ACKNOWLEDGMENTS

9

ABBREVIATIONS

4HB	4 helical bundle
53BP1	53 binding protein 1
AD	Alzheimer's disease
AMP	Adenosine monophosphate
APC/C	Anaphase promotin complex / cyclosome
APOBEC	Apolipoprotein B mRNA editing enzyme catalytic polypeptide
APPBP	Amyloid Precursor Protein binding protein
ARIH1	Ariadne RBR E3 ubiquitin protein ligase 1
ARIH2	Ariadne RBR E3 ubiquitin protein ligase 2
ASB9	Ankyrin Repeat And SOCS Box Containing 9
ATP	adenosine triphosphate
BARD	BRCA1 Associated RING Domain 1
BRCA1	Breast cancer associated 1
BTB	bric-a-brack tramtrack broad
C/R domain	Cullin/RING domain
CAND1	Cullin-associated NEDD8-dissociated 1
CBFb	Core-Binding Factor Subunit Beta
CDC34	cell division cycle 34
CR	Cullin repeat
CRL	Cullin RING ligase
CSN	COP9 signalosome
CTD	C-terminal domain
CYLD	cylindromatosis gene
DCAF	DDB1 and CUL4 associated factor 1
DDB1	DNA-damage binding protein 1
DDR	DNA-damage response
DJ-1	Parkinson's disease protein 7
DNA	Desoxyribonucleic acid
DUB	deubiquitinase
EM	electron microscopy
FACT	Facilitates chromatin transcription
FAT10	Leukocyte Antigen-F Associated Transcript 10
FBXW7	F-Box And WD Repeat Domain Containing 7
GST	Glutathione S transferase
GTPase	Guanosine triphosphatase
HD	Huntigton's disease
HECT	Homologous to the E6-AP Carboxyl Terminus
HEPES	4-(2-hydroxyethyl)-1-piperazineethanesulfonic acid
HIV	human immunodeficiency virus
HUWE1	HECT, UBA And WWE Domain Containing E3 Ubiquitin Protein Ligase 1
IBR	In-between-RING
IFN-ɣ	Interferone γ

IKK	IkB kinase
IPTG	Isopropyl-β-D-thiogalactopyranosid
ITCH	Itchy E3 Ubiquitin Protein Ligase
KLHL20	Kelch Like Family Member 20
LB	Luria's broth
LDD	Linare ubiquitin determining domain
LTD	LUBAC C-terminal domain
MBP	Maltose binding protein
Mdm2	Mouse double minute 2
Mg	Magnesium
MIU	Motive interacting with ubiquitin
MLL	Mixed lineage leukemia protein-1
NEDD8	Neural-precursor-cell-expressed developmentally down-regulated 8
NF-kB	Nuclear factor kB
NLRP3	NOD-, LRR- and pyrin domain-containing protein 3
NOXA	Phorbol-12-Myristate-13-Acetate-Induced Protein 1
NS1	non-structural protein 1
NTD	N-terminal domain
OD	Optical density
PABPN1	PolyA bindig protein nuclear 1
PARC	PARKIN-like cytoplasmatic
PCNA	Proliferating cell nuclear antigen
PD	Parkinson's disease
PE	phosphatidylethanolamine
PINK1	PTEN-induced kinase 1
PMSF	Phenylmethylsulfonylfluorid
PTM	Post-translational modification
Ras	Rat sarcoma protein
RBR	RING-in-between-RING
RBX	RING-box protein
Rcat	RING catalytic
RCR	RING-cys relay
RING	Really interesting new gene
r.m.s.d.	Root mean square deviation
RTI	RING-to-IBR
SIM	SUMOl interacting motif
SKP1	S-phase kinase associated 1
SMURF	SMAD-Specific E3 Ubiquitin-Protein Ligase 1
SOCS	Suppressor of cytokine signalling
SOC buffer	Super optimal buffer
SOX	SRY-related HMG-box
SR	Substrate receptor
SUMO	Small ubiquitin-like modifier

TB	Terrific broth
TEV	Tobacco etch virus
TGN	Trans-Golgi network
TLS	translesion synthesis polymerase
TRAF6	TNF Receptor Associated Factor 6
Tris	Tris(hydroxymethyl)aminomethan
UB	Ubiquitin
UBA	Ubiquitin associated
UBA3	Ubiquitin-like modifier-activating enzyme 3
UBD	Ubiquitin binding domain
UBE2F	Ubiquitin Conjugating Enzyme E2 F
UBL	Ubiquitin-like
UBR5	Ubiquitin Protein Ligase E3 Component N-Recognin 5
UIM	Ubiquitin-interacting motif
UPS	Ubiquitin-proteasome system
VCP	Valosin-containing protein
WD40 domain	Tryptophan-aspartate 40 domain
WHB	Winged helix B
Wnt	Wingless and Int-1 signaling pathway
ZnF/ZF	Zinc finger
β-ME	beta mercaptoethanol
β-TrCP1	(beta-transducin repeat containing protein 1

INTRODUCTION

The Ubiquitin Code

Ubiquitin (UB) and ubiquitin-like proteins (UBLs) are part of the versatile toolbox of posttranslational modifications (PTM) eukaryotic cells employ to transfer information about protein fates across the cell. Information regarding protein stability, activity, localization and affinity towards binding partners is encoded on the surface of modified proteins and subsequently "read" by downstream effector proteins. Ubiquitin is a small globular protein which itself can be altered through the attachment of modifying groups such as acetyl, phosphoryl, glycosyl and methyl groups. Additionally, ubiquitin molecules can be conjugated to each other, thereby forming polyubiquitin chain configurations which adds to the enormous diversity of the ubiquitin code. Together, they enable the cell and organisms to respond rapidly to changes in their environment and regulate signaling pathways without the need for degradation or *de novo* protein synthesis.

Eukaryotic regulation has evolved through modular post-translational modification cascades, wherein "writers" catalyzing PTMs and "readers" recognizing them collaboratively transduce input signals into specific cellular outputs[7]. Much of our understanding of the principles underlying modular signaling derives from studies of kinase or acetyltransferase catalytic domains, and the motifs that read their phosphorylation or acetyl marks, respectively[8,9]. Signaling has been likened to a "code", determined by the arrangements of "writer" enzymatic domains, their targets, "reader" motifs, and regulatory sequences within multidomain proteins and higher-order assemblies. As a part of this "code", the spatial and temporal addition and removal of PTMs has to be highly coordinated to ensure the smooth progress of many fine-tuned processes with an organism.

Although ubiquitin and ubiquitin-like protein modifications are distinctive in that they are proteins themselves, the UB and UBL code is often interpreted based on principles of modular signaling[10-12]. The ubiquitin code is "written" by E3 ligases that mark proteins with distinct UB or UBL modifications. The extent of the modification ranges from linking a single UB or a UBL site-specifically to a particular target lysine to polyUB "chains" wherein multiple UBs are conjugated to each other. The code is subsequently

14

"read" by downstream machineries that selectively bind and alter the fates of modified proteins.

Numerous eukaryotic processes, including signal transduction, transcription, cell division, differentiation, and many homeostatic pathways are regulated by the protein ubiquitylation code (Fig.1a) (reviewed in ref.[13]). The significance of this information processing system becomes obvious when a dysregulation of UB and UBL pathways occurs, causing many diseases, including cancers, neurodegeneration, and developmental disorders (see below and reviewed in ref.[14,15].

Chemical ubiquitin modifications

Ubiquitin opens countless possibilities to specifically regulate cellular processes. It is a very versatile tool as it is subject to PTMs which expand the versatility and complexity of the ubiquitin code. Ubiquitin contains several serine and threonine residues on its surface which can be phosphorylated as well as seven lysine residues from which six are found to be acetylated[16,17,18,19]. One of the best studied ubiquitin PTM is the phosphorylation of Ser65 by PINK1 during mitophagy[20]. Additional phosphorylation sites are Ser57[21]. Thr12[22], Thr14[23], Ser20[24], Thr22, Thr55, Thr66[25], Tyr59[26], and Ser65[27] (Fig. 1b). Unfortunately, for most of these modifications the involved "writers" (acetyltransferases and kinases), "erasers" (deacetylases and phosphatases and "readers" (phospho-ubiquitin or acetyl-ubiquitin binding domains) are unknown.

Structure

Ubiquitin is ubiquitously found in all eukaryotic cells (hence the name) with a sequence conservation of 96% between human and yeast. Structure-wise, five β-sheets form a compact β-grasp fold with an additional α-helix and a short 3_{10} helix, which altogether increases its stability under denaturing conditions. Hydrophobic surfaces around Ile44 and Il36 are often recognized by binding partners such as the proteasome, E2 and E3 ligases and ubiquitin binding domains (UBDs) in general[28].

E1-E2-E3 cascade

The protein modification mechanism with ubiquitin is achieved by the consecutive activity of the three enzymes E1, E2 and E3. Ubiquitin is activated and transferred it from one enzyme to the next until it finally ends up on the substrate (Fig. 1c). During

15

the activation of ubiquitin, the E1 enzymatically couples the hydrolysis of adenosine triphosphate (ATP) to the conjugation of the C-terminus of UB and the E1 catalytic cysteine via an thioester bond[29-34]. The UB activation starts with the E1 enzyme which binds both MgATP and ubiquitin, followed by the formation of a ubiquitin adenylate intermediate that is subsequently coupled to the catalytic cysteine under the release of adenosine monophosphate (AMP) (Fig. 1c). The E1 can bind two molecules of ubiquitin, one conjugated to AMP and the other as a thioester. Structures of the E1 revealed a multidomain protein containing an adenylation domain involved in binding ATP and activating UB, a catalytic domain with the reactive cysteine and a ubiquitin-fold domain playing a role in recruiting the E2[29-34]. Next, UB is transferred to the E2 which is subsequently recruited to an E3 ligase (Fig. 1c). The exact mechanism of E2~UB ("~" refers to a thioester bond) binding and E3-dependent ubiquitin transfer are described in more detail below.

The E1-E2-E3 cascade results in a covalently linked C-terminus which preferentially (but not exclusively) connects to the lysine amino group on the substrate protein. Research in the ubiquitin field for the last 35 years has shown that UB also forms thioester, hydroxyester and peptide bonds with cysteines, serines, threonines and the N-terminal amino group of substrate proteins, extending the toolbox even further[35]. Placing the UB on the target protein is often enough to provoke drastic changes for its localization, activity and stability.
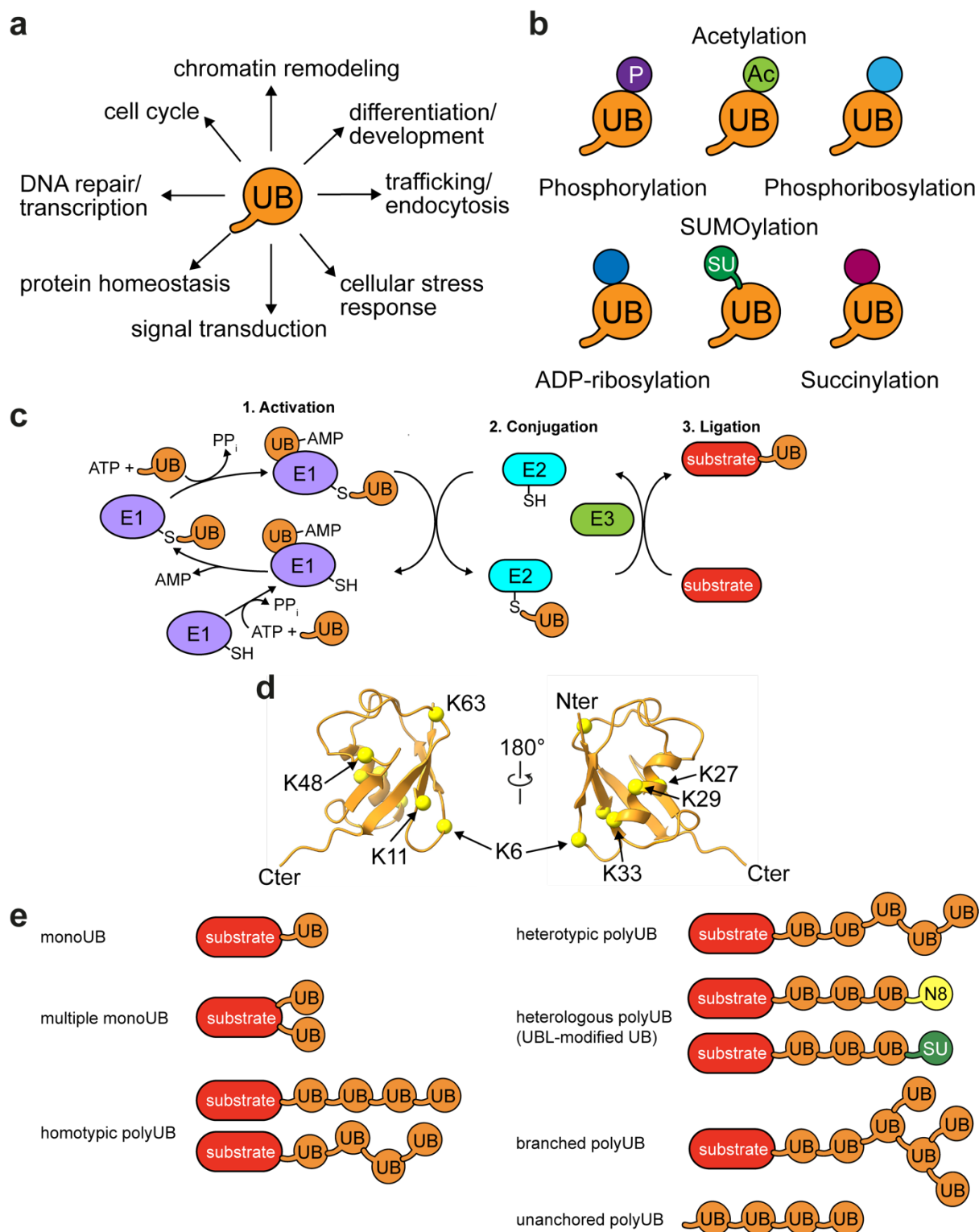
Fig. 1. Ubiquitin serves as a versatile tool in multiple cellular processes
a, Modifications with ubiquitin are involved in virtually all cellular pathways ranging from cell cycle regulation to endocytosis **b,** Residues on the surface of ubiquitin can be modified with different chemical units. Phosphorylation is shown in purple, acetylation in red, phosphoribosylation in light blue, ADP-ribosylation in blue, SUMOylation in green and succylation in violet. **c,** Activation, conjugation and ligation steps of the ubiquitylation cycle. E1 is shown in purple, UB in orange, E2 in cyan, the E3 in green and the substrate in red (based upon ref.[33]; Informations regarding this article can be viewed under <https://pubs.acs.org/doi/10.1021/acs.chemrev.6b00737>. For further permission related to the material excerpted please contact ACS directly.) **d,** Ubiquitin features seven lysinse residues on its surface that can be modified with another ubiquitin unit (PDB ID: 7B5N, chain U). The right panel is rotated 180° to

show the backside of Ubiquitin **e,** Single and multiple ubiquitin can be conjugated in different ways to a target substrate. UB chains can be linear, branched, homotypic or heterotypic (based upon ref. [36])

Monoubiquitylation

Tagging a substrate with just one ubiquitin has been shown to have distinct cellular functions apart from serving as the primer for a polyUB chain (Fig. 1d-e)[37,11,38]. Monoubiquitylation plays a role in receptor endocytosis[39], protein trafficking[40], viral budding[41] and DNA repair[42]. It often works together with other PTMs to target proteins such as small GTPases, cytoskeletal proteins, and scaffolding proteins to specific cellular compartments. Together with farnesylation (a C15 lipid PTM), monoubiquitin relocates the prominent oncogene H-Ras (Harveys rat sarcoma virus; a GTPase involved in regulating the cell division) from the plasma membrane to endosomal sites, which leads to reduction in MAPK (mitogen-activated protein kinase) signaling[40]. Moreover, it has been also shown that single UBs on proteins influence the ability of proteins to form complexes. This is the case for the interaction between the FACT (facilitates chromatin transcription) complex and histone H2A. During transcription, FACT mainly associates with non-ubiquitylated H2A and displaces the H2A/H2B dimer from the nucleosome so that RNA polymerase II can continue to transcribe DNA[43]. Ubiquitylated H2A prevents association of the FACT complex[44].

Ubiquitin chains: sometimes one is not enough

The first UB on a substrate protein often sets the stage for the attachment of additional UBs: Ubiquitin contains seven lysine residues on its surface (Lys6, Lys11, Lys27, Lys29, Lys33, Lys48, and Lys63) plus the N-terminal amino group that can be conjugated to another ubiquitin and form polyUB chains. The different types of UB linkages generate distinct surfaces between the individual UB moieties which in turn can be bound by specific UB-binding domain (UBD)-containing effector proteins (Fig. 1d-e). Together, they enable a huge variability in linkage types and specific functions for substrates[45].

Ubiquitin chain types

Lys48

18

Among the eight possible UB linkage types, the most prominent and abundant is the Lys48 linkage. It makes up nearly half of all linkage types and generates a proteasomal degradation signal (also known as a "degron"). The Lys48-linked chain is specifically recognized and bound by subunits of the proteasomal cap (19S subunit)[46], thereby contributing to the degradation of the modified target protein in the so-called ubiquitin-proteasome system (UPS). The ubiquitin are then removed from the substrate as it travels through the proteasome and is ultimately unfolded and degraded in the central proteolytic chamber[47].

Lys63

Second most important to linkage type is the Lys63 linkage. The Lys63-linked UB modification is associated with the degradation of proteins during autophagy. Autophagy is a cellular degradation mechanism that removes damaged or unnecessary cellular components as well as invading pathogens through a lysosome-dependent pathway. Apart from degradative processes, Lys63 linkages is involved in the transport of proteins[48,49], repair of DNA damage and the activation of protein kinases[50]. Lys63 is established by the E3 ligases TRAF6 (TNF receptor-associated factor 6; which also forms other types of UB-linkages, see below), NEDD4-1[51] and many others.

Met1

Linking the C-terminal carboxyl group and Met1 results in a peptide bond and linear ubiquitin chains compared to the isopeptide bond of lysine-linked UBs. Linear chains are established by the LUBAC complex[52] often involved in inflammatory and immune responses. Linear UB-chains are involved in regulating the activity of the transcription factor NF-κB. Without activating stimuli, NF-κB is bound and kept in an inactive state in the cytosol by its inhibitor IκB. The IκB kinase (IKK) can phosphorylate IκB which serves as a degradation signal, releasing NF-κB and enabling its transfer to the nucleus. Ubiquitylation of a IKK with Met-1 linked chains start the whole activation cascade by activating the IKK kinase[53,54]. The LUBAC complex is also recruited to and ubiquitylates invading bacteria and protein aggregates [55,56]

Lys6

K6-linked ubiquitylation has been repeatedly linked to the control of the DNA damage response (DDR) signaling[57,58]. The major DDR-complex BRCA1-BARD1 (Breast cancer type 1 and BRCA1-associated RING domain protein 1) has been shown to be K6-linked autoubiquitylated during double strand break repair and replication stress[59,60]. Further evidence for this unusual linkage type during DDR comes from recent studies on the E3 ligase HUWE1 (HECT, UBA and WWE domain-containing protein 1). Studies found HUWE1 to be responsible for generating the majority of cellular K6-linked substrates targeting them for degradation via the UPS. It is part of the cellular quality control system where it targets mainly unassembled proteins for ubiquitylation, thereby controlling protein homeostasis. An increase of K6-linked proteins was observed upon the inhibition of the valosin-containing protein (VCP) which indicates that VCP is responsible for the disposal of protein specifically targeted by HUWE1[61,62,63].

Lys11

K11- and K48-linked chains are often found together on proteins being targeted for proteasomal degradation, although either one of these conjugates can lead to degradation[64]. Combined with chain branching, studies performed in yeast show that the recognition by the proteasomal receptor subunit is strongly enhanced[65]. A prominent example for an E3 ligase that specifically puts K11-linked chains on substrates is the Anaphase-promoting complex (APC/C)[66]. The APC/C complex is critical regulator of eukaryotic cell-cycle progression and consists of a multiple subunits, one of which is a RING E3, which forms a complex with the E2's UBE2C and UBE2S and modifies substrates with K11/K48 targeting them for degradation[66]. Combined with other E3s, a vast array of substrates including NOXA (PMA-induced protein 1)[67], β-TrCP1 (F-box/WD repeat-containing protein 1A)[68] and SOX[69] are earmarked for degradation. Additionally, K11-chains are involved in modulating protein-protein interactions [70] or even stabilize the substrate as was shown for β-Catenin[71].

Lys27

Host immune responses to viral infections rely heavily on ubiquitylation of involved proteins of both the host and the virus along the way[72]. A special type of UB-linkage implicated in the regulation of the interferon signaling are K27-linked chains. Studies

showed their involvement in the regulation of the transcription factor NF-κB (nuclear factor 'kappa-light-chain-enhancer' of activated B-cells) and Interferon regulatory factors pathways[73,74,75]. Additionally, K27 conjugates are assembled on histone H2A by the RING-type E3 ligase RNF168 (RING finger protein 168) and serve as binding hub for DNA repair proteins such as 53BP1[76,77].

Lys29

K29-linked ubiquitin modifications have often been connected to neurodegenerative disorders such as Parkinson's Disease (PD)[78]. The E3 ligase TRAF6 assemblies K29-, K6-, and K27-linked ubiquitin-chains on mutated DJ-1 (Parkinson's disease protein 7) and α-synuclein in sporadic PD. Mutated DJ-1 increases the sensitivity to oxidative stress-induced cell death and forms insoluble aggregates. Mutated α-synuclein assembles in aggregates as well, leading to the severe pathologies of PD. Both proteins are polyubiquitylated and assembled into cytoplasmic aggregates[78]. Additionally, studies found K29-linked chains to be involved in downregulating Wnt/β-catenin signaling[79,80]. Under normal conditions, Axin interacts with Wnt receptors and protects them from degradation. K29-polyubiquitylation by Smurf1 (SMAD Specific E3 Ubiquitin Protein Ligase 1) disrupts this interaction, leading to β-catenin disposal and stalling the Wnt pathway[80].

Lys33

The least studied type of ubiquitylation are K33-linked chains. So far, the only known role for this specific type of modification is for protein trafficking. The CUL3^{KLHL20} (Kelch-like protein 20) E3 ligase ubiquitylates the F-actin regulator coronin 7 which is subsequently targeted to the trans-Golgi network (TGN). Together with a partner protein, it forms a pUB-dependent assembly and induces the biogenesis of TGN-derived transport carriers[81].

Branched chains

Ubiquitin chains are known to contain not only a single type of UB-linkage (homotypic) but are of more complex and heterotypic nature with multiple alternating linkage types (Fig. 1e). Heterotypic chain types can be further classified into branched and mixed chains. Whereas mixed chain types contain multiple different UB linkage types which

are linked via just one acceptor site on the ubiquitin, branched chains consist of at least one ubiquitin which is linked to other ubiquitin moieties on multiple acceptor sites[82].

Only a couple of branched chain-types are well-described in terms of functionality. These include K11/K48, K29/K48, and K48/K63 linkages[83,66,84,85] although the mechanisms underlying the formation of these branched polymers are even less well established. What is known is that for the assembly of branched chains, different types of E3 ligases with distinct linkage specificities have to collaborate. This is the case for branched K48/K63 chains which are installed during NF-κB signaling by TRAF6 and HUWE1 and by the HECT E3s (the different types of E3s are explained below) ITCH (Itchy homolog) and UBR5 during the apoptotic response[85,86].
Another mechanism depends on E2 enzymes which have different linkage specificities and are recruited to a single E3 ligase. Such a mechanism is employed by the APC/C: in a two-step mechanism, short chains of mixed K11, K48, and K63 UB-linkages are first established by UBC2C, followed by a second step, where multiple K11-linkages are added to the existing short chains by UBE2S. This type of mechanism leads to the formation of branched K11/K48 polymers[83].

Another interesting feature of the heterotypic chain type is that one of the ubiquitin units can also be a ubiquitin-like protein. Consequently, this leads to the formation of hybrid chains, which expand the ubiquitin code even further and allow a widespread crosstalk between the different UBL pathways[87-89].
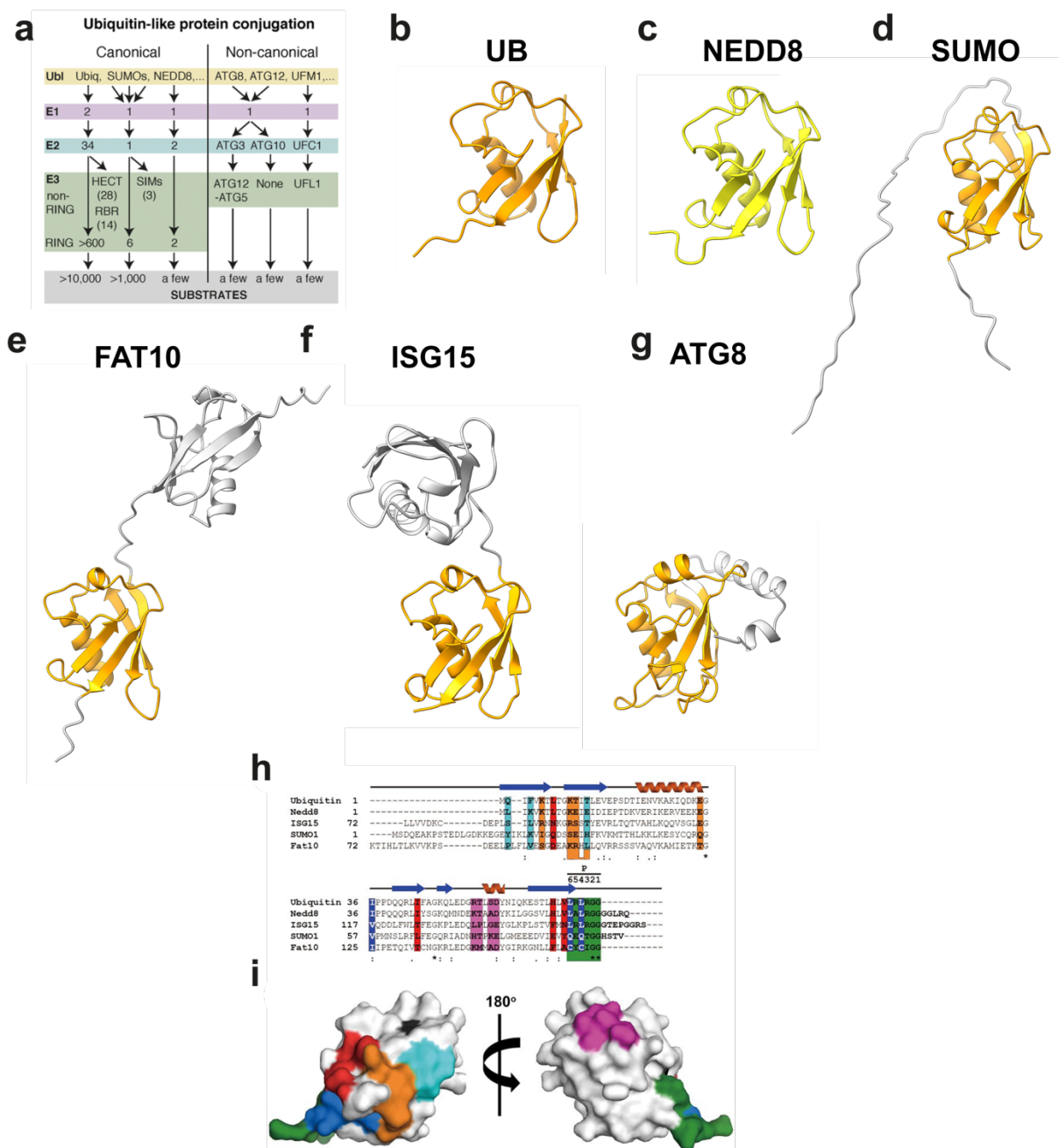
Fig. 2. Ubiquitin-like proteins share the structure but diverge in functions

a, Schematic of the E1-E2-E3 cascade for ubiquitin and canonical and non-canonical UBLs (taken from ref.[33]; Informations regarding this article can be viewed under <https://pubs.acs.org/doi/10.1021/acs.chemrev.6b00737>. For further permission related to the material excerpted please contact ACS directly) **b-g,** Structures of UB and 5 different UBL reveal the common UB-fold (orange). Structures of UB and NEDD8 (yellow) are taken from PDB ID: 7B5N[90]. The models of SUMO, ISG15, FAT10 and ATG8 are taken from Alphafold[91] **h,** Sequence alignments of ubiquitin and ubiquitin-like proteins. Different surface patches are colored. (taken from ref. [92]) **i,** Surface patches on ubiquitin are colored according to **h**. The Phe4 patch is colored cyan, the TEK box is colored orange, the Ile36 patch is blue, the Ile44 patch is red, the Asp58 patch is purple, LRLRGG motif is colored green, and Ser65, which gets phosphorylated by PINK1, is black. (taken from ref. [92])

Ubiquitin-like proteins

The ubiquitin fold is shared among a small family of eukaryotic proteins that also share a common biochemical mechanism: the carboxyl group of the modifier's C-terminus is conjugated to the target residue (Fig. 2a). As with ubiquitylation, the most commonly modified amino acid is an easily accessible surface lysine residue on the surface of the substrate. Furthermore, N-terminal amino groups can also be utilized[93]. Regarding their evolutionary appearance, the UBLs NEDD8 and SUMO are basically found in all eukaryotes, while other members such as FAT10 and ISG15, arose much later during evolution and are only found mammals[94,48]. Another special member of the UBL family is ATG. It shares the common ubiquitin fold, but rather that modifying proteins, it is found to be attached to the headgroup of the phospholipid phosphatidylethanolamine[95] during (but no solely) autophagy[96] (Fig. 2b-i).

Small ubiquitin-like modifier (SUMO)

SUMO shares only a 18% sequence identity with ubiquitin but adopts the same overall three-dimensional structure with its C-terminus oriented in the same direction (Fig. 2d)[97]. What distinguishes it from the ubiquitin structure is a N-terminal extension and a different distribution of charged residues on its surface, which adds to the unique biological functions compared to ubiquitin[98]. The biological effects of SUMOylation are determined by specific reader domains similar to ubiquitin. Functionally, SUMOylation covers a great variety of cellular processes: it is involved in the DDR, where it regulates the functions of DNA damage sensing and repair proteins in the nucleus[99]. It is further involved in nucleocytoplasmic transport[100], cell signaling, chromatin remodeling, cell cycle regulation[101] , apoptosis[99,102] and many other essential processes.

Leukocyte antigen-F adjacent transcript 10 (FAT10)

As mentioned above, FAT10 is found exclusively in mammalian cells, especially in cells of the immune system. Other cell types can also express FAT10, but mostly in response to inflammation[103,104]. FAT10 consists of a tandem β-grasp domain (Fig. 2e) and directly targets modified proteins for proteasomal degradation independently of their ubiquitylation status[105,106,107]. Since the half-life of endogenous FAT10 conjugates is comparable to that of free FAT10, it seems that it is degraded along with its substrates[108]. Another possible role of FAT10 was found in cytokine-induced apoptosis[109].

24

Interferon-stimulated gene product 15 (ISG15)

ISG15's structure contains a tandem UB-fold similar to FAT10 with its own conjugation machinery (Fig. 2f). Unlike the other UBLs however, it does not seem to target proteins directly for degradation[110,111,112]. This UBL is a key component of the host anti-viral response where modifications with ISG15 of both viral and host proteins tries to stop viral replication. In addition to being conjugated to target proteins and thereby influencing protein-protein interactions, it can also exist in an unconjugated state, acting as a cytokine[113].

ISG15 also regulates antiviral signaling pathways via negative feedback suppression. For instance, the activation of type I interferon (INF) signaling has to be tightly regulated in order to prevent excessive immune responses[114]. The negative regulation of type I IFN signaling occurs through the reduction of INF promotor activity by ISGylated RIG-I[115,116]. ISG15 can also be secreted from cells acting as a cytokine by stimulating the secretion of IFN-ɣ of natural killer cell and T-lymphocytes[117,118]. IFN-ɣ directly inhibits viral replication and plays a major role in stimulating and modulating immune response[119]. Consequently, a deficiency in ISG15 leaves patients highly susceptible to mycobacterial disease because of their IFN-ɣ deficiency[120].

Neural-precursor-cell-expressed developmentally down-regulated 8 (NEDD8)

NEDD8 which shares 58% sequence[121] identity and 80% sequence similarity with ubiquitin and is consequently its closest relative (Fig. 2h). It employs a similar three-step enzymatic cascade to be conjugated to target proteins[122]. Readers for ubiquitin modifications are often found to be rather promiscuous when it comes to binding also NEDD8[121,123,124]. Neddylation often modulates the efficiency of ubiquitin transfer, the most prominent example being the family cullin RING E3 ligases (CRL) which have to be first neddylated before they can receive ubiquitin and transfer it to its cognate substrate [122,125].

Neddylation reaction

NEDD8 is transferred to its substrate target in the same manner as ubiquitin: it starts with the activation of NEDD8 through conjugating AMP to its C-terminus, mediated by adenylation domain of the NEDD8 E1 APPBP1-UBA3 (amyloid-β precursor protein-binding protein 1 and ubiquitin-activating enzyme 3) (Fig. 2a). Structurally, APPBP-

25

UBA3 shares similarities with the ubiquitin E1 (UBA1), as APPBP1 and UBA3 correspond to its N- and C-terminal half-domains[29,122,126]. NEDD8 then forms a thioester intermediate with the catalytic cysteine in UBA3, thereby releasing AMP. In the subsequent transthiolation reaction, NEDD8 is conjugated to the E2's catalytic cysteine. Either UBE2M (for CRL1-4) or UBE2F (specific for CRL5 in metazoan) serve as E2's for NEDD8[127]. In the third and last step of the neddylation reaction, the E2~NEDD8 binds the substrate protein and forms an isopeptide with a specific lysine ε-amino group[128,129].

The tight relationship between neddylation and ubiquitylation is highlighted by the fact that all known NEDD8 E3 enzymes also act as E3 ligases for ubiquitin. One of the most prominent examples are the RING-box proteins 1 and 2 (RBX1 and 2). The RING domain of RBX1/2 serves as the binding site for the neddylated E2, transferring NEDD8 to the WHB (Winged-helix B) domain of its partner cullin[127,130,131]. RBX proteins form a so-called cullin RING E3 ligase (CRL) complex with cullins. Cullin neddylation leads to conformational changes (the extent of the remodeling depends on the individual cullin) which increases CRL ubiquitin transfer activity[132].

In addition to CRLs, a broad range of other non-RBX-family E3 ligases are modified with NEDD8. Most of these proteins are found to be involved in cell cycle regulation, tumor suppression, signal transduction and are part of the apoptotic machinery. Examples include c-Cbl (Casitas B-lineage lymphoma proto-oncogene), Smurf1, Mdm2/HDM2 (mouse double minute 2), RNF111, and Parkin which highlights the potential involvement of NEDD8 in various cancer-related processes[133-138].

Writers, readers and erasers of ubiquitin modifications

Information passed through UB modifications is subsequently translated into function through "reader" elements, specific motives and domains that bind single or multiple UBs. To counterbalance and regulate UB signaling, deubiquitinases (DUBs) can cleave peptide and isopeptide bonds between two UBs or an UB and a lysine, thereby "erasing" single or multiple UB modifications and preventing constitutively active ubiquitin signaling.
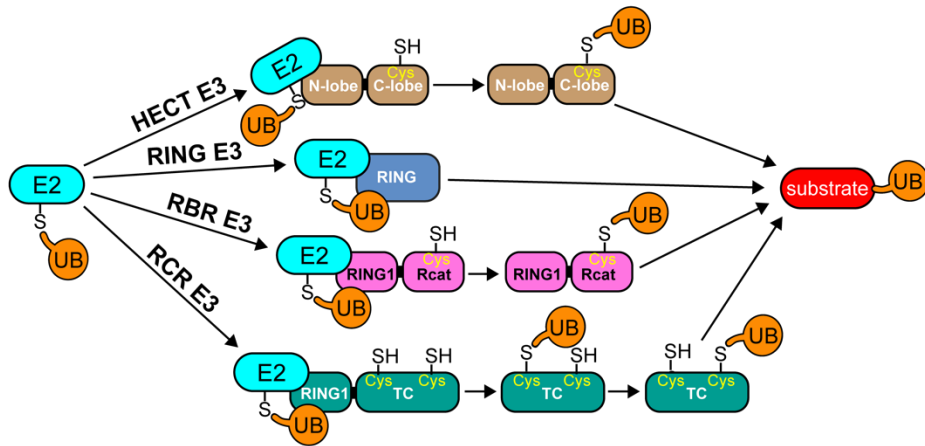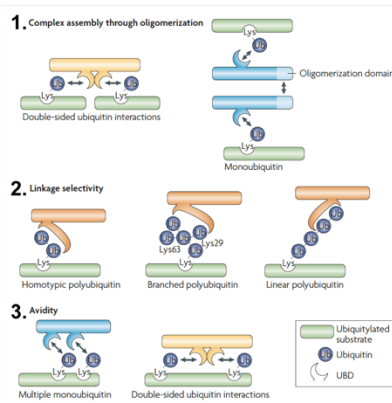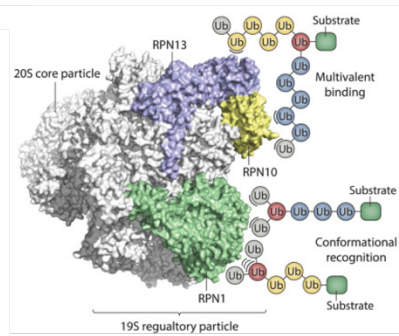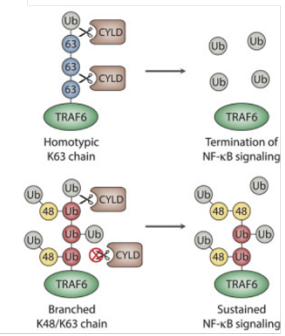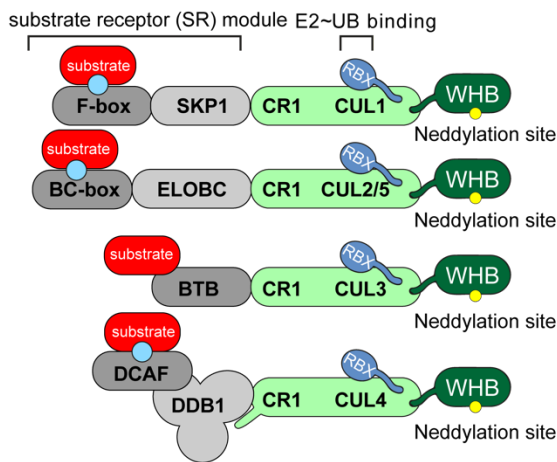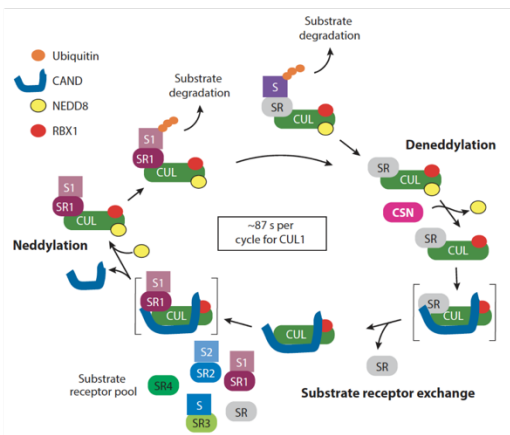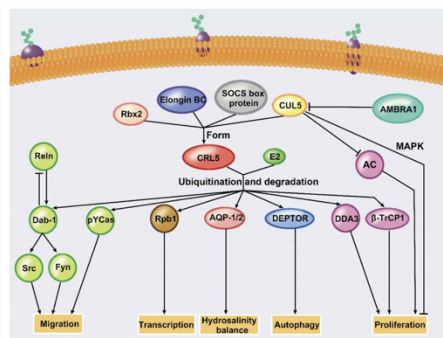
Fig. 3. The ubiquitin code is established, deciphered and removed by specialized enzymes

a, Ubiquitin (orange) transfer mechanism starting from the E2 (cyan) via E3 ligases to the substrate. Four different families of E3s transfer UB either via a thioester intermediate (HECT E3 ligases, brown), just act as a facilitator of substrate ubiquitylation and do not covalently bind UB (RING E3-ligases, blue) a hybrid RING/HECT-type mechanism (RBR E3 ligases, magenta) and a mechanism where the UB is transferred from one Cys to another before reaching the substrate (RCR E3 ligases, petrol). The catalytic cysteine is shown in yellow. The thiol groups are indicated. (taken from ref.[139]; Reprinted by permission from EMBO Press: John Wiley and Sons; "RBR E3 Ligases at work", Judith J Smit, Titia K Sixma, (2014). © 2014 The Authors). **b,** Ubiquitin-binding domains read different modification types. 1.UBDs on the same protein can together assembly ubiquitinated substrates. Also, proteins can recruit UB and then form an oligomer through their oligomerization domains. In both cases a complex is formed, which may lead to a signal amplification or activation of downstream processes. 2. UBD are specific for certain linkage types. 3. Two or more UBDs on a protein increase the binding avidity despite the general low affinity of UBD-UB interactions. The same is true if the substrate contains multiple ubiquitylations. UBDs are depicted as half-moons. UB is colored blue. Arrows indicate protein-protein interactions (taken from ref.[140]; Reprinted by permission from Springer Nature, *Nat Rev Mol Cell Biol* **10**, 659-671 "Ubiquitin-binding domains - from structures to functions". Dikic, I., Wakatsuki, S. & Walters, K. J., (2009). © 2009 The Authors). **c,** Specific UB-linkage types bind different UB-binding subunits on the 19S regulatory particle (PDB ID: 5T0J). The UB-binding sites are colored in blue, yellow, and green. Branched chains increase the binding through a higher local "UB concentration". The UBDs recognize either the newly formed interaction surface of the branch or the branching points itself (taken from ref.[141]). **d,** the DUB CYLD cleaves K63-linked UBs from TRAF6 to terminate NF-κB signaling. Branched K48/K63 chains cannot be cleaved (taken from ref. [141]). **e,** SR modules are specific for different cullins and allow for a rapid assembly of new active CRL complexes. SR modules consist of at least one subunit (adaptor, grey) that binds the substrate and one domain/subunit that connects the receptor (dark grey) to the cullin scaffold. The substrate is normally modified (e.g. phosphorylation, light blue) to be recognized by the receptor. On the other side (cullin CTD), the RING box protein (RBX1 for CRL1-4, RBX2 for CUL5; in blue) forms a tight assembly. The WHB domain (green) contains the neddylation site (yellow) which activates the cullin. CUL1s CR1 binds the SKP1-F-box assembly. CUL2 and CUL5 bind the ELOBC heterodimer that binds a BC-box protein. CUL3 binds BTB-containing proteins that directly recruit substrates. CUL4 bind DDB1-DCAF via the CR1 and a N-terminal tail. Abbreviations: CR-cullin repeat, CRL-cullin RING ligase, CUL-cullin, ELOBC-ElonginB/C, WHB-winged helix B (taken from ref.[142]; Reprinted by permission from Annual Reviews, *Annu Rev Biochem* **90**, 403-429, "Cullin-RING Ubiquitin Ligase Regulatory Circuits: A Quarter Century Beyond the F-Box Hypothesis" (2021). Harper, J. W. & Schulman, B. A. © 2021 The Authors). **f,** The regulatory circuit of the CRL system senses and transmits feedback via the neddylation-deneddylation-SR exchange cycle. Neddylation activates fully assembled CRLs and leads to substrate ubiquitylation. Once the substrate is degraded, the CSN complex deneddylates the cullin followed by SR exchange via CAND1. Now, a new CRL complex can assembly with different SR modules. Assembly of a new SR favors neddylation and start of a new ubiquitylation cycle. Abbreviations: "CAND-cullin-associated NEDD8-dissociated, CRL- cullin-RING ubiquitin ligases, CSN-COP9 Signalosome, S-substrate." (taken from ref.[142]; Reprinted by permission from Annual Reviews, *Annu Rev Biochem* **90**, 403-429, "Cullin-RING Ubiquitin Ligase Regulatory Circuits: A Quarter Century Beyond the F-Box Hypothesis" (2021). Harper, J. W. & Schulman, B. A. © 2021 The Authors) **g,** CUL5 assembles RBX2, ELOBC and SOCS box proteins into the CRL5 complex which recruits the UB conjugated E2 enzyme. CRL5 ubiquitylates different substrates such as Dab-1, pYCas, Rpb1, AQP-1/2, DEPTOR, DDA3, and β-TrCP1. These proteins are part of cellular processes such as transcription, autophagy and cell migration. AMBRA1 can inhibit CRL5 (taken from ref.[143])

UB writers

To transfer UB onto substrates, the E2~UB conjugate has to associate with its cognate E3s, which ensures that only the right substrate is selected and ubiquitylated. The human genome harbors over 600 E3 enzymes which can be categorized into 4 classes based on their reaction mechanism: RING type, HECT (Homologous to E6-AP C-terminus), RBR (RING-in-between-RING) type and RCR (RING-Cys-Relay) (Fig. 3a).

Most E3 ligases are part of the **RING type E3 ligase** family, which comprises a RING domain characterized by coordinating Zn^{2+} ions to adopt a cross-braced conformation. The RING domain forms the E2~UB binding platform and enables the transfer of ubiquitin to the substrate[144,145,146].

The second family, **HECT type E3 ligases,** employs a different mechanism based on their bipartite structure: binding of the E2~UB conjugate is mediated by the N-terminal lobe, while the catalytic cysteine, which receives the UB, is located on the C-terminal lobe. For there, the UB is passed on to the substrate[147,148].

RBR type family member share a common domain organization: they contain three Zn^{2+}-coordinating subdomains: (1) a RING1 domain, which is closely related to the canonical RING domains and forms the E2~UB binding platform; followed by (2) an In-Between-RING domain, which allosterically binds UB molecules that regulate protein activity; and (3) RING2 or Rcat, which comprises the catalytic cysteine to form the final step, the E3~UB[34,149]. RBR type E3 ligases are therefore a mix between RING and HECT E3 ligases (Fig. 3a)[150].

Recently, a novel mechanism of transferring UB from the E2 to the substrate has been found by Pao *et al.* Their study shows that the E3 ligase MYCBP2 (myc binding protein 2), which is involved in neurodevelopment and axon maintenance, uses a **RING-Cys-Relay** mechanism to target proteins for ubiquitylation. Similar to RING E3s, the RCR's RING domain binds the E2~UB[151,152] in an closed conformation. Next to the RING domain lies a tandem cysteine domain which surprisingly contains two cysteine residues both of them sequentially binding ubiquitin[119,120]. Similar to RBR/HECT E3s, the upstream cysteine first receives the UB from the E2, undergoing transthiolation then passing it on to the downstream cysteine (UB relay mechanism). In the final step, RCR E3 ligases show an esterification activity and preferentially target a threonine on the substrate protein (Fig. 3a)[119,120].

After priming the substrate with a single UB, additional UB moieties can be added by specific chain elongation E2 (f.i. CDC34). Consistent with this notion, the specificity of the polyUB linkage type is considered to be dictated by the last thioester-forming enzyme.

UB and UBL modifications are ultimately read by downstream machineries that selectively bind to and alter the fates of modified proteins. Structural studies of readers bound to polyUB chains and to UB- and SUMO-modified proteins have established paradigms for how these PTMs are translated into new functions. The linkage type of polyUB modified proteins often influences its function. PolyUB chain readers, including the 26S Proteasome (Fig. 3b-d), typically display multiple UB-binding domains. In many readers, UB-binding domains that individually bind a UB hydrophobic patch are arranged to synergistically recognize multiple UBs in a linkage-specific manner (for examples, see ref.[54,153-160]). This concept was further validated through design of artificial linkage-specific sensors, which bind selectively to particular UB chain-types[161,162].

Alternatively, some readers recognize site-specifically monoubiquitylated proteins or those bearing a single UBL. Much like readers of specific polyUB chain types, site-specifically monoubiquitylated proteins are cooperatively recognized by tandem reader motifs. This principle emerged from structures of the Srs2 helicase bound to PCNA (Proliferating Cell Nuclear Antigen) SUMOylated on Lys164 and of several different histone methyltransferases bound to histone H2B ubiquitylated on Lys120, wherein each of the two motifs on their own bind weakly to UB (or SUMO), or to the targeted protein[163-170]. When two reader motifs are combined they avidly and selectively recognize the monoSUMOylated or monoubiquitylated target[163].

Ubiquitin binding domains (UBDs)

UBDs interact with UB mono- or polymers via a diverse range of surface areas. Like many other interactions, the contact between UB and the corresponding UBD induces small conformational changes on UB to better accommodate the modification[171]. Interactions between the UB and the UBD are mostly mediated via hydrophobic patches on the surface of UB, such as the Ile44/Val70 and Ile36/Phe4 patches (Fig. 2i)[172,173]. A third hydrophobic stretch is localized around Leu8 and was so far only identified for being used by members of Y-family translesion synthesis (TLS) polymerases[174]. Moreover, other interaction surfaces include the C-terminal part of ubiquitin (which interacts with the DUB USP5[175]) and a polar interface around Asn58[176].

UBDs are modular domains with a size ranging from just 20 amino acids (ubiquitin interacting motives or UIMs) to up to 150 amino acids. They adopt a variety of different folds and can be categorized into nearly 25 classes based on their structure (Fig. 3b). They are classified into four major classes: (1) helical domains or motifs e.g. motifs interacting with ubiquitin (MIU), UB-interacting motif (UIM), UB-associated (UBA), coupling of ubiquitin conjugation to endoplasmic reticulum (CUE); (2) domains coordinating Zn^{2+} ions: zinc finger (ZnF), (3) UB-conjugating-like, (4) pleckstrin homology (PH) and other domains[177,178].

Surprisingly, single UBDs bind ubiquitin with relatively low affinity, with a K_d ranging in high micromolar ranges[179,180]. This makes sense when considering that most UB-interacting proteins contain multiple UBDs or that one UBD has multiple UB-interaction surfaces (UB chains) adding to higher avidity[181].

To mediate specificity and amplify the signal transferred by ubiquitin, UBDs are required to bind ubiquitin in a rapid, timely and reversible manner. This can be achieved by the low affinity but high avidity recognition of specific UB linkage types. Linkage-specific UB recognition can be accomplished in two ways: domains that specifically recognize the linker region between two ubiquitin units, or UBDs with multiple UB-binding surfaces that can find the position of UBs without binding the actual linkage[140]. An increase of avidity in UBD-UB binding is accomplished by various strategies, such as sensing the length of the UB chain or cooperative binding by tandem or different combinations of UBDs. UB-binding modules can regulate the accessibility to the ubiquitin chain and can induce the recruitment of multiple UB-modified proteins and/or UB receptors to the ubiquitin modification (multimerization)[10,54].

UB erasers

Every modification reaction requires a controlling and removal mechanism to prevent escalation. In the case of ubiquitylation, dedicated proteases called deubiquitinases (DUBs) remove and counterbalance the amount of ubiquitylated substrates within cells (Fig. 3d). They are responsible for removing mono-UB from their substrates and altering the topology of ubiquitin chains thereby editing the ubiquitin code[182,183]. The catalytic domains of DUBs and ubiquitin-like proteases are specifically targeting

modifiers such as SUMO, ISG15 and NEDD8. There are different modes of action for DUBs: They can either directly bind the substrate and cleave off UB or bind the UB-chain itself via UBDs. The arrangement of UB-binding sites in the DUB specifies whether the polyUB chain is cleaved at the end (exo-) or within (endo-cleavage)[184]. Branched UB chains can also be trimmed by targeting branching points (Fig. 3d)[156]. Independent of the cleavage site, DUBs share a common cleavage mechanism: ubiquitin is bound by the S1 site, where its C-terminus and the isopeptide bond are positioned in the right conformation to be hydrolyzed. When a diUB bond has to cleaved, both UB are bound by two ubiquitin binding sites: the distal UB is bound by the S1 site and the proximal UB binds the S1' site[185,186].

Cullin RING E3 Ligases (CRLs)

CRLs are part of the RING-type E3 ligase family and contains eight members (CUL1-3, CUL4A, CUL4B, CUL5, CUL7 and CUL9). To form an functioning complex, all of them have to assemble with a RING-box protein, either RBX1 (CUL1-4,7 and 9) or RBX2 (CUL5)[187]. Structure-wise, the cullin-RING assumes an elongated shape comprising multiple regions that mediate protein-protein interactions essential for ubiquitylation. The N-terminal region contains a module that enables the binding of interchangeable and cullin-specific substrate-binding receptors (SRs). Located opposite on the C-terminus sits the RING protein with the E2-binding domain (Fig. 3e)[130].

Cullin structure

All cullins share a common domain organization: three cullin-repeat domains (CR1-3) which bind the SR exchange factor CAND1 (Cullin Associated And Neddylation Dissociated 1)[188] are followed by a 4-helical bundle (4HB)[189]. CR1 also engages the adaptor and substrate receptor proteins. Next to the 4HB subdomain lies the C/R domain which is named for intercalating the N-terminal β-sheet of the RBX-protein (Fig. 3e)[189]. In addition to holding the RBX-protein in place, the C/R domain interacts with the deneddylation machinery, the COP9 signalosome (CSN)[190,191]. Moving further along to the C-terminus, we find the last cullin domain: The C-terminal WHB domain which harbors the conserved lysine residue where the UBL NEDD8 is covalently and reversibly attached. Neddylation plays an essential role in activating the cullin-RING ubiquitylation machinery (Fig. 3e)[132,192].

The SR system

The elegance of the CRL system lies in the vast number of interchangeable SR that bind the cullin either directly or via adaptors and recruit diverse substrates for ubiquitylation[193]. For example, F-box and BC-box proteins function as SRs with CUL1-RBX1 and CUL5-RBX2, respectively (reviewed in ref.[194]). Numerous assorted SRs, e.g. ≈70 F-box and ≈40 BC-box proteins in humans, assemble into distinct substrate-specific CRLs, collectively regulating a great variety of biological processes (Fig. 3e). For a uniform nomenclature, individual CRLs are written in capitals with their respective adaptor and substrate receptor proteins indicated in superscript. CRL1[β-TRCP] refers to CUL1-RBX1 assembled with the adaptor protein SKP1 and the substrate receptor β-TRCP. Different cullins bind to different SR families, each of them containing unique domains which mediate the specific interactions with the cullin CR1 or the adaptor protein. CUL3's SR directly interacts with the CR1 domain via its bric-a-brack/tramtrack/broad (BTB)-box domain which dimerizes[195]. CUL4A/B form together with the substrate-binding DCAFs and the adaptor DDB1 the DCAF-DDB1 SR module[196]. CUL5 and CUL2 both use the adapter pair ElonginB and C (Fig. 3e, referred to as ELOBC)[194].

E2~UB binding

Directly across the SR module resides the RING domain of the RING E3 ligase (RBX), which does not directly catalyze the ubiquitin transfer but recruits and activates the UB-carrying E2 enzyme[197]. The UB is conjugated to the E2 via a thioester bond, and binds to the RING domain in a closed conformation. The RING domain contains a linchpin residue (Asn98 in RBX1) that stabilizes the E2~UB conformation, bringing it face to face to the receiving lysine residue on the substrate.

The RING domain of RING-box protein is not the only location a charged E2 can bind. CRLs were also found to collaborate with another class of E2~UB binding E3's. These proteins, namely ARIH1 and ARIH2, are members of the RING-in-between-RING E3 Ligase family and carry and deliver ubiquitin to CRL substrates[6,90].

Regulatory circuit

The activity of cullins depends on a dynamic regulation of the position of its WHB domain and the RBX RING domain. Without an activating stimulus in terms of the

33

neddylation, these two domains are preferentially packed against each other and prevent binding of the E2. Consequently, deletion of the WHB increases ubiquitylation of some substrates[198]. Neddylation alters the positioning of the WHB domain and is part of the regulatory circuit of cullin RING ligases where it provides new binding sites for CRL partners proteins[132,199].

The regulatory circuit is separated into individual steps ("substrate-SR association, SR-cullin binding, cullin neddylation, ubiquitylation, CSN-mediated NEDD8 deconjugation, and CAND1-catalyzed SR exchange"[142]) (Fig. 3f) and is induced by a specific stimulus. Upon receiving the correct stimulus to ubiquitylate a substrate, the SR binds this substrate and together associated with the corresponding cullin protein. Substrate-SR binding blocks deneddylation by the CSN and induces NEDD8 conjugation to the conserved lysine on cullin WHB domain. Interactions between the WHB, RBX RING domain and C/R are disrupted by neddylation, enabling catalytically active conformations of the WHB and RING domain. The RING domain can now engage the E2 and UB is transferred to the substrate. Thus, NEDD8 stabilizes the substrate-bound CRL and stimulates substrate ubiquitylation. Successful ubiquitylation and dissociation of the substrate subsequently enables binding and deneddylation by the CSN ending the activity of the CRL. The exchange of the substrate-SR pair through CAND1 marks the beginning of a new round of the CRL regulatory circuit (Fig. 3f).

Taken together, SR-bound substrates are ubiquitylated by a RING E3-bound UB carrying enzyme recruited by the RBX1 RING domain in a manner that depends on cullin modification by NEDD8. Thus, UB-carrying enzymes are readers of neddylated CRLs[200].

The black sheep within the family: CRL5
Within the cullin-RING family, CRL9 and CRL5 assume somewhat special positions: whereas CUL9 is a fusion between a CRL and an RBR ligase, CUL5 adopts a classical cullin shape but uses its own RING protein RBX2 and its own neddylation machinery.

Structurally, CUL5 shares the same domain organization as all the other cullins: Three CR domains, followed by a 4HB, a C/R domain and a WHB domain with the conserved lysine (Lys724) for neddylation. The most N-terminally located CR1 binds the adaptor

pair ELOBC and a SR protein which contains a SOCS (suppressor of cytokine signaling) box[201]. Two interaction interfaces make up a SOCS box: A BC box that binds ELOBC and a CUL5-interaction box. Proteins with a SOCS-box can be further classified into 4 groups depending on additional domains they feature for interactions. SH2 domain-containing proteins, the ankyrin repeat-containing proteins, the WD40 repeat containing protein and the SPRY (SplA/ryanodine-receptor) domain-containing proteins [201]. Together, 37 SR form CUL5-based E3 ubiquitin ligase complexes to target substrates of different regulatory pathways for ubiquitylation. Surprisingly, SOCS box elements are also found in viral proteins. The HIV-1 viral infectivity factor (Vif) uses its SOCS box motive to hijack the CRL5 system and promotes the degradation of host immune response proteins[2].

Directly across the SR assembly, the RBX2 RING domain is placed to bind the the E2 for ubiquitylation. In-vitro studies and crystal structures[132] have shown that neddylated CUL5^{CTD} forms also a complex with RBX1, suggesting both RING proteins can assemble with CUL5, but whether this is physiological relevant requires further investigations. Similar to CUL1, CUL5 employs a member of the ARIH E3 ligase family, ARIH2, to ubiquitylate substrates[5].

Biological function of CUL5
The biological function of CUL5 is quite diverse, ranging from angiogenesis[202], to downregulating aquaporins[203] and inhibiting autophagy[204] to viral replication (Fig. 3g). Some of these processes are essential for cancer survival (f.i. angiogenesis) which is why CUL5 is an of interest for cancer and viral research. Two approaches are taken in the pursuit of potential CRL5 inhibitors: (1) neddylation inhibitors and (2) inactivating molecules. In theory, the uniqueness of CUL5 with its specific neddylation machinery could be exploited to find suitable drug targets (1a) blocking the interaction between the NEDD8 E1 NAE and its E2 UBE2F; (1b) the interface between UBE2F and the RING domain of RBX2; (2a) the interaction between NEDD8–CUL5 and SOCS proteins, and (2b) SOCS-substrates ("–" refers to an isopeptide bond). The only drug currently undergoing clinical trials the small molecule inhibitor Pevonedistat (also known as MLN4924), which inhibits the neddylation E1[205].

a

ARIH2 — E2 binding / RBR module — acidic · UBAL · RING1 · IBR · Rcat (cat Cys) · Ariadne — 493 — binding to neddylated CRL5

ARIH1 — acidic · UBAL · RING1 · IBR · Rcat (cat Cys) · Ariadne — 557 — binding to neddylated CRL1/2/3/4

HOIP — UBA · RING1 · IBR · Rcat (cat Cys) · LDD — 1072 — binding to LUBAC (SHARPIN + HOIL)

PARKIN — UBL · RING0 · RING1 · IBR · REP · Rcat (cat Cys) — 465 — binding of pUB and phosphorylation of UBL by PINK1

HOIL — LTD · UBL · ZF · RING1 · IBR · Rcat (cat Cys) — 510 — binding to HOIP

mode of activation

b autoinhibited ARIH1 (PDB: 4KBL)

c activated ARIH1 from complex with neddylated CRL1 (PDB: 7B5L)
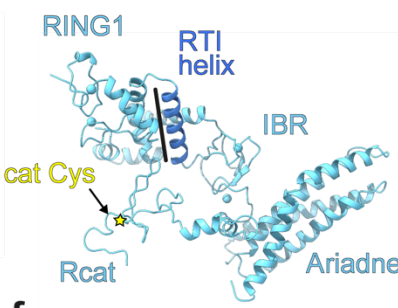
d HOIP + UB (PDB: 5EDV)
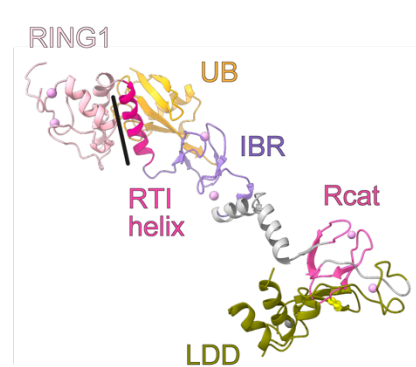
e autoinhibited PARKIN (human, PDB: 4BM9)
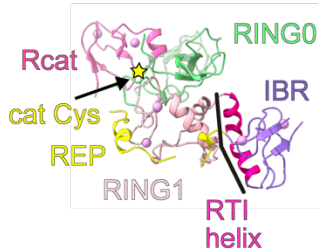
f PARKIN (human) + pUB (PDB: 5N2W)

g canonical RINGs stabilize closed E2~Ub states — linchpin and Ub contacts — long Zn²⁺ loop II — RBR RING1s favor open E2~Ub states

h

i HHARI/UbcH7-Ub complex

j HHARI^APO (PDB: 4KBL, chainB)

36
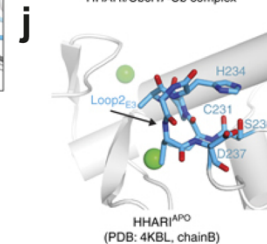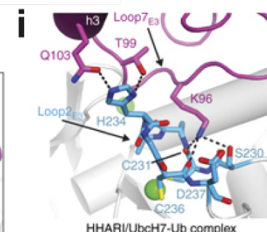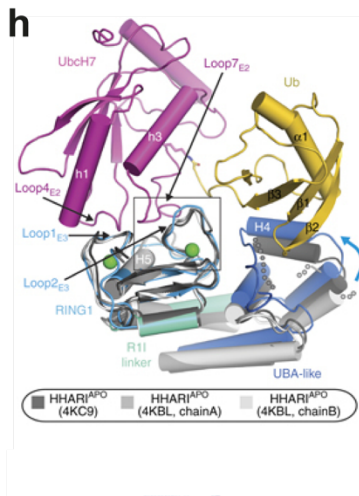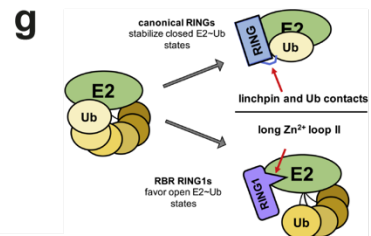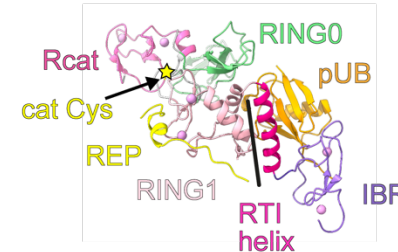
Fig. 4. Common and uncommon structures and mechanisms of RBR E3 ligases

a, RBR E3 ligases share a common RING1 (pink) IBR (medium purple) Rcat (deep pink) module. RING1 binds the E2 (cyan) and Rcat contains the catalytic cysteine (yellow stars). ARIH1/2 contain an additional autoinhibitory Ariadne domain (purple) a UBAL and a stretch of acidic residues on their N-terminus. Both are activated by binding to their respective CRL. HOIP contains an inhibitory LDD domain and is activated by binding to LUBAC. PARKIN is kept inactive by a repressor element (REP) and a RING0 (green). Binding to pUB and phosphorylation of its UB-like (UBL, brown) domain relieves autoinhibition. HOIL contains a zinc finger (ZF, light blue) and LUBAC C-terminal domain (LTD, blue) (based upon ref.[31]; Reprinted from "RING-Between-RING E3s ligases: Emerging themes amid the variations" Volume 429, Issue 22, Dove, K. K. & Klevit, R. E., (2017) Pages 3363-3375, with permission from Elsevier). **b-f,** the E2~UB-binding platform (RING1-RTI-helix-IBR domains) as well as individual inhibitory elements of different RBRs (autoinhibited ARIH1 PDB ID: 4KBL[206] , neddylated CRL1 bound ARIH1 PDB ID: 7B5L[90], HOIP PBD ID: 5EDV[207], autoinhibited human PARKIN PDB ID: 4BM9[208], human PARKIN PDB ID: 5N2W[209]) are shown. They all aligned over their RING1 domains and colored as in **a**. The cat Cys is indicated by a yellow star **g,** Model of E2~Ub conformations. In an unbound state, E2~Ubs are highly dynamic and can assume open and closed states depending on the E2. The open state is stabilized in canonical RING domains (e.g. RBX proteins) by a linchpin residue (red arrow) that favors the UB-transfer to amino groups. RING1 domains contain a Zn^{2+}-loop that acts as wedge and stabilizes the extended (open) conformation for transfer to cysteines (taken from ref.[210]). **h,** Conformational changes between different apoARIH1 crystal structures (PDB ID: 4KC9, 4KBL, greys) and the UBE2L3 (UBCH7)~UB bound state (colored). Close-up view of the $Loop2_{E3}$ region shows how His234 is rotated towards UBE2L3/UBHCH7 and forms a wedge separating the E2 and UB. UBE2L3/UBCH7 is colored violet, UB is yellow, ARIH1/HHARI RING1 light blue, RTI linker turquois and UBA-L domain in blue, zinc atoms are green spheres (taken from ref.[211]). **i,** Close up of residues of the ARIH1/HHARI $Loop2_{E3}$ (blue) which form interactions with UBE2L3/UBCH7 (violet). The amino group of Lys96 of UBE2L3/UBCH7 is coordinated by electrostatic interactions with Ser230 and Asp237. (taken from ref.[211]). **j,** Same view as in **i,** but of the apoARIH1 crystal structure (taken from ref.[211])

RING in-between RING (RBR) E3 Ligases

RBRs share a common architecture

The RBR family comprises 14 different members which all share a conserved catalytic RING1-IBR-Rcat (RBR) core and mechanism. Despite their mechanistic similarity, RBR ligases display a remarkable functional heterogeneity. Each of them has their own specific substrate, is localized to different cellular compartments, puts a specific type of ubiquitin-linkage (or just monoUB) onto the substrate and is regulated in different ways. All of these unique functions arise from ancillary domains that add to their respective functions (Fig. 4a).

The RBR module consists of the three zinc binding domains: the RING1, the IBR and the Rcat (also RING2). The RING1 assumes the three-dimensional structure of a canonical RING domain, coordinating two Zn^{2+}. Next come an IBR domain (also coordinating two Zn^{2+} ions) and the Rcat domain (again two Zn^{2+} ions) with catalytic cysteine. Structurally, the Rcat is related more to the IBR domain that to the RING1[212]. The RING1-IBR and IBR-Rcat are connected by flexible linker sequences, which allow large-scale conformational rearrangements of the individual domains when switching from autoinhibited to active forms. This could be shown for the more prominent family

37

members ARIH1, HOIP (HOIL1-interacting protein) and PARKIN (Fig. 4a-f)[206,207,213,214]. Only this flexibility allows all domains to align all reaction components correctly for the transfer of UB to the RBR and from there to the substrate[207,215].

To successfully transfer UB to the right substrate, each domain takes over specific functions in this multistep process: 1) the E2~UB conjugate is bound by the RING1, 2) ubiquitin is then passed onto the catalytic cysteine (transthiolation reaction results in a thioester) in the Rcat, and 3) finally, the transfer onto the substrate nucleophile (amino group) which can be a lysine or serine/threonine (Fig. 4a-f)[211]. The amino group can either be located on a substrate targeted for degradation or another ubiquitin targeted to form polyUB chains.

Catalytic mechanism

The RING1 domain interacts and stabilizes the E2~UB conjugate

After getting charged with UB by the E1, E2~UB conjugates are quite flexible but relatively stable and undergo aminolysis only slowly, most likely to prevent off-target effects and aberrant ubiquitylation. Therefore, the UB transfer from the E2 to a substrate has to be stimulated by specific mechanisms. This is achieved by stabilizing the dynamic E2~UB through binding the RING1 domain in conformation facilitating the UB transfer[216-219].

The E2~Ub conjugate binds the RING1 domain via the central α-helix of the E2 with UB being positioned distal from the E2 in an open conformation. This configuration answers the question of how an aberrant discharge of UB onto a lysine residues on the RBR is prevented: the open E2~Ub conformation suppresses the transfer to a lysine and instead promotes the transfer to a cysteine[149]. Interestingly, both UBE2D~UB and UBE2L3~UB are bound by the RING1 in an open confirmation, despite the fact that UBE2L3 is anyway unable to transfer ubiquitin onto lysine residues (Fig. 4g)[210]. Interactions between the RBR and the E2~UB are dominated by the RING1-E2 interface as it was shown for structures of ARIH1-UBE2L3~Ub complexes. Minor contacts can also be formed between the UBA-like (UBA-L) domain of ARIH1 (which sits N-terminal of the RBR domain) and ubiquitin but these contacts play no role in the overall functionality[210,211,220].

Taking a closer look into the UBE2L3 (UBCH7)-RING1 interface reveals essential interactions between UBE2L3's Loops4 and 7 and Loop1$_{E3}$ and Loop2$_{E3}$. What distinguishes ARIH1's RING1 domain from canonical RINGs is the length of the second Zn^{2+} loop (Loop2) (Fig. 4h-j)[212]. In ARIH1 it is two amino acids longer and prevents UBE2L3~UB from adopting a closed conformation by wedging the two proteins apart (Fig. 4i-j) [210,211]. Lys96 of UBE2L3 forms essential interactions with residues of RING1 Loop2 (Fig. 4i), adding to the preference ARIH1 has for UBE2L3 compared to UBE2D2[211]. Canonical RINGs feature a conserved "linchpin" residue (asparagine, arginine or lysine) which stabilizes the closed conformation of the E2~Ub conjugate through contacts with both proteins. Interestingly, while HOIP lacks the additional residues in Loop2, the bound UbcH5~Ub conjugate is also stabilized in the open conformation[207]. In contrast to the ARIH1-UBE2L3~UB interaction, HOIP binds ubiquitin through residues along the entire RBR domain, not just the RING1[207]. These extensive contacts are essential for forming a complex with UBE2L3~UB, as the binding affinity for UbcH5 alone is very low. This suggests that only the ubiquitylated E2 can form a stable complex with the HOIP RBR domain[220].

Taken together, RBRs ensure the cysteine-specific transfer of ubiquitin from the E2 in multiple ways: 1) evolving an interaction surface that favors binding of an E2 that prefers transthiolation (UBE2L3) over aminolysis (UBE2D2), 2) by harboring additional residues in its Zn^{2+} loop that "stretch" the UBE2L3~UB thioester bond and prevent a "closed" conformation, and 3) strengthen the "stretching" through extensive contacts between the dedicated UB binding domains (UBA-L in ARIH1) or the whole RBR domain (HOIP).

Ubiquitin transfer to the catalytic cystein

Interlude 1: Most RBRs exist in an autoinhibited state

The structures of autoinhibited Parkin and ARIH1 (PDB ID: 5N2W and 4KBL) show that their respective catalytic cysteines (Cys431 in Parkin and Cys357 in ARIH1) are restricted in their accessibility by unique structural elements[146,206,221]. Cys431 in Parkin is blocked by its RING0 domain (Fig. 4a, e-f), thus deleting it or abrogating the interaction with the Rcat surface through point mutations results in an increase of Parkin activity. This is likely due to an enhanced access to the catalytic cysteine[222]. For ARIH1, Cys357 is sequestered by residues in its Ariadne domain (Fig. 4a-c)[206].

39

Binding of the UB-charged E2 does not result in a release of the Rcat from the autoinhibitory state, which is consistent with findings from other studies that show that ARIH1 activation depends on a different mechanism involving another set of E3 ligases[210].

Interlude 2: transfer of UB to the catalytic cysteine requires specific activation mechanisms

To understand how the catalytic cysteine is made accessible and by which mechanism a RBR is activated is key to understand its biological roles and functions. For example, Parkin is activated by binding phosphorylated ubiquitin, which is catalyzed by the kinase PINK1 at Ser65 (Fig. 5a)[20,223]. In addition, Parkin itself has to be phosphorylated at an equivalent serine residue in its inhibitory UBL domain, which is again carried out by PINK1[224]. Binding of phosphoubiquitin (pUB) is not enough to activate Parkin, the same way as E2~UB binding to ARIH1 is not enough to release its autoinhibitory mechanism. The RING0 of pUB-bound Parkin is still occluding the catalytic cysteine and the repressor element still covers the proposed E2-binding site[225,209].
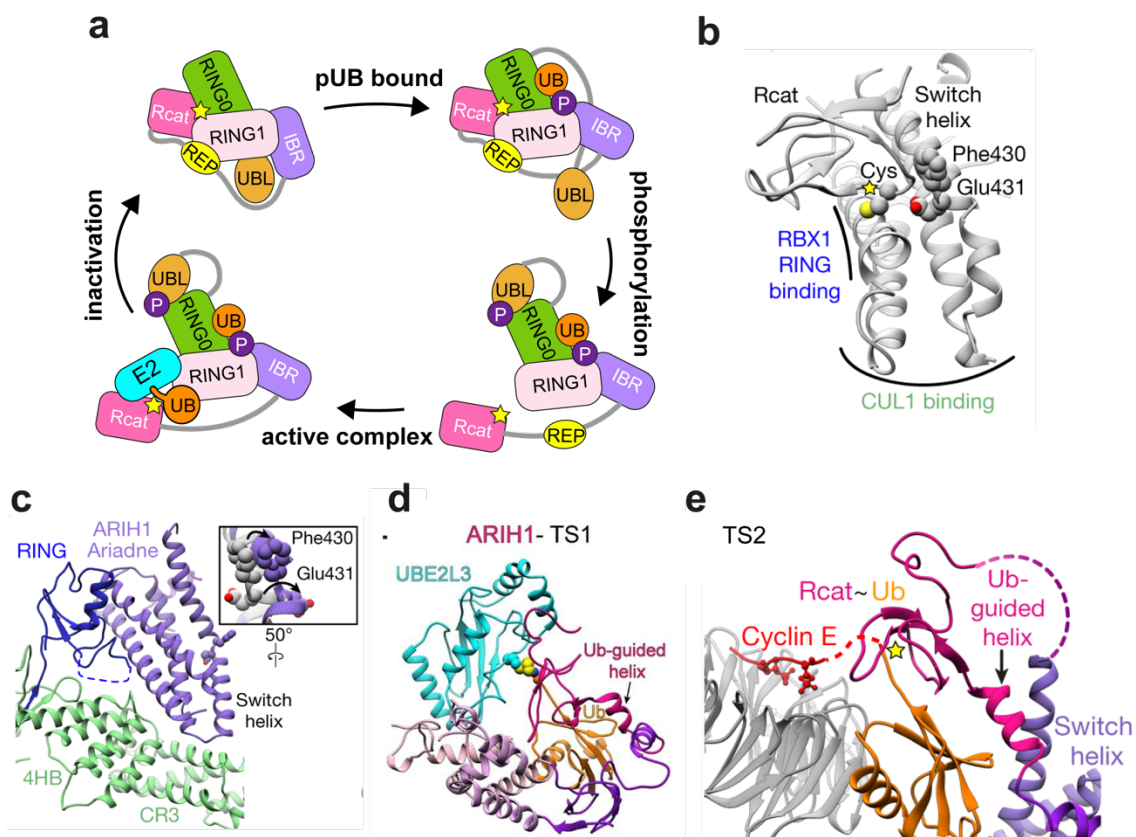
Fig. 5. Activation and transfer mechanism of RBR E3 ligases
a, Regulatory cycle of PARKIN activation. In the autoinhibited state, the RING0 occludes the catalytic cysteine and the UBL and the repressive element (REP) prevent E2 binding. Binding of pUB to the RING1 displaces the UBL domain. Further activation through PINK1-mediated phosphorylation of the UBL domain completely frees the E2 binding sites and the catalytic cysteine (yellow star). Domains are colored as in **4a**. for simplicity, the REP is not shown in the activated complex (based upon ref.[215]; Reprinted by permission from Springer Nature, *Nat Struct Mol Biol 25*, 623-630, "Mechanism of parkin activation by phosphorylation", Sauve, V. *et al.,* (2018) © *2018, The Author(s)*) **b,** The Rcat with the catalytic cysteine (yellow star) of autoinhibited ARIH1 is secured in place by residues of the Ariadne domain. Regions that bind to the RBX1 RING and CUL1 are indicated (taken from ref.[90]). **c,** The ARIH1 Ariadne domain (purple), the RBX1 RING (blue) and the CR3/4HB domains of CUL1 (green) are forming the E3-E3act superdomain. The switch helix bends and the residues holding the Rcat in place are rotated outwards (taken from ref.[90]). **d,** Transition state 1: UB-transfer from UBE2[215]L3 (cyan) to the ARIH1 Rcat (magenta). UBE2L3 is bound by the RING1 domain and UB is positioned by the UB-guided helix (magenta) (taken from ref.[90]). **e,** Transition state 2: UB-transfer from the ARIH1 Rcat (magenta) to the Cyclin E substrate (red). The UB-guided helix and switch helix (purple) hold the Rcat-bound UB (orange) in place and position the thioester bond for the nucleophilic attack (taken from ref.[90])

ARIH1s Rcat with its catalytic cysteine is held in place through interactions with its family-specific Ariadne domain (Fig. 4b-c, Fig. 5b). A cryo-EM structure of ARIH1 in complex with its activation partner CUL1 shows the mechanism of how two E3 ligase work together to ubiquitylate a substrate[90]. ARIH1 Ariadne domain forms interaction surfaces with RBX1s RING domain as well as the 4HB and CR3 of CUL1 (Fig. 5c). One major conformational change between the bound and the autoinhibited state can be observed in its switch helix (Fig. 5b). Named for its movement upon activation, it releases the Rcat and makes the catalytic cysteine accessible to receive UB from the E2. Mutations of resides securing the Rcat to the Ariadne (Asp503) as well as in the exact location where the switch helix undergoes is rotation (Phe430 and Asp431) lead to ARIH1 activation[90,206,210]. With the Rcat now released from Ariadne's grasp, it is now able to move to receive UB. Additionally, the linker connecting the IBR and Rcat domain is remodeled into a UB-guiding helix upon release of the Rcat and holds UB into place for the Rcat (Fig. 5d). The extended C-terminus of UB is finally gripped by catalytically important residues in the Rcat and forms the thioester bond with the cysteine (Fig. 5d-e)[90].

Substrate ubiquitylation

The concluding step of the UB-transfer mechanism was nicely shown in the cryo-EM structure of the ARIH1-CRL1 complex (Fig. 5e)[90]. The already mentioned UB-guiding helix plays an essential role in restricting the mobility and positioning the active site thioester towards the substrate lysine. Together with the Rcat it forms the "transferase module" which brings the UB close to the F-box-bound substrate[90].

Studies of the closely related RBR ARIH2 showed that it works with another cullin family member, namely CUL5-RBX2. The high sequence similarity tempt to speculate that employs a similar mechanism as ARIH1-CRL1 to target its substrates[1,5,6].

ARIH2

ARIH2 is another member of the family of RBR E3 ubiquitin ligase which forms together with ARIH1 its own branch of RBR ligases due to its prominent autoinhibitory Ariadne domain. ARIH2 shows the characteristic domain organization: starting with disordered N-terminus which contains a high number of acidic residues, followed by a UBA-like domain, a RING1, which binds the UB-conjugated E2, an IBR domain, a catalytic domain (Rcat) which harbors the catalytic cysteine (C310) and the autoinhibitory Ariadne domain[139]. RBR family members, such as the above-mentioned Parkin, HOIP, ARIH1 and many others have been found to play major roles in many regulatory pathways including protein degradation and stability, transcription and translation, subcellular tethering and cellular signaling. Consequently, RBR E3 ligases have to be tightly regulated with dysregulation found to be the cause of various diseases[139], making them potential targets for future drug developments.

ARIH2 is a negative regulator of inflammation

Studies performed in dendritic cells and macrophages show that one of the hallmarks of aberrant inflammation is a deficiency in ARIH2. ARIH2 negatively regulates inflammation through controlling the activation of NF-κB signaling and constitutively active inflammatory responses[226,227].

Furthermore, ARIH2 negatively regulates the NLRP3 inflammasome activity. As a part of the innate immune system, NLRP3 (nucleotide-binding oligomerization domain-like receptor family pyrin domain containing 3) recognizes extracellular ATP[228], which is released from damaged cells. Upon activation it stimulates caspase-1 activity which results in interleukin IL-1β secretion. ARIH2 directly binds NLRP3 without the involvement of the CRL5 system and ubiquitylates its target with K48 and K63-linked UB-chains. Deleting endogenous ARIH2 resulted in increased NLRP3 levels and activity which consequently lead to an increase in IL-1β production[227].

Regulator of endosomal transport

Additionally, ARIH2 ubiquitylates substrates with K48 and K63-linked UB-chains both of which are also shown to play a role in the endosomal sorting system[229]. Here, membrane and protein components originating from the plasma membrane and other membrane systems are collected and then returned to their place of origin or transferred to the lysosome for degradation. Two plasma membrane receptors, the epidermal growth factor receptor and the growth hormone receptor normally accumulate at endosomes and are recycled. Depletion of ARIH2 changes the morphology of these sorting endosomes, indicating that it plays are role in the sorting mechanism of both membrane proteins[230,231].

Role in aging-associated muscle degeneration

A decrease of athletic activity leads to a reduction of muscle mass and strength called hypotrophy[232]. The molecular mechanism underlying muscle hypotrophy depends on a complex system of protein synthesis and degradation that have to be in homeostasis[233]. One of the cellular signatures of aging and many neurodegenerative disorders is the decline of this protein homeostasis[234,235]. Accumulation of misfolded proteins and formation of insoluble aggregates are histologic hallmarks of diseases such as Huntington's disease (HD), Parkinson's disease and Alzheimer's disease.

An example of accumulation of a pathological polyalanine expansion concerns the poly(A)-binding protein nuclear 1 (PABPN1) which, when mutated, causes muscle weakness in occulopharyngeal muscular dystrophy (OPMD)[236]. Under normal conditions, PABPN1 controls the length of the poly(A) tail of nascent proteins and is regulated by the UPS. Mutated, expanded PABPN1 forms aggregates and depletes the levels of soluble PABPN1 in affected muscles leading to a complete dysregulation of the ubiquitin proteasome system. Normally, ARIH2 regulates PABPN1 through ubiquitylation and its expression in return regulated by PABPN1[237].

ARIH2 role as tumor suppressor

Mixed lineage leukemia 1 (MLL1) is a histone methyltransferase which positively regulates the transcription of genes during early development and hematopoiesis. Fusion proteins with MLL were found to induce the transcription and expression of ARIH2 in myeloid progenitor cells. Knockdown of ARIH2 in mice transplanted with Mll-

Ell-transduced bone marrow shortened the latency period to develop acute myeloid leukemia[238].

Cullins and RBRs team up

Ubiquitylation is either achieved by the RBX RING domain partnering with a UB carrying enzyme (E2~UB) or with another E3 ligase which contains a RING domain on its own. Much like other RING E3s, the RBX RING domain collaborates with a set of cognate E2~UB intermediates, which preferentially transfer UB directly to substrates or extend polyUB chains (reviewed in [199]). CRLs can also employ ARIH-family RBR E3s as their partner UB carrying enzymes[1,6,210]. This latter "E3-E3" mechanism differs from conventional E1-E2-E3 cascades in that after E1-loading of E2, UB is transferred to the ARIH-family E3, and from there to a neddylated CRL-bound substrate[1,6,239]. The binding and activation of both classes of UB carrying enzyme, E2 or E3, is stimulated by site-specific cullin modification by NEDD8[5,6]. Hence, UB carrying enzymes are readers of neddylated CRLs.

Cryo-EM structures of these two classes of NEDD8 reader - each with a distinct UB carrying enzyme, i.e. writer, catalytic mechanism - bound to neddylated CUL1-RBX1-based CRL1s revealed principles in common with UB and SUMO readers[90,199]. Both UB carrying enzymes, either the E2 UBE2D or the RBR-family E3 ARIH1, display tandem reader motifs, one binding the RBX1 RING domain (and also CUL1 in the case of ARIH1) and another directly binding NEDD8. The Mechanisms by which UB carrying enzymes "read" neddylated CRL1s were revealed with chemically-trapped complexes representing ubiquitylation[90,199]. The structures showed two entirely distinct mechanisms: One is a canonical RING E3-E2 mechanism wherein RBX1 activates UB transfer from the E2 UBE2D to a substrate of neddylated $CRL1^{\beta\text{-TRCP}}$ (ref.[199]). The other one is a distinctive E3-E3 mechanism, where UB is shuttled from the E2 over ARIH1 to neddylated CRL1's F-box protein-bound substrate[90]. Both of them revealed common molecular principles underlying the reading of neddylated CRL1s. First, noncovalent interactions between NEDD8 and its covalently-linked CUL1 shapes NEDD8 to recruit its readers. NEDD8's Ile36 hydrophobic engages the CUL1 WHB domain helix that culminates in the isopeptide linkage between them. These intra-complex interactions restrict the positions available to NEDD8, although its relative location differs with the two UB carrying enzyme. Importantly, the NEDD8-CUL1 interface also templates

44

NEDD8's malleable structure[199], resulting in the exposure of NEDD8's Ile44 patch in a particular "loop-out" conformation. Second, in the loop-out conformation, NEDD8's properly displayed Ile44 patch binds a reader, either UBE2D and ARIH1, which mediates ubiquitylation of the CRL1 substrate[199].

In addition to modifying CUL1's K720, NEDD8 also becomes covalently linked to other cullins, including the homologous K724 in the WHB domain of CUL5[130]. Interestingly, however, CUL5 has its own specific pathway writing and reading neddylation. Neddylation of CUL5 requires the metazoan-specific NEDD8 E2 UBE2F and its essentially built-in E3, the cognate RING domain from RBX2[240]. These differ the E2 and E3 UBE2M and RBX1 that neddylate cullins 1-4. Moreover, neddylated CRL5s employ the ARIH-family RBR E3 ARIH2 instead of ARIH1 as a UB carrying enzyme[1]. Despite 35% sequence identity, ARIH1 predominantly associates with neddylated CRL1-3s, while ARIH2 copurifies exclusively with neddylated CRL5-based CRLs[5,6].

CUL5 and ARIH2

Despite this progress in understanding mechanisms of NEDD8 regulation, and thereby also of CRL1-mediated ubiquitylation, it remained unknown if the established principles of UBL regulation apply to all CRLs, particularly those harboring CUL5. As mentioned above CUL5 employs its own NEDD8 E2, which neddylates a homologous lysine residue (Lys724) on CUL5[240]. Moreover, neddylated CRL5s uniquely employ the ARIH-family RBR E3 ARIH2 instead of ARIH1 as their UB carrying enzyme[1,5,6].

Hijacking the viral defense system

The importance of CRL5-specific neddylation "writers" and "readers" is highlighted by their roles in the evasion of the host cell immune response where HIV-1 hijacks components of the antiviral defense mechanism. HIV-1 replication in host cells depends on usurping cellular UB-dependent proteasomal degradation pathways to dispose of anti-viral restriction factors, including proteins in the APOBEC3-family.

APOBEC proteins belong to the family of deaminases, which removes the amino group from cytosine under oxidizing conditions and converts it to uracil. This process is f.i. involved in generating new combinations of antibodies in B cells[241]. It is also part of the innate immune response where, upon viral infection, the C to U conversion introduces

45

hypermutation in the viral genome. Additionally, it prevents the successful integration of reverse transcribed viral DNA into the genome. The human genome encodes for seven different APOBEC3 proteins which share a common structural feature, the zinc-containing deaminase-like domain[242]. Some APOBECs, such APOBEC3G (short A3G) and A3F contain two deaminase domains. Both of them contain a C-terminally active deaminase domain (CTD) and a inactive N-terminal domain (NTD) which is important for the integration of A3G into the newly formed virus particle (encapsidation)[243]. A3G and A3F are bound by the viral protein Vif through distinct interfaces and motifs that partially overlap. Within the APOBEC family, A3G and A3F are the most efficient in hampering HIV-1 replication. Their close relative A3C contains only one deaminase domain and restricts SIV replication in gorillas[244]. Vif together with its conscripted host protein CBFβ form a heterodimeric BC-box SR recruiting APOBEC3-family restriction factors to CUL5-RBX2[2-4]. Under normal conditions, CBFβ forms a heterodimeric complex with the transcription factor RUNX1, thereby allosterically enhancing the sequence-specific DNA-binding capacity of RUNX1. Following viral infection, CBFβ plays a critical role in stabilizing Vif and its interaction with CUL5.

Multiple studies use pharmacological inhibition, shRNA-mediated knockdown, or CRISPR/Cas9-mediated deletion studies, to show that neddylation of CRL5 is required for Vif-mediated APOPEC3 degradation. However, the exact structural mechanism of how CUL5, RBX2 and ARIH2[1,245] work together remained elusive so far. Here we use structural and biochemical analyses to reveal the mechanism with which ARIH2 overcomes autoinhibition and assembles with neddylated CUL5-RBX2 into a E3-E3act superdomain. Comparing the cryo-EM structure with the already published NEDD8–CRL1-ARIH1 assembly shows that different cullins are specifically regulated by NEDD8. In the case of CUL1, ARIH1 is directly bound and recruited by NEDD8, whereas CUL5-linked NEDD8 makes no direct contacts with ARIH2, but instead allosterically enables ARIH2 binding and activation. NEDD8 is covalently linked to CUL5 in a unique orientation, opening a previously blocked ARIH2 binding site. Taken together, our data reveals the novel allosteric activation of a cullin E3 ligase through a ubiquitin-like protein.

Results from this thesis have been published in:

Together with Arno F. Alpi and my supervisor, Brenda Schulman, the project was conceived. I purified proteins, optimized crystallization conditions, performed biochemical assays and made cryo-EM samples. I screened grids for optimal complex conditions and performed the initial modeling into the cryo-EM maps. Together with Brenda Schulman, I analyzed the data. Rajan Prabu and Jerome Basquin collected the crystal dataset. "Rajan Prabu refined the crystallographic and cryo-EM datasets and built and refined the final structures."[198]

Figures as well as Tables 4 and 5 used in the Results section were taken from the same publication. This article was published as an **Open Access** article. A copy of the license can be accessed under http://creativecommons.org/licenses/by/4.0/.

RESULTS

Structure of the RBR E3 Ligase ARIH2

Based on its close relationship to ARIH1 and previous biochemical studies, ARIH2 employs a similar UB-transfer mechanism as other RBRs: UB is transferred from the catalytic cysteine (cat Cys) to a substrate[90,150,246]. However, in the absence of activating factors, many RBR E3s employ unique domains to mediate autoinhibition[5,146,206,221,222,247]. For the RBR E3s ARIH1 and Parkin, the cat Cys is buried through intramolecular interactions that prevent its receipt of UB from an E2 enzyme[146,206,221,222]. For ARIH1 this involves the ARIH-family specific Ariadne domain binding to the Rcat domain[206]. Additionally, the conformation and orientation of E2~UB binding platform (consisting of RING1 and IBR) differ substantially between the autoinhibited states of Parkin and ARIH1, due to bending of their RTI-helix[90,146,206,209-211,221,222,248]. RBR E3s are generally activated by binding regulatory factors that effectively release the Rcat domain, straighten the RTI-helix, properly orient the

E2~UB binding platform and/or align a recruited E2~UB[90,146,206,207,209-211,213,215,221,222,225,249]. ARIH1 is activated through the formation of a E3-E3act superassembly with the neddylated CUL1-RBX1-based CRL. Cryo-EM structures of this assembly show that WHB-bound NEDD8 directly engages one side of the ARIH1 UBA-L domain through specific hydrophobic residues. The other side of ARIH1's UBA-L domain intercalates between the RING1, a straightened RTI-helix, and IBR elements[90].
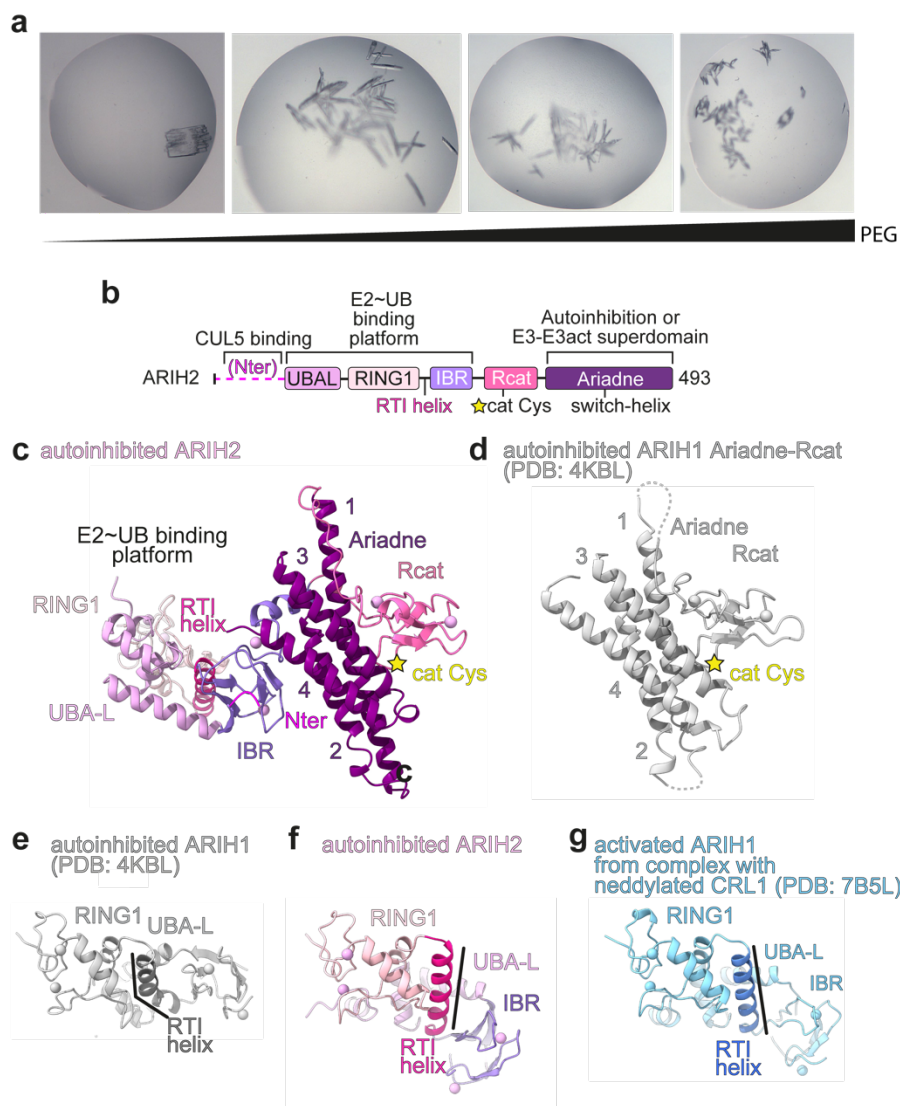
Fig. 6. Crystal structure of ARIH2 E3 reveals unique conformation
a, Pictures of drops with ARIH2 51-C crystals at increasing PEG concentrations (15%, 20%, 25% and 30%). **b,** Domain organization of the ARIH2 construct used for crystallization colored as in **4a**. The N-terminal region (N-ter) is predicted to be disordered and is not part of the crystal structure. The E2~UB binding platform, autoinhibition domains and domains binding to neddylated CRL5 are indicated. The location of the catalytic Cys (Cys310) is highlighted by a yellow star. **b,** Crystal structure of ARIH2 (residues 56-493). The individual domains are colored according to the schematic in **a**. The E2~UB-binding platform consists of the UBA-L, RING1, RTI-helix, and IBR. **d,** Ariadne-Rcat domains of autoinhibited superimposed on the ARIH2 Ariadne. The cat Cys is indicated by a yellow star.

e-g, Side-by-side comparison of autoinhibited ARIH2's UBA-L-RING1-IBR (colored), autoinhibited ARIH1's UBA-L-RING1-IBR (gray, PDB ID: 4KBL[206]), activated ARIH1 (blue, PDB ID: 7B5L[90]). RTI helices are highlighted by a black line. The domains were aligned over the RING1.

For better understanding of the regulation and activation mechanism of ARIH2, we first had to solve the crystal structure of an autoinhibited version that lacked the intrinsically-disordered N-terminal region. For setting up crystal trays, samples of purified ARIH2 51-C (details in the Method section) were submitted to the Crystallization Facility of the Max Planck Institute for Biochemistry where suiting conditions were screen with commercially available screening suites. First crystals appeared in the PACT (Qiagen) suite with 20% PEG 3350, 0.1 M Bis-Tris propane pH 8.5 and 0.2 M Sodium nitrate at 4°C (Fig. 6a). During the optimization process, different concentrations of ARIH2, PEG, different pH of Bis-Tris propane as well as other buffers (HEPES, MES, TRIS, etc) were tried (Fig. 6a). Additionally, other constructs of ARIH2, comprising the full-length version along with a version lacking the Ariadne domain were sent for crystallization but without success confirming the hindering nature of the ARIH2 N-terminus.

The sequence of ARIH2 exhibits canonical RBR E3 catalytic elements[250] (Fig. 6a). RING1, RING1-to-IBR (RTI) helix, and IBR domains that bind and present an E2~UB intermediate[90,207,249]. Unexpectedly however, the structure of ARIH2 shows striking differences from other autoinhibited RBR E3s[146,206,208,211,221,239]: When comparing the structures of autoinhibited ARIH2 and ARIH1 one can immediately make out similarities and differences. Individual domains superimpose nicely (Fig. 6c-f), with ARIH2's Ariadne-Rcat domains assuming the same orientation as for ARIH1 (Fig. 6d). The same holds true for the IBR, RING1 and UBA-L domain when superimposed onto ARIH1 as a single unit. However, mayor differences can be observed when the overall domain orientation is compared (Fig. 6c, g).

ARIH2 autoinhibition is mediated by the family-specific Ariadne domain

Without any activating factors, ARIH2 exists in autoinhibited state where its Rcat domain is sequestered by residues of the Ariadne domain (Fig. 7a). One of the first step to asses the activity of ARIH2 was by replacing the residues responsible for securing the Rcat to the Ariadne domain with alanines (Leu381, Glu382, Glu455), and generating a constitutively active mutant we termed ARIH2*. These mutations mirror those of the corresponding ARIH1* mutant[6,90,206]: they release autoinhibition as

49

monitored by ARIH2 autoubiquitylation, while maintaining NEDD8-dependency for ubiquitylating substrates of CRL5$^{Vif/CBF\beta}$ and CRL5^{ASB9} (Fig. 7b-e).
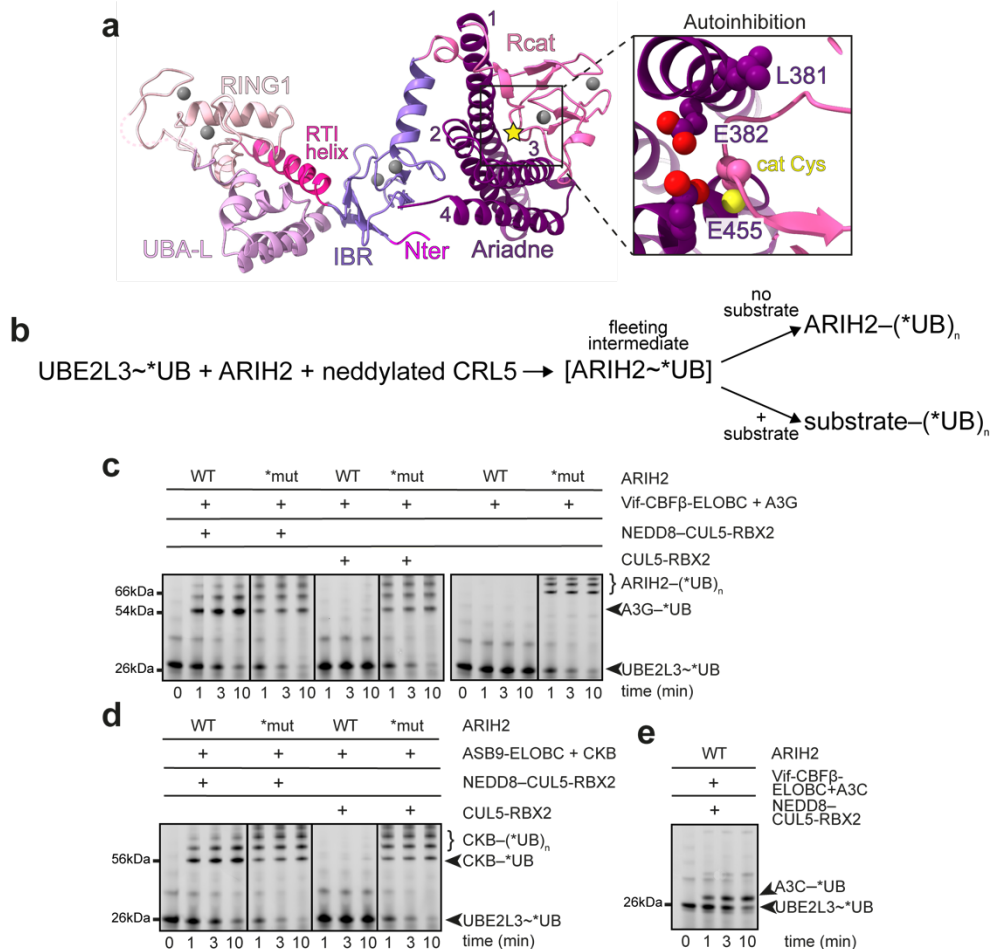
Fig. 7. ARIH2 exists in an autoinhibited state
a, The inset on right shows close-up of L381, E382 and E455 that mediate autoinhibition by securing the Rcat domain. The thiol group of ARIH2 catalytic Cys is indicated as yellow sphere. Zinc atoms are gray spheres. Helices of the Ariadne domain are numbered from 1-4. **b,** Schematic of the pulse-chase assay format. The assay examines the activity of E3-E3 complexes and detects fluorescent ubiquitin (*UB). The E2, UBE2L3 is charged with *UB in the E1-dependent "pulse" reaction. After quenching by removing ATP with apyrase, the "chase" reaction is started by adding variants of ARIH2 and neddylated CRL5. *UB is then transferred from UBE2L3 to the substrate or to ARIH2 (when no substrate is present) via non-detectable, fleeting ARIH2~*UB intermediate. **c,** The ubiquitylation of A3G substrate is monitored by *UB-transfer. The effect of NEDD8–CRL5, Vif-CBFβ and activated ARIH2* (mut* contains the autoinhibition-relieving mutations L381A E382A E455A) on substrate ubiquitylation and ARIH2 auto-ubiquitylation were tested. The UBE2L3~*UB containing chase-mix was added to the indicated E3–E3 and Vif-CBFβ-A3G components. $N = 2$ independent technical replicates. **d,** A different substrate-SR-adaptor complex was tested by the same pulse-chase format as in **c**. ASB9-ELOBC was the new SR-adaptor pair and CKB then new substrate. **e,** The same format as in **c**, but with A3C as substrate

Unique orientation of the E2~UB-binding platform

Perplexingly, ARIH2 differs from ARIH1 in that its domains assume the same spatial orientation as activated ARIH1. The arrangements of ARIH2's RING1, RTI helix and IBR domains reflect that of ARIH1 in complex with neddylated CRL1 rather than in the autoinhibited crystal structure (Fig. 8a-b). In the cryo-EM structure of activated ARIH1,

50

its E2~UB-binding platform and the UB-guided helix are poised in a conformation where UB is oriented with its C-terminus towards the catalytic cysteine (Fig. 5d). Autoinhibited ARIH2 exhibits a similar E2~UB binding platform orientation, stabilized through the tight packing of UBA-L domain to straight RTI helix (Fig. 8a-b). On the other side of the structure, the four-helical bundle-containing Ariadne domain packs against the Rcat, thereby burying the catalytic cysteine in the same manner as for autoinhibited ARIH1.
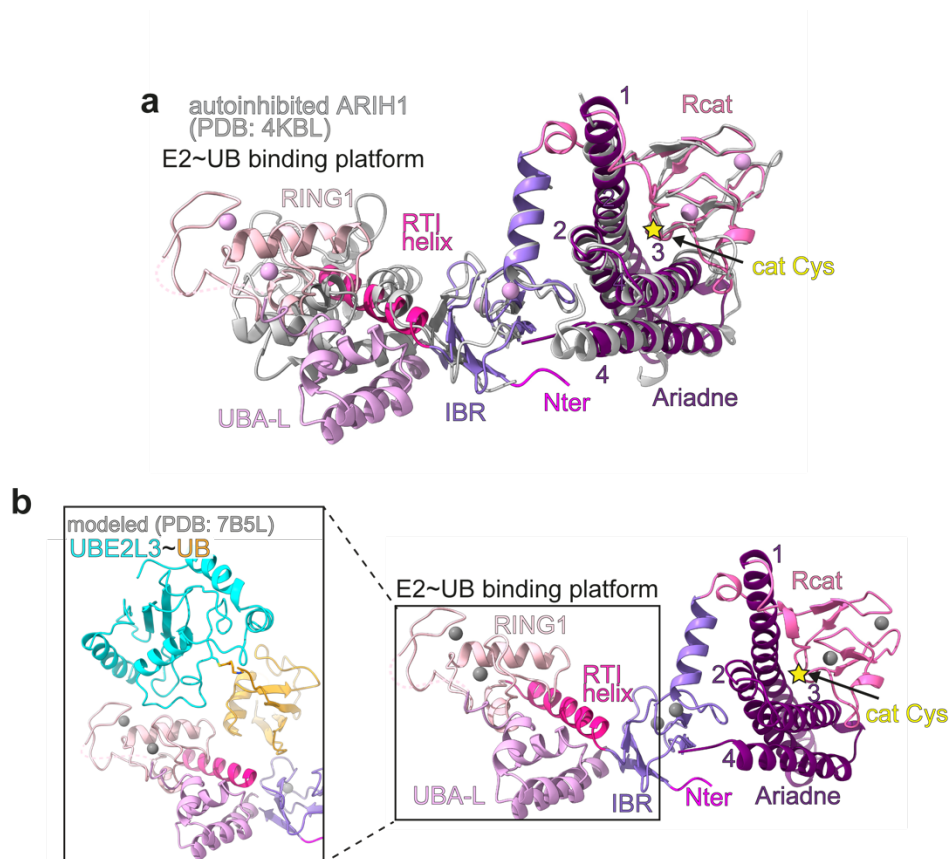
Fig. 8. Major differences between autoinhibited ARIH1 and ARIH2 can be observed in the orientation of the E2~UB-binding platform
a. Crystal structure of autoinhibited ARIH1 (PDB ID: 4KBL) superimposed over the novel ARIH2 structure. Notice the E2~UB-binding platform is misaligned. The E2~UB-binding platform consists of the UBA-L, RING1, RTI-helix, and IBR. Domains are colored as in **Fig. 6b**. **b,** Left inset shows UBE2L3~UB grafted onto E2~UB-binding platform after superimposing the corresponding region with that of neddylated CRL1 (PDB ID: 7B5L[90]).

Overall structure of ABOBEC-bound neddylated CRL5$^{Vif-CBF\beta}$-ARIH2 E3-E3 complex

To understand how neddylation alters CUL5-RBX2 and enables its specifically employing ARIH2, we solved the cryo-EM structures of two NEDD8–CRL5-ARIH2* assemblies with the multiprotein substrate receptor ELOBC-HIV-1 Vif-CBFβ. Both complexes contained a substrate of the APOBEC family, one with A3C and A3G (Fig.

51

Using the ARIH2 WT did not result in the formation of a stable complex. We assumed that the autoinhibited form of ARIH2 only transiently binds neddylated CRL5. For this reason, we employed the ARIH2* mutant where autoinhibition is relieved by the Leu380 Glu381 Glu455 triple mutant. As can be seen in Fig. 11, a stable and more homogeneous complex is formed when using ARIH2*.
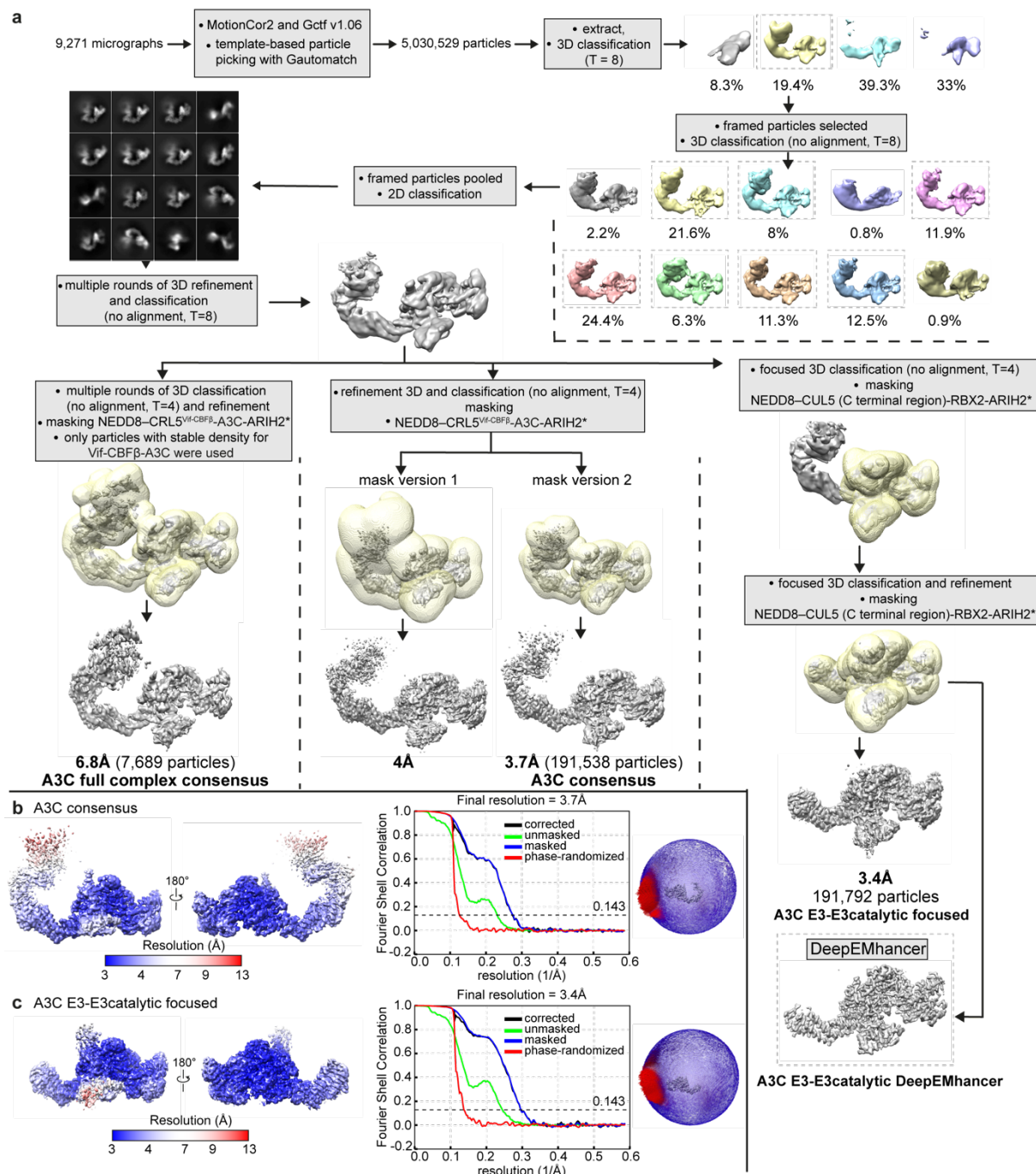
Fig. 9. Flowchart of processing steps for the NEDD8–CRL5$^{Vif-CBF\beta}$-ARIH2*-A3C complex
a, Flowchart depicting all processing steps for the neddylated CRL5$^{Vif-CBF\beta}$-ARIH2*-A3C complex. Transparent yellow masks are superimposed onto grey density maps. **b,** Left, heat maps of two views of local resolution maps of the A3C consensus maps with resolution ranging from 3 to 13 Å. Middle panel shows the FSC curve. "The overall resolution of 3.7 Å is indicated by the FSC = 0.143 criterion." [198] To the right, the angular orientation distribution is shown. **c,** The heat map, FSC curve and angular

52

distribution curve of the A3C E3-E3catalytic focused map of the NEDD8–CUL5 (CTD)-RBX2$^{Vif-CBF\beta}$-ARIH2* part.
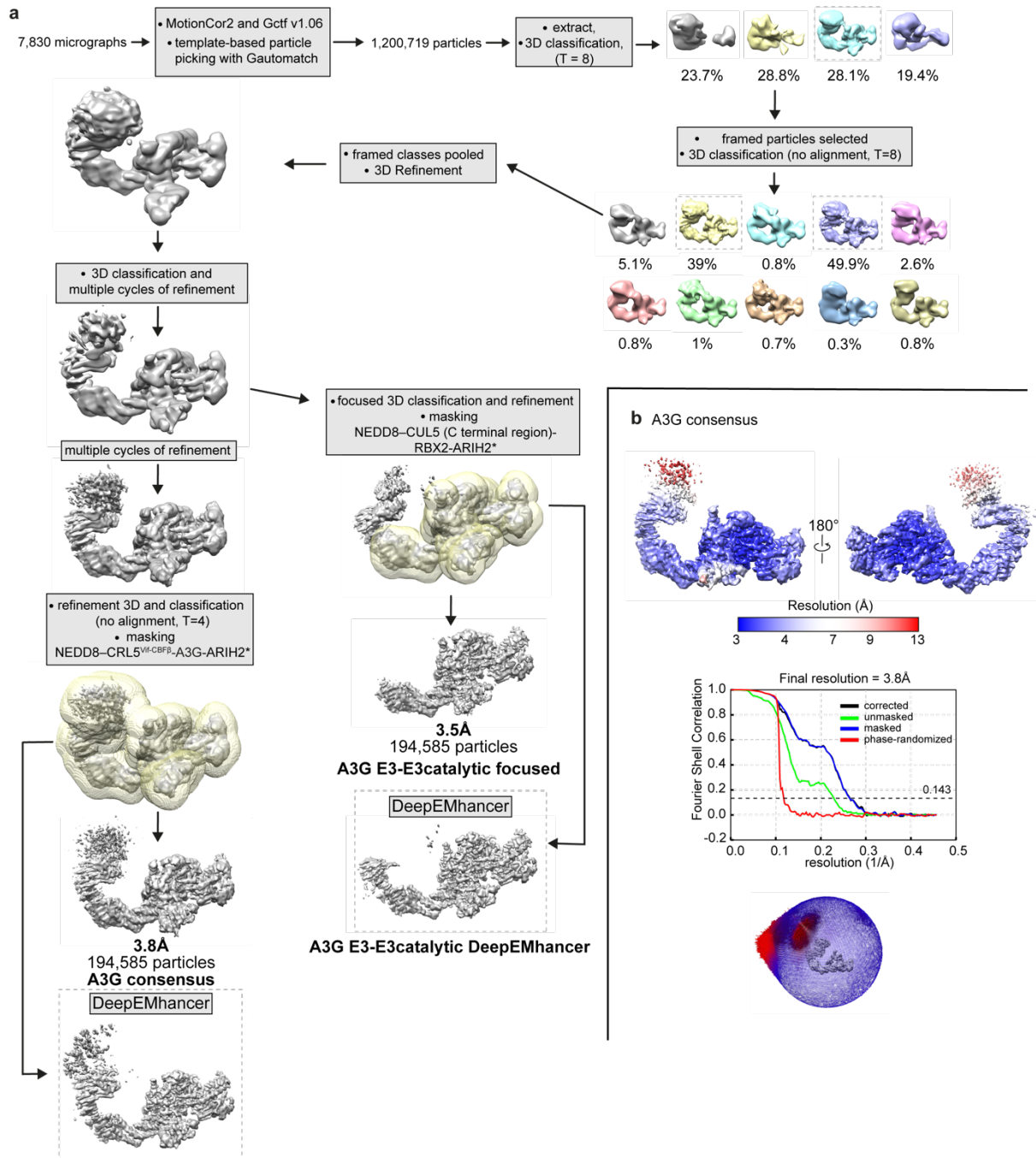
Fig. 10. Flowchart of processing steps for the for the NEDD8–CRL5$^{Vif-CBF\beta}$-ARIH2*-A3G complex

a, Flowchart depicting all processing steps for the neddylated CRL5$^{Vif-CBF\beta}$-ARIH2*-A3G complex. The portion of map where A3G-Vif-CBFβ-ELOBC are located can only be seen at low contour indicating high flexibility of this region. Transparent yellow masks are superimposed onto grey electron densities. **b,** Top, heat maps of two views of local resolution maps of the A3C consensus maps with resolution ranging from 3 to 13 Å. Middle panel shows the FSC curve. "The overall resolution of 3.8 Å is indicated by the FSC = 0.143 criterion."[198] On the bottom, the angular orientation distribution is shown.

Fig. 11. ARIH2* forms tighter assembly with NEDD8–CRL5 than ARIH2 WT
Neddylated CRL5$^{Vif\text{-}CBF\beta}$-A3C mixed with WT ARIH2 (green) or ARIH2* (blue) were run on sizing columns with the chromatograms shown on the top. Corresponding fractions of the UV absorbance peaks were run on SDS-PAGE gels (shown below) and stained with Coomassie-brilliant blue.

As both complexes yielded similar classes during refinement, only the reconstructions with A3C which resulted in higher resolutions are described. The entire A3C-CRL5$^{Vif\text{-}CBF\beta}$-ARIH2 complex could be visualized in a 6.8 Å resolution map ("low-pass filtered to 7.5 Å"[198]), which allowed fitting prior atomic coordinates. Already published structures of the CUL5 NTD with the ELOB-ELOC-Vif-CBFβ subcomplexes, an APOBEC3 substrate, CUL5 CR3, 4HB, C/R, RBX2, NEDD8, and our ARIH2 crystal structure were used to build a low-resolution model[251,252,132,253] (Fig. 12a-h). The high flexibility of the A3C substrate limited the resolution of the whole complex to 6.8 Å. A3C was fit into the density with the same orientation as A3F adopts when it binds Vif-CBFβ[244]. ELOB-ELOC-Vif-CBFβ assume the same position as in the crystal structure albeit with some room for movements[251].
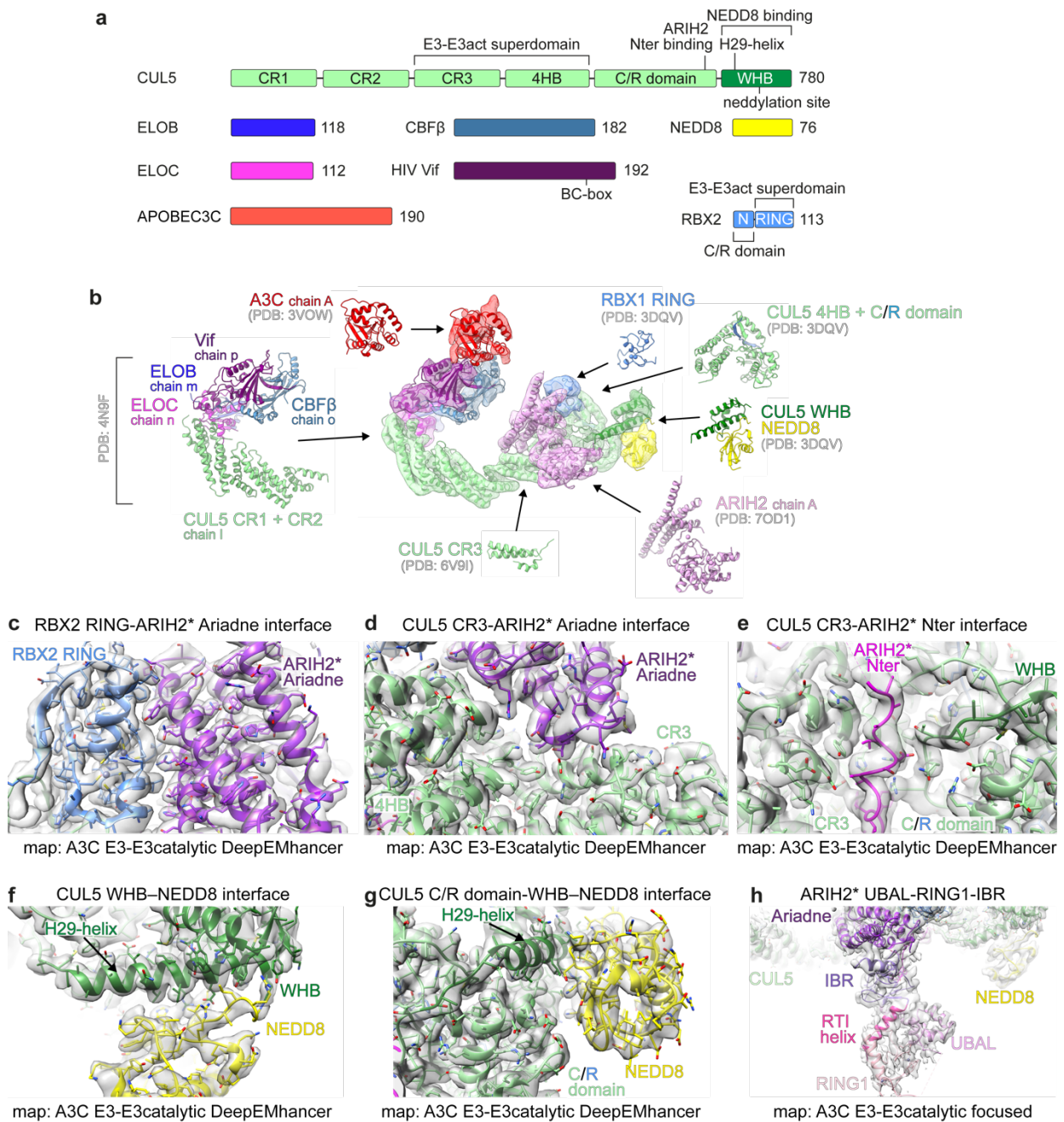
Fig. 12. Building the cryo-EM structure

a, Subunits and domains of neddylated CRL5[Vif-CBFβ]-A3C assembly are color-coded. Domains involved in the E3-E3act supedomain as well as ARIH2 binding are indicated. **b,** 6.8 Å resolution cryo-EM reconstruction of ARIH2* (violet, full-length ARIH2* harboring the L381A, E382A and E455A activating mutations) assembled into the NEDD8–CRL5[Vif-CBFβ]-ARIH2*-A3C complex, color-coded as in **a**. Atomic coordinates from ARIH2 crystal structure, RBX1 RING (PDB ID: 3DQV[132]) and part of neddylated CUL5 spanning the 4HB domain to the C-terminus (PDB ID: 3DQV[132]). CUL5 CR3 was taken from PDB ID: 6V9I[254]. Other domains or subcomplexes fit into the density are: A3C (PDB ID: 3VOW[255]), ELOBC-Vif-CBFβ and CUL5 NTD (PDB ID: 4N9F[251]). Density for ARIH2's Rcat domain is not clearly resolved, and is presumably mobilized upon ARIH2 binding to a neddylated CRL5. **c-h,** Close up of different interfaces between ARIH2* and RBX2, ARIH2* and CUL5 and NEDD8 and CUL5 in the A3C E3-E3catalytic Deep EMhancer map.

The 3.4 Å resolution focused refinement map of the CRL5[Vif-CBFβ]-ARIH2-A3C assembly enabled us to visualize the interaction surfaces between the atomic coordinates of neddylated CUL5-RBX2 and ARIH2 (Fig. 13a-b). The neddylated CRL5-ARIH2 E3-E3 assembly differs substantially from a recent model[253], although it is entirely consistent with protection from hydrogen-deuterium exchange on which that model was based[253]. The cryo-EM data show both general neddylated CRL-ARIH E3-E3 features, and unique ARIH2 interactions and CUL5-specific regulation by NEDD8. The most prominent feature is that CUL5-linked NEDD8 and ARIH2 are separated by more than 30 Å, whereas NEDD8 linked to CUL1 directly binds readers including ARIH1[90,199](Fig. 13a-b). The new model confirms several prior predictions[1,6,90,189,253]. First, similar to the CRL1[FBXW7-SKP1] structure[90], the substrate is located at the N-terminal side of the elongated NEDD8–CRL5 scaffold whereas the ubiquitin carrying enzyme ARIH2 is found at the opposite end. To ensure successful catalytic encounter, A3C leans toward the location where the Rcat with the bound UB would be. Second, ARIH2's E2~UB-binding platform occupies the same orientation as in the crystal structure suggesting that NEDD8 assumes an entirely different function in the activation mechanism of ARIH2[90] (Fig. 13c-d). Mutation of Val141 (Ile188 in ARIH1) in the RING1 of ARIH2 confirmed that ARIH1 and ARIH2 share the same overall ubiquitin transfer mechanism and E2 binding site on the RING1. Substituting it with an aspartate completely abrogated its ability to recruit UBE2L3~UB and prevented substrated ubiquitylation (Fig. 14a-b).
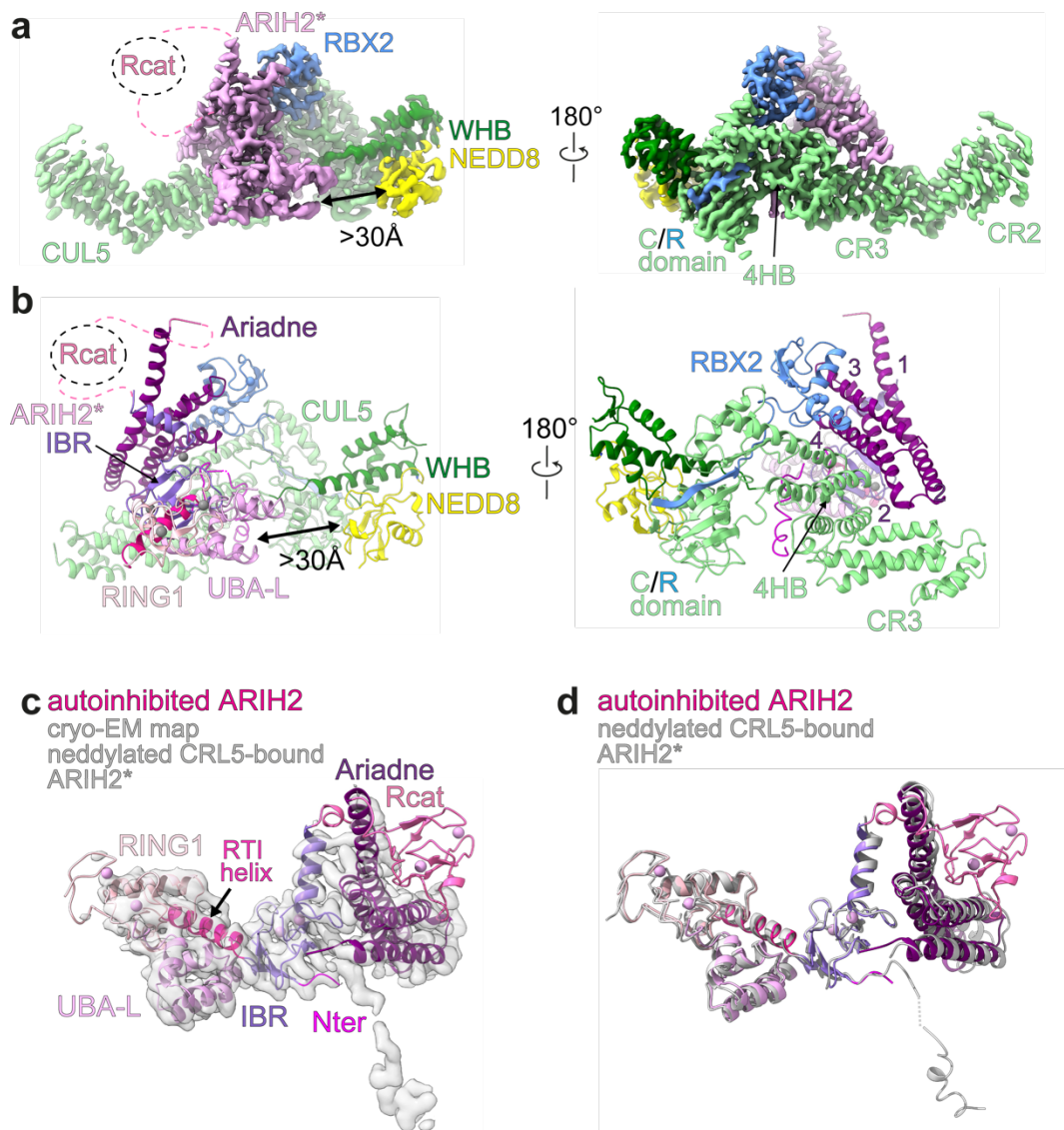
Fig. 13. Cryo-EM structure of CRL5$^{Vif\text{-}CBF\beta}$-A3C-ARIH2* complex displays NEDD8-dependent remodeling

a, 3.4 Å resolution focused refined map showing assembly between ARIH2* (violet) and its interacting region of neddylated CRL5$^{Vif\text{-}CBF\beta}$-A3C, color-coded as in **12a**. The C/R domain joins CUL5 and RBX2 in an intermolecular β-sheet, from which the C-terminal domains of both proteins emanate. CUL5's C-terminal domain consists of the rod-like H29-helix and ensuing WHB domain, which contains the neddylation site. RBX2's C-terminus is the RING domain. Other CUL5 domains encompassed in map include CR3 (3rd cullin repeat) and 4HB (4-helix bundle). No density for ARIH2's Rcat domain could be observed in the map, presumably due to mobility relative to the remainder of the assembly. Rcat domain connections are indicated in dotted lines. The UBAL domain and NEDD8 are separated by >30 Å indicated by a black arrow. **b,** The final refined coordinates for NEDD8–CUL5 (270-C)-RBX2-ARIH2* are shown in ribbon diagram. Domains are colored as in **Fig. 6b**, zinc atoms as gray spheres, and helices of the 4 Ariadne domain are numbered. The ARIH2 Rcat domain not contained in the model, presumably due to mobility relative to the remainder of the assembly, and its connections are indicated in dotted lines). The UBAL domain and NEDD8 are separated by >30 Å indicated by a black arrow. **c,** The autoinhibited ARIH2 structure fits nearly perfectly into the density of ARIH2* in the 3.4 Å resolution focused-refined cryo-EM map. Domains are colored as in **Fig. 6b. d,** Superposition of the ARIH crystal and ARIH2* cryo-EM structure reveals the same overall domain orientation

57
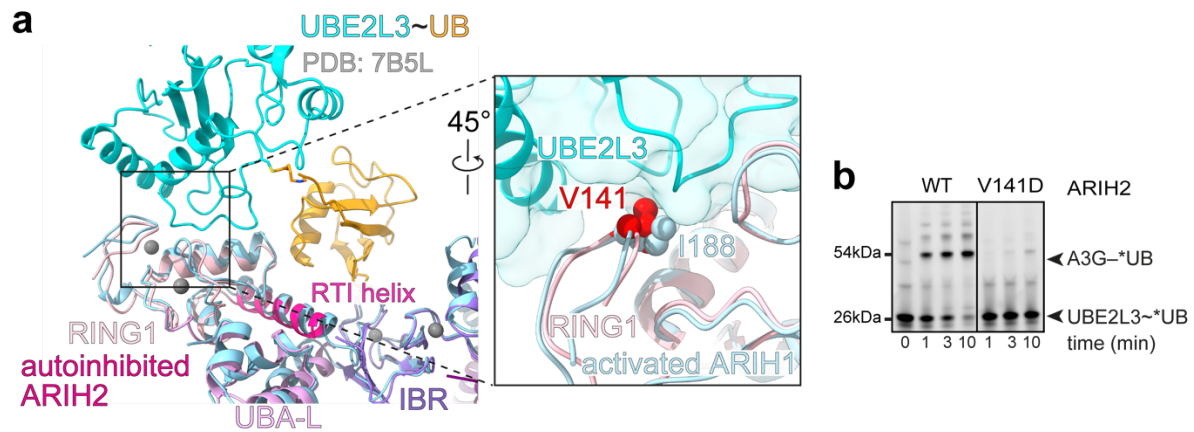
Fig. 14. Unique interface between ARIH2 UBA-L and NEDD8

a, Close-up of the E2~UB binding platform of ARIH2. Superimposed the corresponding region of activated ARIH1 with UBE2L3~UB (light blue, cyan and orange) showing the central Ile188 residue which corresponds to ARIH2 Val1441. Activated ARIH1 (PDB ID: 7B5L[90], light blue) was superimposed onto the E2~UB binding platform. **b,** SDS-page gel of neddylated CRL5$^{Vif-CBF\beta}$-catalyzed *UB transfer from UBE2L3 to A3G comparing the WT ARIH2 and Val141D mutant. $N = 2$ independent technical replicates.

Third, the NEDD8-linked CUL5 WHB and RBX2 RING domains are repositioned relative to a structure of an unneddylated CRL5 complex, consistent with the notion that neddylation favors alternative, active CRL conformations[132] (Fig. 15a-b). Neddylation of CUL5's WHB domain results in an astonishing ≈110° rotation of the CUL5 helix 29 and WHB where before it interacts with the RING domain of RBX2 in unneddylated CUL5 to now novel interfaces with the C/R domain[132,253] (Fig. 15a). Additionally, the RBX2 RING domain undergoes a 50° relative rotation to bind ARIH2 (Fig. 15b). Below we describe conformational changes and protein-protein interactions underlying NEDD8's distinctive, indirect allosteric activation of ARIH2-mediated ubiquitylation of CUL5-RBX2 substrates.
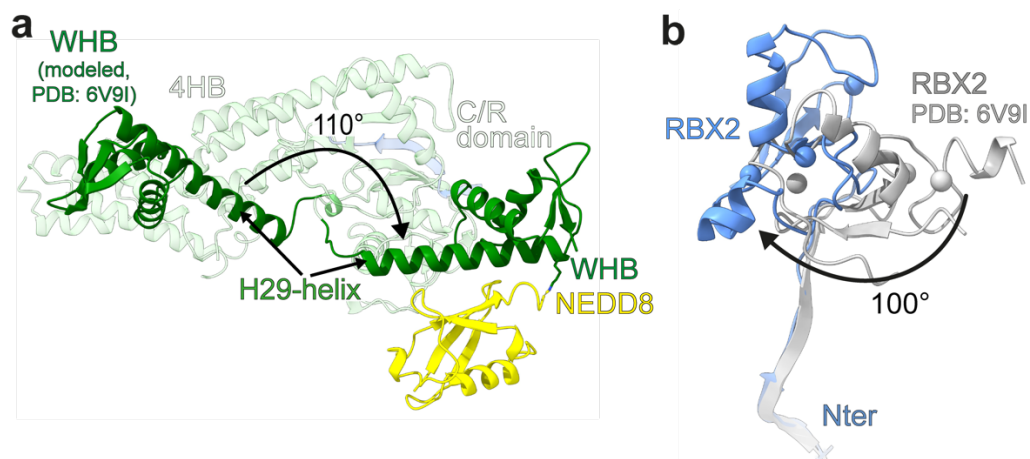
Fig. 15. CRL5 assembly undergoes unique structural rearrangements upon neddylation
a, Neddylation induces a 110° rotation of the CUL5 WHB domain and its H29-helix (both in dark green). The neddylated CRL5[Vif-CBFβ]-A3C-ARIH2* complex and unneddylated CUL5-RBX2 (PDB ID: 6V9I[254]) and are superimposed over their C/R domain (translucent). For simplification, ARIH2* and RBX2 are not shown. **b,** A similar structural transition is caused in the RBX2 RING domain. It is rotated 100° to the side between unneddylated (white, PDB ID: 6V9I[254]) and neddylated (blue) state. The structures were superimposed over the C/R domain, but only RBX2 is shown for clarity.

Distinctive NEDD8 activation of ARIH2 ubiquitylation of CRL5 substrates

To probe ARIH2 activation by neddylated CRL5 E3s, we reconstituted pulse-chase ubiquitylation reactions with two different substrate receptors (ELOBC complexes with CBFβ and HIV Vif, and with ASB9), three substrates (APOBEC3C, APOBEC3G, and CKB), the E2~UB conjugating enzyme UBE2L3, and various versions of CUL-RBX complexes and ARIH2 and ARIH1[1,6]. These assays detect fluorescent UB (*UB), starting with UBE2L3~*UB generated in the pulse reaction, and track its linkage to substrate after adding other proteins in the chase. Control reactions confirmed that CUL5 substrate ubiquitylation depends on ARIH2, its cat Cys, cognate receptor-substrate pairing (i.e., CBFβ-HIV Vif and APOBEC3C or APOBEC3G, and ASB9 and CKB), and NEDD8 (Fig. 16a). We also generated a neddylated CRL1 with RBX2 substituted for RBX1, and a CRL5 with RBX1 substituted for RBX2. The data confirm that CUL5, RBX2, and neddylation are required for CRL substrate ubiquitylation by ARIH2 (Fig. 16b-c).
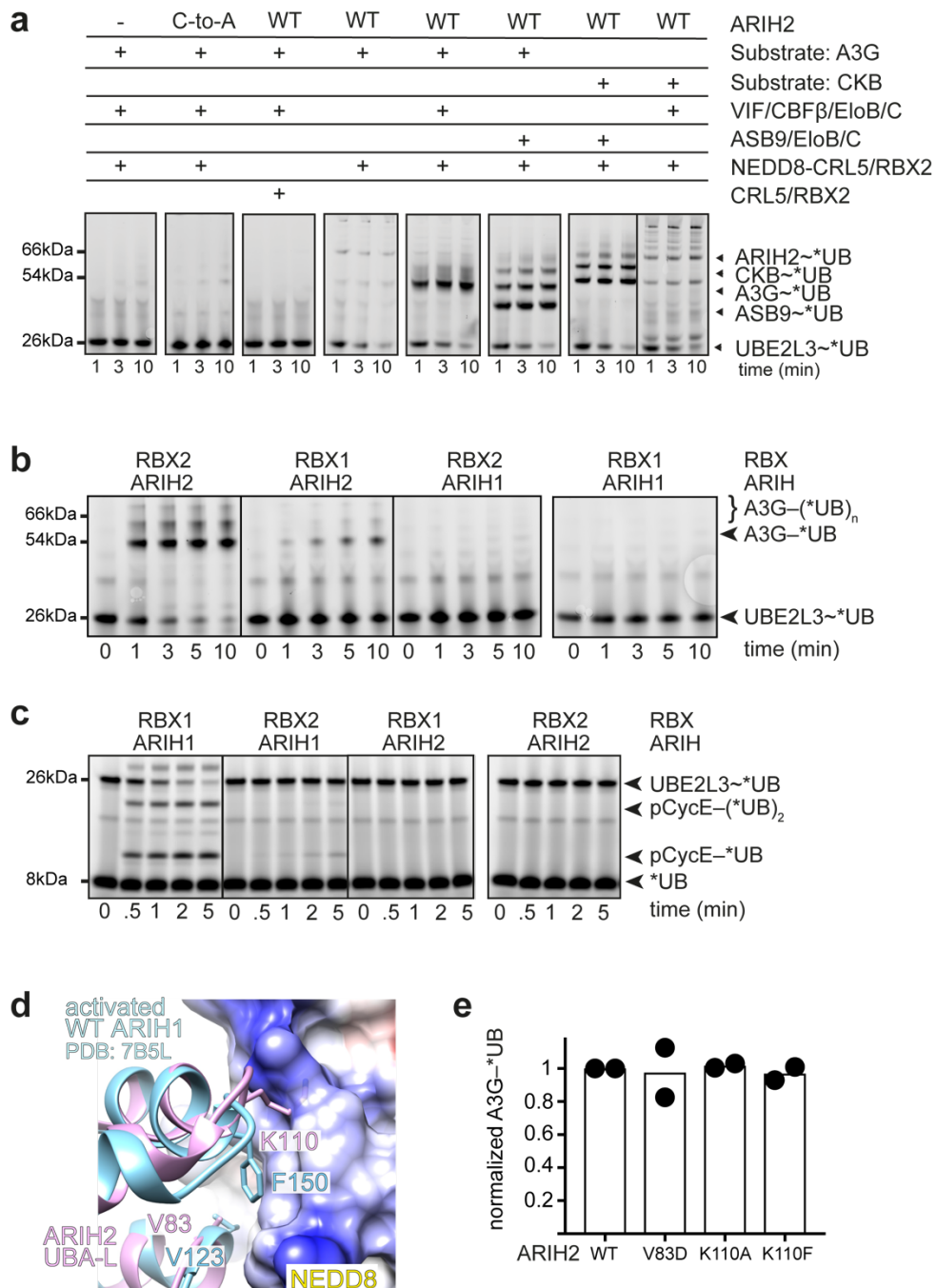
Fig. 16. Proper assembly of all CRL components is required for substrate neddylation

a, SDS-page gels of pulse-chase reactions highlighting the roles of individual components of E3-E3act superassembly for a successful transfer of *UB transfer from UBE2L3 to A3G or CKB. The pulse-chases show that the catalytic cysteine as well as the correct substrate-SR pairing is necessary to ubiquitylate the substrate. Incorrect pairing only results in ARIH2 autoubiquitylation. **b,** SDS-page gels of pulse-chase reactions showing that the correct NEDD8–CUL-RBX-RBR pairing is required to successfully ubiquitylate A3G. Here, CUL5 is expressed with RBX1 and RBX2 and tested in its ability to ubiquitylate A3G with either ARIH1 and ARIH2. **c,** Pulse-chase assay testing the right RBX protein with neddylated CRL1[FBXW7]-pCycE. **d,** The UBA-L domain of ARIH2 (pink) is superimposed onto that of activated ARIH1 (blue). ARIH1 UBA-L is binds NEDD8 (colored by electrostatic surface; positive areas are colored blue, red negative, and white uncharged) via Phe150 and Val123 (PDB ID: 7B5N[90]). **e,** Graphs show the neddylated CRL5[Vif-CBF]-dependent transfer activity of ARIH2 WT and UBA-L mutants of *UB from UBE2L3 to A3G in 10 min. Results were normalized to values with WT ARIH2. N = 2 independent technical replicates.

A major difference between neddylated CRL1-ARIH1 and neddylated CRL5-ARIH2 is that CRL1-linked NEDD8 binds ARIH1's UBA-L domain whereas CRL5-linked NEDD8 doesn't bind ARIH2's UBA-L. Studies have shown that ARIH1 is activated by its UBA-L domain binding to NEDD8 and mutations in this interface lead to a loss of activity[5,6,90], which lead us to examine the structure of ARIH2's UBA-L domain. ARIH2 displays strikingly divergent properties at the site corresponding to ARIH1's NEDD8-binding surface (Fig. 16d). ARIH2's Lys110 is incompatible with hydrophobic interactions like those between ARIH1's corresponding Phe150 and NEDD8's Ile44 hydrophobic patch. Whereas mutating the NEDD8-binding site on ARIH1's UBA-L-domain (F150A and V123D) abolishes ubiquitylation of neddylated CRL1 substrates[5,6,90], mutating the corresponding Val83 and Lys110 in ARIH2 had no effect (Fig. 16e). This suggested that ARIH2's UBA-L domain may not bind CUL5-linked NEDD8, and that ARIH2 could "read" NEDD8 modification of CUL5 in a unique manner.

Distinctive NEDD8 noncovalent interactions with CUL5

NEDD8 makes extensive noncovalent interactions with CUL5. First, NEDD8's concave β-sheet envelops the CUL5 WHB domain (Fig. 17a). Compared to the CUL1-NEDD8 interface, unique interactions are made between residues of NEDD8's Ile44 hydrophobic patch (Ile44 and Val70) and hydrophobic residues of CUL5's H29 helix (Leu710 and Leu713). Helix29 connects the CUL5 C/R domain with the WHB domain and forms one of the two interfaces with NEDD8. H29 and H30 form a hydrophobic pocket where the side-chain of NEDD8 Leu8 is inserted. On the opposite side, Leu73 and Arg74 are wedged between a number of aromatic and small hydrophobic residues (Ile720, Trp759, Tyr765, Tyr778). Further electrostatic interactions with NEDD8 are mediated by CUL5's Glu717 (Fig. 17b).
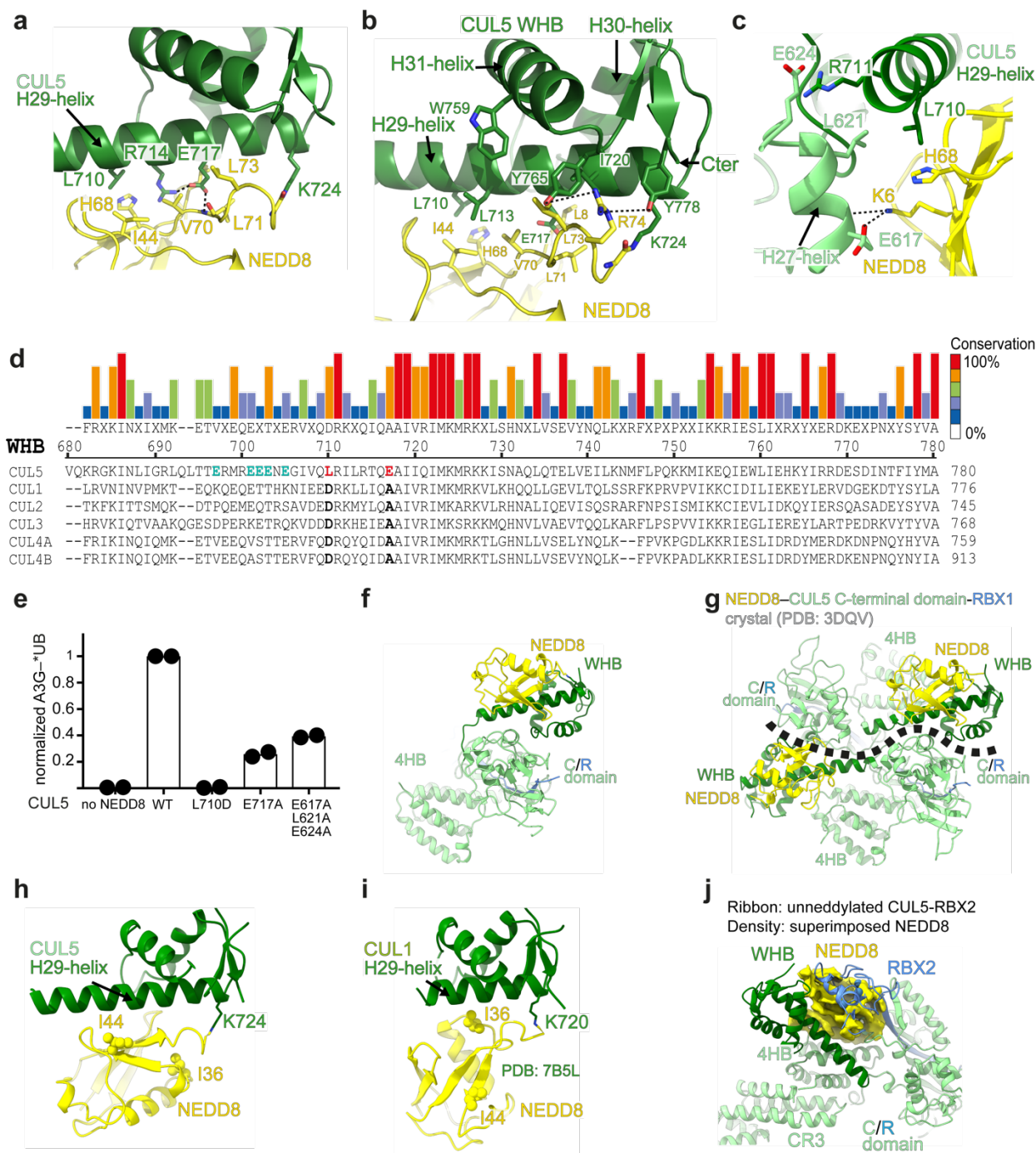
Fig. 17. CUL5 WHB binds NEDD8 differently to CUL1

a, The CUL5 H29-helix part of the WHB (dark green) interacts with residues of the Ile44 patch of NEDD8 (yellow) close to their covalent isopeptide bond. **b,** Hydrophobic residues of H29, H30 and H31-helices (dark green) form an interface with NEDD8 (yellow). **c,** Three-way interface between residues of H27-helix of the C/R domain (light green), H29-helix of the WHB (dark green) and its covalently-linked NEDD8. The structure is oriented relative to **a** by rotations of 40° in *y* and 80° in *x*. **d,** Sequences of human cullin 1-4 WHB domain are aligned and compared to that of CUL5. The percent of conservation is shown as color-coded bars above the individual residues. CUL5's unique residues Leu710 and Glu717, are highlighted in red with the homologous residues from CUL1-4 in bold. Five Glu mutated to "mimic" neddylation are highlighted blue. **e,** Graphs show the ARIH2-catalyzed transfer of *UB to A3G in 10 min. The assays show the ability of neddylated CRL5 mutants to activate ARIH2 and compare it to NEDD8–CUL5 WT and unneddylated CRL5[Vif-CBFβ]. N = 2 independent technical replicates. **f,** Cryo-EM structure of the CUL5 CTD (WHB, C/R and 4HB, the N-terminal β-sheet of RBX2 and the covalently linked NEDD8. **g,** Interfaces between the WHB domain and NEDD8 are formed between two complexes

of NEDD8–CUL5 CTD-RBX1. These contacts correspond to the same interactions made in the cryo-EM structure. The dotted line separates the two NEDD8–CUL5[CTD]-RBX1 complexes from the crystal lattice. **h,** Close-up of the Ile36 and Ile44 (shown as spheres) positions in NEDD8 (yellow) when bound to H29-helix of the CUL5 WHB domain (dark green). **i,** Close-up of the Ile36 and Ile44 (shown as spheres) positions in NEDD8 (yellow) when bound to H29-helix of the CUL1 WHB domain (dark green, PDB ID: 7B5N). The contacts made by CUL1 are conserved across CULs1-4. **j,** Structure of CUL5-RBX2 (PDB ID: 6V9I[254]) is shown in cartoon. The density for NEDD8 from the cryo-EM structure was superpositioned onto the place it would assume when linked to the WHB (dark green). The superposition highlights the fact that the WHB domain has to be displaced.

Ultimately, the H29-helix is repositioned through a 3-way junction involving NEDD8's Lys6 and His68, CUL5's WHB and C/R domain. Residues Leu710 on the H29-helix and Glu617, Leu621 and Glu624 of the C/R domain stabilize the newly formed NEDD8–H29-helix assembly (Fig. 17c). The cullin-specific NEDD8 configurations are rationalized by the sequences of their respective WHB domains (Fig. 17d). Leu710 and Glu717 are specific for CUL5 and make unique contacts with NEDD8's Ile44 patch. Both residues fit into pockets formed by His68, Val70 and Leu73 but would conflict with NEDD8 in the CUL1-bound conformation. Likewise, the CUL5-bound conformation of NEDD8 would not be able to accommodate the corresponding Asp and Ala residues conserved in cullins 1-4 (Fig. 17d). Indeed, homolog swap mutations of Leu710 and Glu717, as well as mutations of residues at the 3-way-junction between the C/R, H29-helix and NEDD8 greatly reduced the amount of ubiquitylated A3G (Fig. 17e). Meanwhile, as a control for proper folding, none of the mutations impaired CUL5 neddylation (Fig. 18).
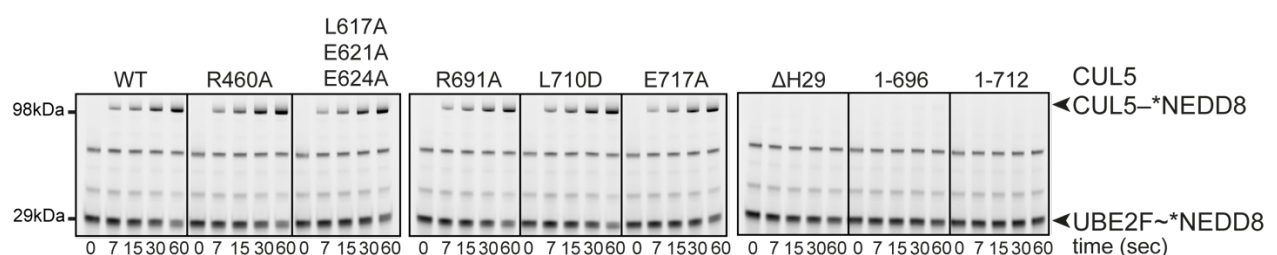
Fig. 18 Neddylation of CUL5 variants to test folding

SDS-gels of pulse-chase assays with fluorescent *NEDD8. All CUL5-RBX2 constructs were tested for proper folding by neddylation. Details of the reaction can be found in the Methods section. CUL5 ΔH29 lacks residues 693-725, the 1-696 truncation terminates at residue 696 and lacks residues 697-780, and 1-713 lacks residues 714-780 - all lack the CUL5 neddylation site (K724).

Interestingly, the same 3-way interface can be found when analyzing the crystallographic data of NEDD8–CUL5 C-terminal region with RBX1. However, these

interactions do not occur within a single complex, but are formed between two neighboring molecules of neddylated CRL5 in the lattice[132] (Fig. 17f-g).

As mentioned above, CUL1's WHB domain binds NEDD8' Ile36 patch, so that the Il44 hydrophobic patch is exposed and can directly recruit the UB-carrying enzyme ARIH1[90,199]. Conversely, CUL5-RBX2 distinctly employs NEDD8's Ile44 hydrophobic patch to mediate large-scale structural remodeling of CUL5. Superimposing the WHB domains of unneddylated[132,253] and neddylated CUL5-RBX2 shows that if CUL5's helix-29 and WHB domain were positioned as when unneddylated, NEDD8 would clash with CUL5's C/R domain, and with RBX2's RING domain (Fig. 17j). This may explain how after the neddylation reaction, NEDD8 would prevent these domains from accessing their orientations in the unneddylated complex, and thereby presumably promote their mobility.

CUL5-RBX2-ARIH2 interactions 1: the E3-E3act superdomain

Previous studies confirmed the notion that ARIH1 and ARIH2 require their specific neddylated CRL to be activated and rely on the specific CUL1-RBX1 or CUL5-RBX2 pairing. A closer look reveals the reason behind their specificity: Domains from CUL5/CUL1 and RBX2/RBX1 engage the ARIH2/ARIH1 Ariadne domain and fulfill similar functions (Fig. 19a-b).
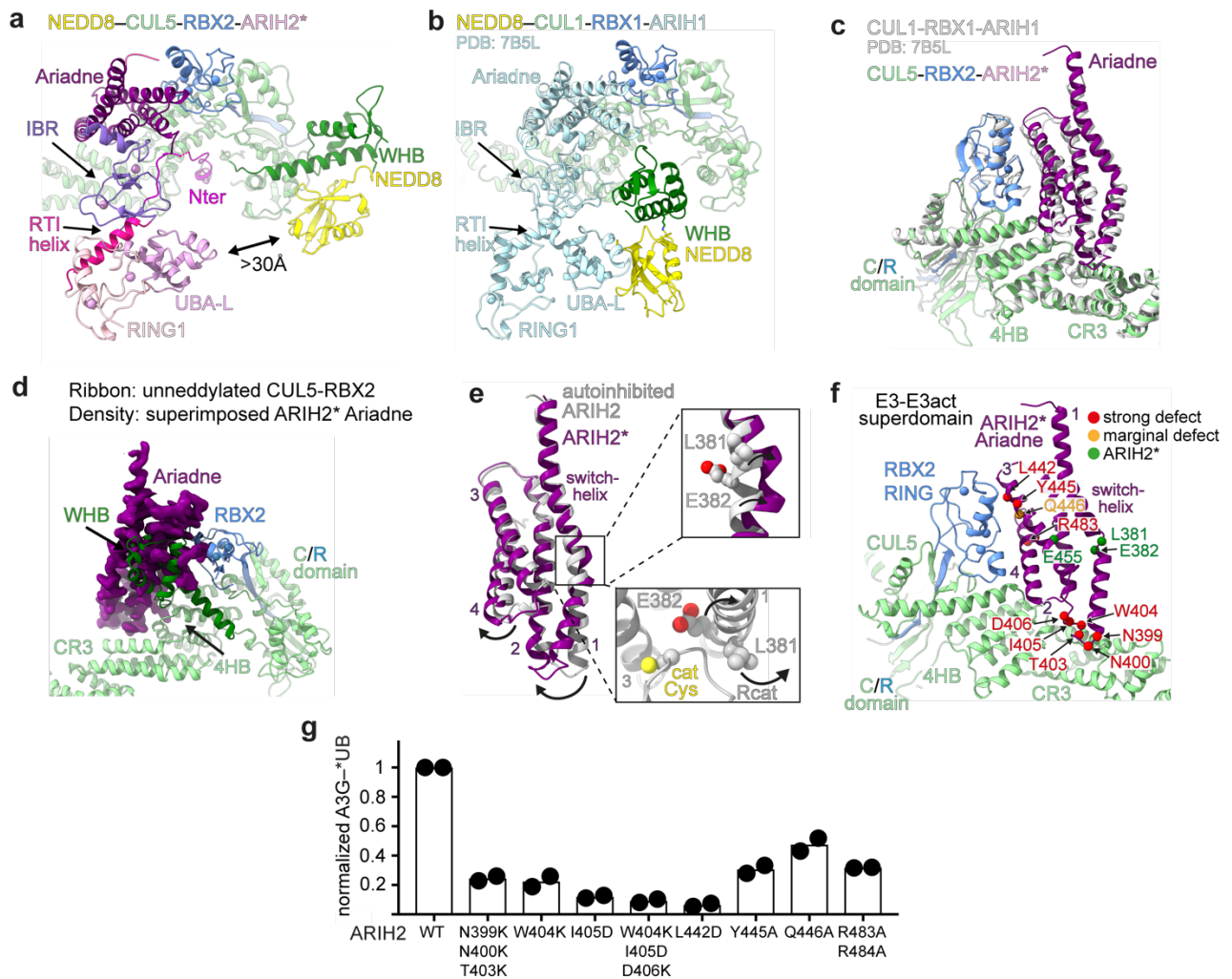
Fig. 19. The NEDD8–CUL5-RBX2–ARIH2* E3-E3act superassembly

a, Top view of the NEDD8–CUL5 (CTD) RBX2-ARIH2* E3-E3act superdomain highlights the 30 Å distance (black arrow) between the UBA-L (orchid) and NEDD8 (yellow). ARIH2* is colored as in Fig. 6a, CUL5 WHB in dark green, the rest in light green. RBX2 in blue. **b,** Same view as in **a.** of NEDD8–CRL1-ARIH1 (PDB ID: 7B5L[90]). ARIH1 UBA-L domain and NEDD8 form close contacts. **c,** Superposition of the NEDD8–CRL1-ARIH1 (light gray, PDB ID: 7B5L[90]).and NEDD8–CRL5-ARIH2* (colored) E3-E3act superdomains. **d,** Structure of CUL5-RBX2 (PDB ID: 6V9I[254]) is shown in cartoon. The density for the ARIH2* Ariadne domain from the cryo-EM structure was superpositioned onto the place it would assume when forming part of the E3-E3act superdomain. Again, the superposition highlights the fact that the WHB domain has to be displaced. **e,** The ARIH2 Ariadne domain undergoes a structural transition from the autoinhibited conformation in crystal structure (white) to the NEDD8–CRL5 bound state (purple). Residues of the switch helix, which secure the Rcat and the catalytic cysteine (yellow spheres), rotate outward and relieve autoinhibition. **f,** Residues along the ARIH2* Ariadne-RBX2-CR3 interfaces were mutated into alanines and charged residues trying the disrupt the interaction. Mutations showing strong or marginal defects are shown in red and orange spheres, respectively. Residues relieving autoinhibition are shown in green spheres. **g,** The ubiquitylation of A3G substrate is monitored by *UB-transfer. The effect of the mutations from **f** in their ability to transfer *UB to A3G in 10 min are shown in the graphs $N = 2$ independent technical replicates.

CUL5's CR3 and 4HB domains and RBX2's RING domain assemble with ARIH2's Ariadne domain into a singular E3-E3act superdomain which superimposes with 1.1 Å r.m.s.d. to that of NEDD8–CUL1-RBX1-ARIH1 (Fig. 19c). The E3-E3act superdomain

was named for its roles in amalgamating two E3s - neddylated CUL1-RBX1-based E3s and the ARIH1 E3 - and in activating ubiquitylation[90].

Formation of the neddylated CRL5-ARIH2 E3-E3act superdomain requires conformational changes in both E3s. Superimposing the Ariadne domain of E3-E3 superdomain with ARIH2 over the C/R domain of unneddylated CUL5-RBX2[253] shows that CUL5's WHB domain must be displaced to expose the ARIH2 binding site (Fig. 19d).

The Ariadne domain itself has to undergo slight changes to fit against the RING domain of RBX2 and CR3 domain of CUL5.Comparing the autoinhibited and activated form of ARIH2 revealed a ~15° bend of the Ariadne helix 1 which we termed "switch helix" when bound to neddylated CUL5-RBX2 (Fig. 19e). Located directly at the center of the bend, residues Leu380 and Glu381 (alanines in ARIH2* used for the cryo-EM structure) are rotated outwards relative to the autoinhibited conformation. In this kinked conformation, these residues cannot keep ARIH2 autoinhibited and elicits ligase activity. This rationalizes the lack of density which could be attributed to ARIH2's Rcat domain, as it is presumably flexible. Preventing the binding of ARIH2 Ariadne domain to CUL5 and RBX2 by mutating key residues inhibits substrate ubiquitylation and highlights the significance of the E3-E3 superassembly (Fig. 19f-g). Residues located at helices facing RBX2 RING domain as well as the CR3 and 4HB domain of CUL5 form hydrophobic and polar interactions, holding the Ariadne domain in place. Especially, mutating Phe404 on CUL5 and resiudes Ile405 and Leu442 on ARIH2 into polar residues lead to a drastic loss of activity.

CUL5-RBX2-ARIH2 interactions 2: ARIH2 N-terminus binds remodeled CUL5 groove

The NEDD8-induced repositioning of CUL5's WHB domain occurs concomitantly with restructuring of its loop connection to the C/R domain. This loop spans residues 691-694 and forms the so-called "gate/groove-loop" (Fig. 20a). Notably, the location of the gate/groove loop is remote from NEDD8. Nonetheless, in the absence of neddylation, the loop structure gates access to CUL5, while upon CUL5 neddylation, the remodeled loop contributes to one side of a groove cradling part of ARIH2's N-terminal region. The other side as well as the backside of the groove is comprised by helices from CUL5's 4HB domain (Fig. 20b).

66
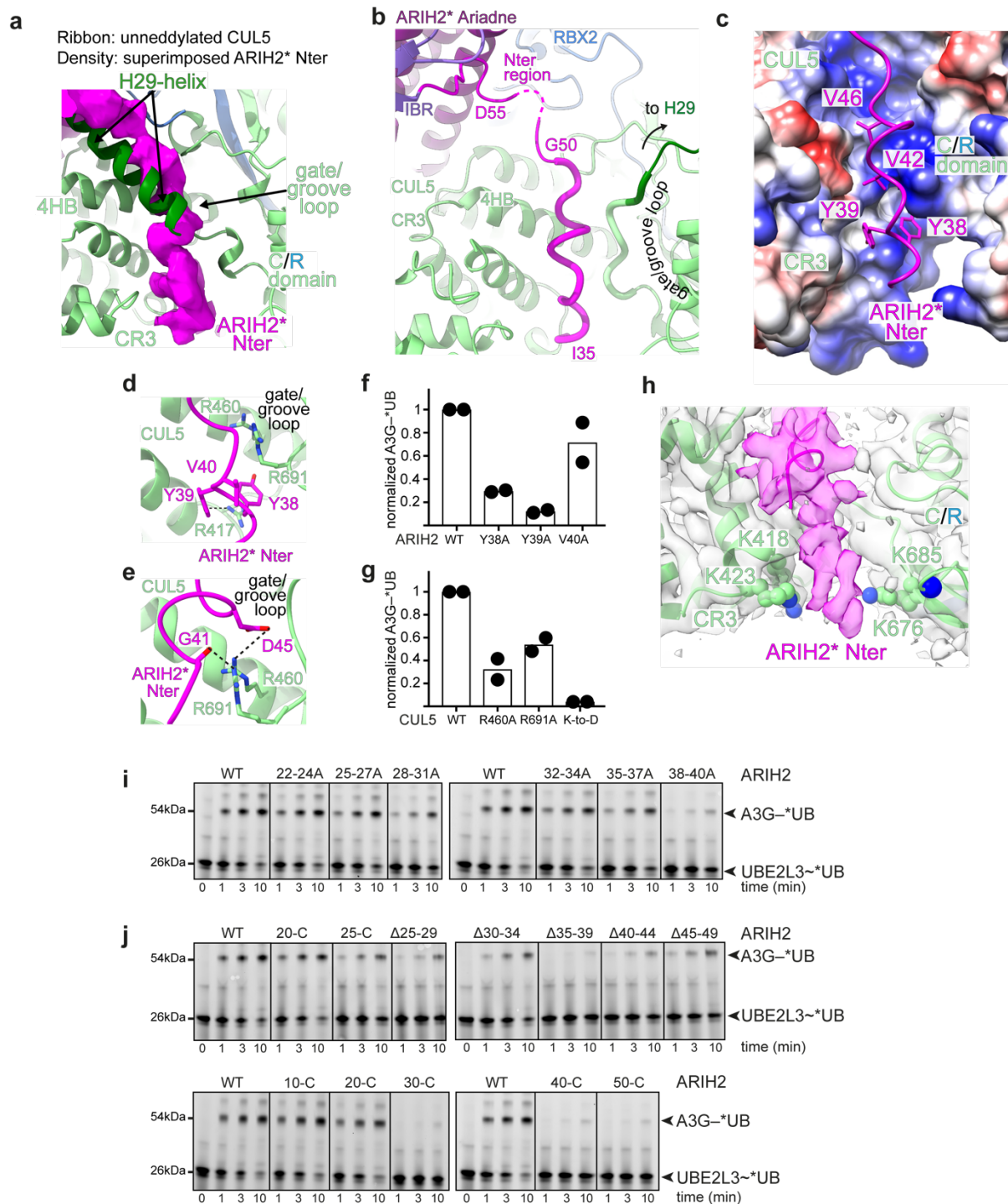
Fig. 20. Neddylation induced exposure of ARIH2 binding surfaces on CUL5

a, Structure of CUL5-RBX2 (PDB ID: 6V9I[254]) is shown in cartoon. The density for the ARIH2* Nter from the cryo-EM structure was superpositioned onto the place it would assume when forming part of the E3-E3act superdomain. Again, the superposition highlights the fact that the WHB domain has to be displaced to form a new binding surface for ARIH2. **b,** ARIH2* N-terminus (magenta) winds along the 4HB and forms novel contacts with the newly formed gate/groove loop of neddylated CUL5 (green). Reorientation of CUL5's H29-helix enables residues 691-695 of CUL5 to contribute to the groove binding of ARIH2*'s N-terminal region. Locations of ARIH2* residues I35 and G50 at the two ends of the CUL5 groove, and D55 approaching the ARIH2* Ariadne domain are indicated. **c,** Surface representation of the CUL5 cryo-EM structure, which forms interactions with the ARIH2* Nter colored by electrostatic potential (positive areas are colored blue, red negative, and white uncharged). The N-terminus is shown in magenta. Hydrophobic residues of the N-terminus fit into hydrophobic pockets formed by the CUL5

67

surface. **d,** Close-up of the key YYV motif (Phe38, Phe39, Val40) forming contacts with Arg460 and Arg691 of CUL5 4HB and C/R domain (light green). **e,** Close-up of Arg460 and Arg691 making further interactions with residues further along the N-terminus. **f,** Graphs showing the amount of ARIH2-catalyzed A3G~UB*. The activity of ARIH2 WT with NEDD8–CRL5$^{Vif-CBF\beta}$ is compared to indicated ARIH2 N-terminal mutations of Results were normalized to activity of ARIH2 WT with neddylated CRL5$^{Vif-CBF\beta}$. N = 2 independent technical replicates. **g,** Graphs show the NEDD8–CRL5$^{Vif-CBF\beta}$-dependent *UB transfer to A3G in 10 minutes. The activity of CUL5 WT with ARIH2 WT is compared to indicated CUL5 mutants. Results were normalized to values with WT CUL5. K-to-D comprises K685D, K676D, K423D and K418D. N = 2 independent technical replicates. **h,** Close-up of the ARIH2* N-terminus (Nter, magenta) fit into the cryo-EM density. At low contour, more of density for the N-terminus wich presumably corresponds to the acidic stretch (residues 22-34) is visible but not modeled. The novel CUL5 groove is lined by four basic residues (K418, K423, K676 and K685). The exact orientation of their side-chains was not visible but they are presumably poised to guide ARIH2's N-terminal acidic stretch. **i-j,** SDS-gels of *UB transfer from UBE2L3 to A3G testing the activity of different ARIH2 alanine mutants over the indicated time. The residues substituted with alanines are indicated by their residue number. N = 2 independent technical replicates.

ARIH2's N-terminal region is predicted to be disordered and its removal was required for crystallization of autoinhibited ARIH2. However, the N-terminus becomes mostly visible upon complex formation with neddylated CRL5 and forms three structurally-distinct regions that mediate interactions with the newly structurally-remodeled CUL5 (Fig. 13b). Residues 47-55 form a taught linker to the canonical RBR elements, whereas residues further along the N-terminus intercalate into the new basic groove.

The central residues 33-46 form a kinked amphipathic helix with the hydrophobic residues Ile35, Tyr38, Tyr39, Val42 and Val46 inserting their side-chains into hydrophobic holes in CUL5 between helices of the 4HB domain (Fig. 20c). The tyrosines mediate aromatic stacking and polar interactions across the groove. In particular, ARIH2's Tyr39 is surrounded by CUL5's 4HB domain Arg417, Arg460 and Arg691 from the newly formed CUL5 gate/groove-loop (Fig. 20d). ARIH2's N-terminus winds horizontally along the 4HB domain until it makes an almost 90° turn and follows the newly formed basic canyon and gate/groove loop of the C/R domain. The positive charges of Arg460 and Arg691 tether the flexible N-terminus into place through electrostatic interactions contacts with from ARIH2*'s Gly41 and Asp45 backbone carbonyl groups (Fig. 20e). Mutating either Arg460 or Arg691 substantially reduces the ability to transfer UB to the A3G substrate (Fig. 20f-g).

On the opposite side of CUL5, between the 4HB and the C/R domain, four lysines (Lys418, Lys423, Lys676, and Lys685) line the edges of the basic groove and form something remotely similar to a gate. Residues N-terminal of the ARIH2 helix also appear to bind in the groove. Limited density, visible only at low contour but above the

noise, fills the remainder of the groove, which is lined by polar residues (Fig. 20h). Interestingly, the ARIH2 residues presumably corresponding to this density (residues 22-31) are entirely acidic, which could enable sampling multiple conformations even in a complex[256,257,258] (Fig. 20h).

The importance of Tyr38 and Tyr39 came to light when examined the roles of ARIH2 N-terminal residues in binding CUL5 and activating ARIH2. Therefore, we substituted 3-4 residues at a time with alanines and tested their activities in a pulse-chase format. These two residues came to our immediate attention when residues 38-40 where replaced with Ala (Fig. 20i). We also tested effects of deletions (Fig. 20j). Residues 1-20 where not observed in cryo-EM and deleting them did not overtly impair ubiquitylation. Unlike the first 20 amino acids, the next 10 residues consisted of aspartates and glutamates, which, when deleted, greatly reduced the amount of neddylated CRL5 substrate ubiquitylation. This would be consistent with the notion that the negative charges bind a part of the basic groove and removing a certain number of charged residues impairs its ability to bind to NEDD8–CRL5.

Neddylation repositions WHB and removes barriers blocking the access of ARIH2
Taken together, the data suggest that different ARIH-family RBR E3s "read" NEDD8 modification of their cullin partners in distinct ways (Fig. 17h-i, Fig. 19a-b). One the one hand, NEDD8's interactions with CUL1 template its Ile44 patch to directly bind and activate partner ubiquitin-carrying enzymes including ARIH1[90,259]. But with NEDD8's Ile44 patch bound to CUL5, how then does it promote ARIH2 binding and ubiquitylation? In the absence of neddylation, CUL5's WHB domain cloaks its 4HB and RBX2's RING domains, thereby blocking binding of ARIH2's Ariadne domain and preventing formation of the E3-E3act domain (Fig. 19d). Also, when unneddylated, CUL5's H29-helix and its preceding loop would gate the groove binding to ARIH2's N-terminal region.

The ultimate test of the importance of NEDD8-mediated barrier removal would be to achieve the same kind of activation through mutations. Thus, two questions remained: would the removal of the WHB domain alone be enough for activating ARIH2-dependent ubiquitylation or do we need to keep the H29-helix as it forms part of the

gate/groove-loop? And secondly, which residues are keeping the unneddylated WHB in a closed position?
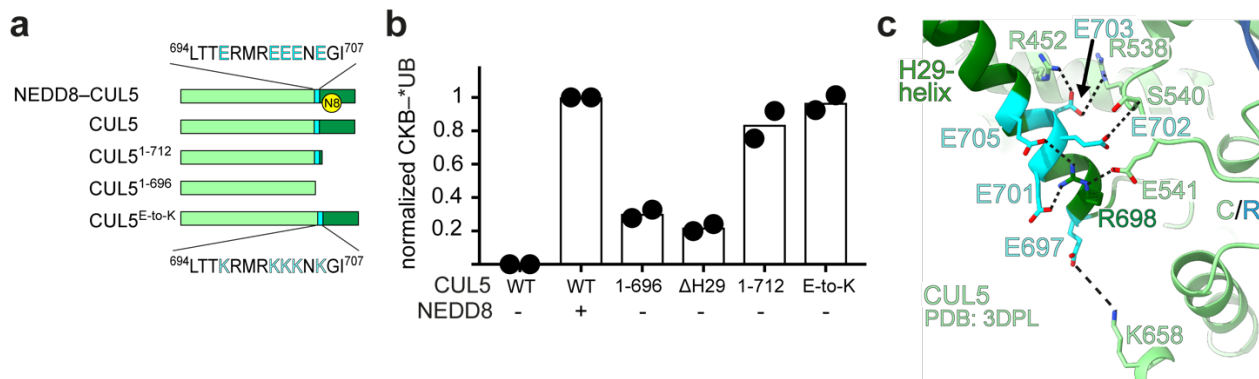
Fig. 21. CUL5 WHB is held in place by negative charges
a, Different CUL5 constructs were used to test the role of the gate/groove loop and the H29-helix in binding the ARIH2 Nter. Additionally, five Glu (cyan) on the H29-helix (dark green) were found to secure the WHB (dark green) to the C/R and 4HB domain. **b,** Graphs show the ARIH2-catalized transfer of *UB to CKB in 10 min. The assays show the ability of CRL5 truncations and mutants to activate ARIH2 and compare it to NEDD8–CUL5 WT and unneddylated CRL5^Vif-CBFβ. N = 2 independent technical replicates. **c,** Structure of unneddylated CUL5 (PDB ID: 3DPL[132]) with the five H29-helix Glu (cyan) forming an extended interaction network with the C/R and 4HB domain holding the WHB (dark green) in place.

Indeed, keeping only part the "gate-groove loop" preserved and deleting the rest of the WHB (CUL5$^{1-696}$) is sufficient to show some level of CKB ubiquitylation compared to the complete absence of activity with unneddylated CRL5^{ASB9} (Fig. 21a-c). Extending the construct so that it contains part of the H29-helix (CUL5$^{1-696}$) lead to a drastic increase of activity, almost to the level of neddylated WT CUL5 (Fig. 21a-c). To answer the next question, we took a closer look at the structure of unneddylated CUL5 to identify candidate residues that keep the anchored but which would not impact the neo CUL5 groove formed upon neddylation. A set of candidate glutamates (701, 702, 703, and 705) mediate electrostatic interactions positioning the H29-helix in the unneddylated CUL5-RBX2 structure, but are solvent exposed in the neddylated CRL5 assembly with ARIH2. Indeed, replacing this collection of glutamates with lysines enabled unneddylated CRL5^{ASB9} and ARIH2 to ubiquitylate CKB at a level approaching activation achieved by neddylation (Fig. 21b-c).

DISCUSSION

Viruses have evolved the ability to subvert multiple cellular processes to fit their own needs, starting from hijacking the replication and translation machinery to preventing immune responses. To thwart host defence mechanisms, they specifically target antiviral restriction factors for degradaton via the UPS, paving the way for unhindered multiplication. While viral proteins do not directly ubiquitylate substrates, they act more as adapter molecules, sequestering the substrate and recruiting it to an host E3 ligase. Prominent examples are proteins from the Epstein Barr virus[260], human Adenovirus [261] and the HIV-1[2]. HIV-1 Vif is of special intrest to us as it evidently ursurps the CRL5-ARIH2 system, binding members of the APOBEC family and targeting them for degradation through ubiquitylation. Additionally, Vif recruits the transcriptional regulator CBFβ thereby influencing the transcription of interleukin 3 and the maturation of lymphocytes[262,263].

Studies have shown that CUL5-RBX2 alone is not sufficient to increase the HIV-1 infectivity in lymphocytes[1]. Another E3 ligase is required to form a functioning unit and target members of the APOBEC deaminase family for degradation. Neddylated CUL5-RBX relies on the RBR ligase ARIH2 to form an interdependent assembly in order to ubiquitylate substrates[5] ARIH2 is a 60 kDa RBR E3 ligase with a typical RING-IBR-RING domain organization and is closely related to ARIH1 which is already known to work together with the CRL1 system. Although these two RBR ligases share 35% overall sequence similarity and comprise the same domain organization, ARIH2 is unique to the RBR family. Already in its autoinhibited state, its RING1-IBR are poised in an orientation that facilitates E2~UB binding and the subsequent transfer of the UB to the Rcat. Conversely, ARIH1 has to bind NEDD8 via its UBA-L domain in order for its domains to be accurately[5] aligned for transferring ubiquitin to the catalytic cysteine.

Historically, the first evidence for an RBR and a cullin being assembled into a multiprotein ubiquitin ligase complex came from the sequence of the atypical cullin protein CUL9 (also known as PARC). CUL9 is by far the largest cullin and functions downstream of the 3M complex which inhibits CUL9 to prevent ubiquitylation of Survivin (BIRC5) and is involved in the localization of p53. Sequence-wise, it is closely related to CUL7 but interestingly harbors an additional RBR domain at its N-terminus.

Thus it was suggested and later proven, that the *CUL9* gene originated from a fusion between a *CUL7* gene duplicate and an *Ariadne* gene[264,265].

Ariadne E3 ligase members ARIH1/2 both contain an autoinhibitory Ariadne domain consisting of a 4-helical bundle, which sequesters the Rcat domain and keeps the catalytic cysteine inaccessible (Fig. 4b-c). To prevent aberrant ubiquitylation, most RBRs remain in an autoinhibited state until they are activated by distinct stimuli. E.g. PARKIN is released from autoinhibition by binding pUB and phosphorylation of its UBL domain via PINK1 [20,247]. HOIP becomes activated through interactions between its UBA domain and LUBAC constituents HOIL-1 or SHARPIN[266]. ARIH1 is activated through binding CUL1/2/3 and interactions mediated between its UBA-L domain and NEDD8. Interestingly the E2~UB binding process and the relief of autoinhibition are structurally separated, providing two ways of regulating the RBR activity. RBRs bind E2~UB in an open conformation, thereby restricting the conformational flexibility of UB to prevent non-productive ubiquitylation. The open state favors transthiolation to the catalytic cysteine ensuring that the RBR determines the type of ubiquitylation and chain formation. HOIP specifically targets its substrate for ubiquitylation by placing its Rcat in the vicinity of the N-terminus of an acceptor UB[267]. As a part of the LUBAC complex, HOIP ensures that linear UB chains are formed with high fidelity even when UBE2K associates with the E3 and normally would generate Lys48 chains[246].

The cryo-EM structures of ARIH1 with neddylated CRL1 elucidated the exact mechanisms of each step of the E2-E3 UB-transfer cascade. ARIH1 UBA-RING1-IBR with RING1-bound E2~UB are aligned in such a way that on one side NEDD8 can bind to the UBA domain and ubiquitin is oriented for the nucleophilic attack of the flexible Rcat. Upon binding the CRL1 and formation of the E3-E3act superdomain Rcat is displaced from the Ariadne domain and swings backwards to the RING1-IBR receiving the UB. The Rcat then swings towards the substrate, positioning the N-terminus of UB towards the substrate lysine.

Understanding the basic principles of the ubiquitin transfer mechanism is essential to illuminate how various substrates are targeted for degradation and how this degradation mechanism could be exploited. This led us to examine the role of ARIH2 in ubiquitinating the host restriction factors APOBEC3C and 3G. Solving the structures

of A3G and A3C-bound neddylated CRL5[Vif/CBFβ]-ARIH2 complexes revealed how the HIV-1 hijacked E3-E3 ligase assembly subdues host immune responses. This structure defined the molecular basis for selective E3-E3 interactions between different members of neddylated CRL E3s and ARIH-family RBR E3s. We elucidated an unexpected mechanism by which a "reader" recognizes its ubiquitin-like protein modified target: rather than the UBL (or UB) directly recruiting the reader, here NEDD8 induces a conformational change in CUL5-RBX2, and it is the restructured conformation that rather than the UBL itself that is directly recognized by ARIH2 (Fig. 22).
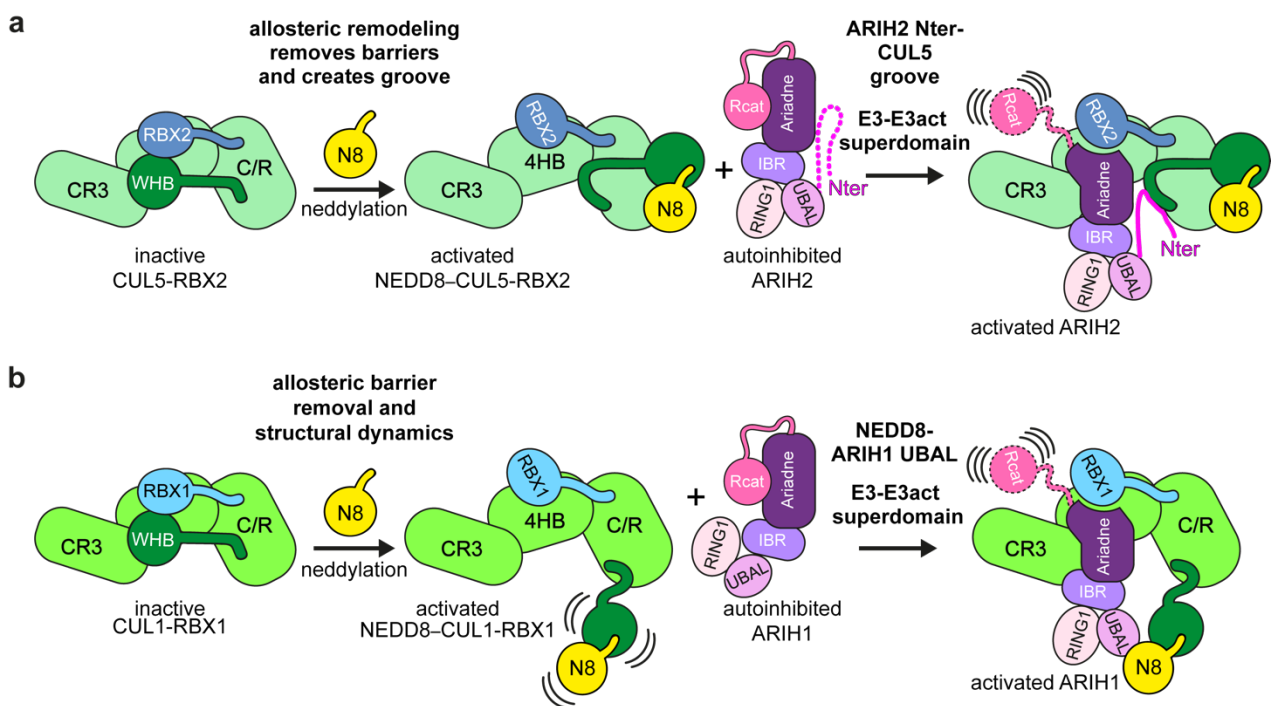
Fig. 22. Model of cullin-specific NEDD8-driven CRL remodeling and E3-E3act superassembly formation
a, NEDD8 forms no direct contacts with ARIH2, driving the assembly of the E3-E3act superdomain between CRL5 and ARIH2 entirely indirectly, via an allosteric mechanism. Barriers blocking ARIH2 binding are removed and novel binding site are created by neddylation. **b,** Conversely, ARIH1 is directly activated by NEDD8. The most prominent differences between the NEDD8–CRL1-ARIH1 and NEDD8–CRL5-ARIH2 assemblies is the position of the WHB relative to the RBR ligase.

The mechanistic details reveal fundamental rules by which UBL-mediated allostery drives binding to a reader. NEDD8-induced structural remodeling enables formation of the CRL5-ARIH2 E3-E3 super-assembly E3 in two broad ways. First, the neddylated conformation has removed the barriers that conceal cryptic ARIH2 binding sites in an unneddylated CRL5. Specifically, the 110° rotation of CUL5's WHB domain exposes CUL5's 4HB and C/R domains and a new groove is formed that together provide
73

surfaces recognizing ARIH2's distinctive N-terminal region and C-terminal Ariadne domains. Thus, UBL-linkage stimulates recognition of the modified target both by removing barricades that prevent reader binding to the unmodified protein, and by allosteric creation of new surfaces not present in the unmodified protein. Notably, ARIH2 and ARIH1 both display tandem reader motifs, and the Ariadne domain interaction similar between them depends on NEDD8-dependent allosteric restructuring of both CUL5 and CUL1 (Fig. 12a-b). However, this allosteric regulation of CUL1 depends on its linked NEDD8 directly recruiting ARIH1, a mechanism conceptually paralleling readers of other UB and UBL modfications[90].

To our knowledge, reader recognition of a UBL (or UB)-driven conformational change - without direct interaction with the UB or UBL itself - has not been structurally characterized so far. What has been shown, are UB- and SUMO-induced conformational changes that inhibit, rather than promote, interactions. For example, SUMOylation of thymine DNA glycosylase (TDG) results in conformational changes that are incompatible with binding to DNA. SUMO binding to a SUMO-interacting motif (SIM) within TDG mediates conversion from the DNA-binding conformation that catalyzes base excision to one that masks the DNA binding site[268,269]. Similarily, the yeast transcription factor Met4 displays tandem UB-binding domains. When a K48-linked polyUB chain is ligated to Met4 as part of a nutrient feedback repression cascade, intramolecular engagement of the covalently-linked UBs prevents transcriptional activation of genes inducing production of sulfur-containing metabolites[270].

CRL5's modular organization in common with other CRLs, the ≈40% sequence identity between CUL5 and CUL1 WHB domains, their orthologous NEDD8 modification sites, ≈35% sequence identity between their ARIH2 and ARIH1 readers, and the same overall outcome of neddylated CRL-ARIH E3-E3 super-assembly raise the question of why NEDD8 modulates CUL5-RBX2 in its own unique way and not like it does with CUL1-RBX1. The sequence identity between ARIH2 and ARIH1 answers only the question of specificity for their CRL partner. The question of why the WHB has to rotated for 110° for CUL5 but not for CUL1 where a minor rotation is sufficient to accommodate the N-terminus still remains unanswered. Although, further studies are required to give a satifying answer, we can for the moment only speculate that

additional regulation mechanisms have co-evolved when CRL5 first emerged in metazoans[240,250].

Allosteric differences may prove useful in therapeutic targeting of specific members within families of proteins in PTM cascades. Indeed, recent studies probing conformational dynamics of a kinase, itself activated by phosphorylation, demonstrated that potential to transiently occupy distinct active and inactive conformational states not only determines physiological function, but also is exploited by chemotherapeutic drugs[271]. Our structural and mutational analyses revealing unique allosteric switches may indicate opportunities for uniquely targeting distinct neddylated CRL-ARIH E3-E3 super-assemblies. As CRL5 and ARIH2 are both involved in regulating immune response pathways this may particularly relevant for further drug developments[226,272].

MATERIALS AND METHODS

Materials

Plasmids

Table 1. List of plasmids that served as templates for site-directed mutagenesis and protein expression

Vector	Insert	Tag+cleavage site	Antibiotic
pRSF	ARIH2 WT	6xHis-MBP-TEV	Kan
pRSF	ARIH2 51-C	6xHis-MBP-TEV	Kan
pRSF	ARIH2 mutants	6xHis-MBP-TEV	Kan
pRSF	Vif (MCS1) Cbfb (MCS2)	6xHis (on Vif)-TEV	Kan
pET3a	ASB9	6xHis-TEV	Amp
pET duet	APPBP1-UBA3	6xHis (on UBA3)	Amp
pACYCDuet-1	ELOB (MCS1) ELOC (MCS2)	none	Cam
pGEX 4T1	Ubiquitin	GST-3C	Amp
pGEX 4T1	Creatine Kinase B	GST-TEV	Amp
pGEX 4T1	UBE2L3	GST-TEV	Amp
pGEX 4T1	UBE2M	GST-TEV	Amp
pGEX 4T1	UBE2F	GST-TEV	Amp
pGEX 4T1	NEDD8	GST-Thrombin	Amp
pLib	CUL5	none	Amp
pLib	RBX1	GST-TEV	Amp
pLib	RBX2	GST-TEV	Amp
pLib	APOBEC3G	GST-TEV	Amp
pLib	APOBEC3C	GST-TEV	Amp
pFastBac	UBA1	GST-TEV	Amp

Abbrev.: Kan-Kanamycin, Amp-Ampicillin, Cam-Chloramphenicol

Buffers

Protein purification Buffers

His Lysis Buffer
50 mM Tris pH 8.0
200 mM NaCL
5 mM β-ME
2.5 mM PMSF

His Buffer A
50 mM Tris pH 8.0
200 mM NaCL
5 mM β-ME

His Buffer B	50 mM Tris pH 8.0
	200 mM NaCL
	5 mM β-ME
	300 mM Imidazole pH 8.0
GST Lysis Buffer	50 mM Tris pH 8.0
	200 mM NaCL
	1 mM DTT
	2.5 mM PMSF
GST Buffer A	50 mM Tris pH 8.0
	200 mM NaCL
	1 mM DTT
GST Buffer B	50 mM Tris pH 8.0
	200 mM NaCL
	1 mM DTT
	20 mM red. Glutathione
Ion exchange Buffer A	50 mM Tris pH 8.0
	5 mM DTT
Ion exchange Buffer B	50 mM Tris pH 8.0
	5 mM DTT
	1 M NaCL
SEC Buffer	25 mM HEPES pH 7.5
	150 mM NaCL
	1 mM DTT
Cryo-EM SEC Buffer	25 mM HEPES pH 7.5
	100 mM NaCL
	1 mM TCEP

Pulse-chase Buffers

10x pulse Buffer	500 mM HEPES 7.5
	25 mM MgCL2

77

	15 mM ATP pH 7.5
	1 M NaCL
1x Dilution Buffer	25 mM HEPES 7.5
	100 mM NaCL
Quench Buffer	50 mM HEPES 7.5
	50 mM NaCL
	5 U Apyrase
10x Chase Buffer	250 mM HEPES 7.5
	1 M NaCL
Neddylation buffer	25 mM HEPES pH 7.5
	150 mM NaCl
	10 mM MgCl2
	1 mM ATP
Dilution buffer	25 mM HEPES pH 7.5
	100 mM NaCl
Ubiquitylation buffer	25 mM HEPES pH 7.5
	100 mM NaCl
	2.5 mM $MgCl_2$
	1 mM ATP

Buffer for DNA transformation and Protein expression

Luria Broth (LB)	1 % (w/v) Peptone
	0.5 % (w/v) Yeast extract
	0.5 % (w/v) NaCl
SOCS	2 % (w/v) Peptone
	0.5 % (w/v) Yeast extract
	0.5 % (w/v) NaCl
	20 mM Glucose
	10 mM $MgSO_4$
	10 mM NaCl
	2.5 mM KCl
Terific Broth (TB)	2 % (w/v) Trypton

78

2.4 % (w/v) Yeast extract
0.4% (v/v) Glycerol
17 mM KH_2PO_4
72 mM K_2HPO_4

Cell lines

Table 2. List of bacterial and insect cell strains used for plasmid generation and protein expression

Name of strain	Organism	Manufacturer
Bacterial strains		
BL21 Rosetta (DE3)	E. coli	Novagen
BL21-Gold (DE3)	E. coli	Aligent
DH5α	E. coli	Thermo Fisher
DH10 EMbacY	E. coli	Geneva
Insect cells		
High Five (BTI-TN-5B1-4)	Trichoplusia ni	Thermo Fisher

Software

Table 3. List of all software used for this thesis

Software	License holder/Reference
Cloning	
SnapGene	Insightful Science
Assay analysis	
Graph Pad Prism v8.4.1 and v8.3	GraphPad Software
Microsoft Excel v16.16.25	Microsoft Corp.
ImageQuant TL v8.2.0.0	Cytiva Lifesciences
Cryo-EM	
RELION 3.1	Ref.[273]
Gautomatch v.056	K. Zhang, MRC Laboratory of Molecular Biology
Gctf v1.06	Ref.[274]
MotionCorr2 v1.2.6	Ref.[275]
Structure visualization	
Chimera v1.14	Ref.[276]
ChimeraX 1.0	Ref.[277]

PyMol 1.5.0.4	The PyMOL Molecular Graphics System, Version 2.0 Schrödinger, LLC

Model Building	
COOT 0.8.9.2	Ref.[278]
Phenix.refine 1.18.	Ref.[279]
SHELXC/D/E	Ref.[280]
DECA	github.com/komiveslab/DECA
DeepEMhancer	Ref.[281]
XDS	Ref.[282]

Methods

Cloning

The DNA templates for cloning into expression vectors were either obtained from the in-house DNA library, synthesized (Twist Biosciences) or from members of our lab. All proteins except HIV-1 Vif contain the human coding sequence.

ARIH2

For crystallographic studies, the N-terminal 50 residues of the autoinhibited form were removed. These residues were deemed disordered by sequence analysis using PONDR. Full-length ARIH2 was used for biochemical assays and cryo-EM studies. For assembling the cryo-EM complex, three residues (L381, E382 and E455) were mutated to alanines via site-directed mutagenesis using the Quikchange system (Agilent). All other residue-substitution mutants were generated using the same protocol. Mutations of ARIH2, where parts of the sequence are deleted are indicated by "Δ". The excluded residues are indicated by their position numbers.

The full-length ARIH2 and its N-terminal deletion versions were cloned into a pRSF vector using the Gibson assembly protocol[283]. They harbor an N-terminal His$_6$-tag for Ni-affinity purification followed by a Maltose-binding protein (MBP) tag for increasing the solubility and a TEV protease cleavage site.

CUL5-RBX2, UBA1, APOBEC's

CUL5 was cloned without a tag into a pLib vector. RBX2, RBX1, APOBEC3C and 3G were cloned into the same vector comprising an N-terminal glutathione S-transferase

80

(GST) tag followed by a TEV site. *Trichoplusia ni* High-Five insect cells were used to express all constructs. The same Quikchange system was used for mutations in CUL5.

Viral infectivity factor (Vif) and CBFβ

The GeneArt software (ThermoFisher) was used to codon-optimize the DNA template for HIV-1 Vif (UniProt: P12504) for *E. coli* expression. The construct was ordered from Twist Bioscience and lifted into the Multiple Cloning Site 1 (MCS1) of a pRSF duet vector with an His$_6$-MBP tag and TEV cleavage site with Gibson assembly. Its binding partner CBFβ was cloned into the MCS2 site without an affinity tag.

ElonginB and C

Elongin B (ELOB) and Elongin C (ELOC) were sub-cloned as full-length and untagged constructs into the MCS1 and MCS2 of pACYCDuet-1 (Novagen), respectively.

Additional constructs

UBE2L3, Creatine kinase B, UBE2F were cloned into a pGEX 4T1 vector as N-terminal GST fusions with intervening TEV sites. Full-length ASB9 was cloned into a pET3a vector and contained a N-terminal His$_6$-tag and a TEV site.

After the Gibson assembly (or Quickchange), the DNA was transformed into DH5α, put on ice for 30 min, heat-shocked for 45 sec, addition of LB and put on a 37°C shaker for 1h. Afterwards the constructs were plated onto LB agarose plates with the corresponding antibiotics.

Protein expression

The ARIH2, CKB, UBE2L3 constructs were transformed into *E. coli* (Rosetta, DE3) for expression. Cultures of TB medium were grown am optical density (OD; was measured with the Biophotometer D30 from Eppendorf) of 0.6-0.8. For protein expression, the temperature was lowered to 18°C. 0.1 mM Isopropyl-β-D-thiogalactopyranoside (IPTG, Sigma) was used to induce the protein production. 0.1 mM ZnCl$_2$ (Sigma) were added to assist in the proper folding of the proteins and increase the yield.

CUL1-RBX1, NEDD8–CUL1-RBX1, SKP1-FBXW7 and ARIH1 WT were kindly provided by Kheewong Baek. UBE2M, NEDD8 and APPBP1-UBA3 were kindly provided by Maren Klügel.

Transfections and expressions of proteins in *Trichoplusia ni* High-Five insect cells were performed by Susanne von Gronau from the insect cell facility within our department.

CUL5 and RBX2 were co-expressed via baculoviral co-infection as previously described for CUL1-RBX1[90,199].

The plasmids harboring Vif-CBFβ and ELOBC were co-transformed into *E. coli* (BL21gold, DE) for co-expression. Cultures were grown in TB to OD 0.6-0.8 upon which the temperature was lowered to 18°C. 0.1 mM IPTG was used to induce the protein production. 0.1 mM $ZnCl_2$ (Sigma) were added to assist in the proper folding of the proteins and increase the yield. The ASB9-ELOBC complex was expressed in a similar way.

Protein purification

The ARIH2 constructs were purified in a three-step purification. First by nickel-affinity chromatography. The cell pellet was resuspended in His Buffer A and sonicated. After centrifugation, the lysate was incubated with HisPur™ Ni-NTA Resin (Thermo Fisher) for at least 1h. The same buffer was used for washing the resin. The protein was eluted with His Buffer B and elution fractions were run by SDS-PAGE to check for protein. The His-MBP tag was removed by adding 1:100 TEV protease to the elution fractions and dialyzing overnight at 4°C to get rid of the imidazole. The next day, a HiTrap Q HP column (Cytiva Life Sciences) was used during the anion exchange chromatography step to remove the remaining impurities. The final step was separation by size to get rid of residual contamination by size-exclusion chromatography (Superdex SD 200 (GE Healthcare) and the buffer exchange into SEC buffer.

CUL5-RBX2, UBA1 and CKB were expressed with a N-terminal GST-tag, so they were purified by a GST-pulldown. Their tag was removed with 1:100 TEV protease

over night at 4°C followed by anion exchange chromatography. The proteins were passed over a HiTrap Q HP column, followed by washing with Ion exchange Buffer A and elution with an increasing concentration of Buffer B. The fractions containing the respective protein were concentrated and put onto a sizing column and buffer exchanged into SEC buffer. All CUL5 mutants were purified the same way. Specific CUL5 mutants are the "Δ29-helix" (lacking residues 694-726), the "E-to-K" "(E697K, E701K, E702K, E703K and E705K)"[198] and the "K-to-D" "(K418D K423D K676D K685D)"[198] mutants.

HIV-1 Vif, CBFβ, ELOB, ELOC APOBEC3C and 3G were purified according to an already published protocol[252].

SKP1-FBXW7$_\Delta$D (mutant version which has the dimerization domain deleted), NEDD8–CUL1-RBX1, and ARIH1 were expressed and purified as previously described[6,90,199].

The ASB9-ELOBC complex was purified by nickel-affinity chromatography using the same protocol as described above.

Components for the neddylation reaction comprise the additional proteins UBE2F, UBE2M, NEDD8 and the E1 APPBP1-UBA3. For expression, they were transformed in *E. coli* (either Rosetta, DE3 or BL21 Gold). Except APPBP1-UBA3, all constructs were GST-fusions with either an thrombin or TEV site. APPBP1-UBA3 was tagged with 6xHis. They were expressed and purified according to already established protocols[6,192].

For fluorescently label ubiquitin (*UB), its N-terminal RRASV sequence was replaced with RRACV so that the fluorescein-maleimide label could be attached to the cysteine. The expression strain BL21 pRIL (DE3, *E. coli*) was used. *UB was purified and chemically labeled according to a published protocol[192].

For identification of successful purification, mutagenesis and sample purity, the intact mass of all protein samples was verified by submitting them to the mass spectrometry facility of the Max Planck Institute of Biochemistry.

Neddylation reaction

For biochemical characterization, all CUL5-RBX2 variants (including the WT) were neddylated. The final concentrations of CUL5-RBX2 was 12 µM, 0.2 µM of APPBP1-UBA3, 1 µM of UBE2F and 25 µM of NEDD8. The reaction was started by adding neddylation buffer. The reaction took place at room temperature and was started by adding NEDD8. The optimal duration of the reaction was judged by taking aliquots at 0, 5, 8 and 12 min time points. The large-scale (1 mL) neddylation reactions were quenched typically after 8 min with 10 mM DTT. The neddylated CUL5-RBX2 construct was put onto a Superdex SD200 column to separate it from the reaction components and buffer exchanged into SEC buffer.

Peptide

A peptide of phosphorylated Cyclin E (pCycE, residues 377-400) with the sequence KAMLSEQNRASPLPSGLL(pT)PPQ(pS)GRRASY was used as a substrate for in-vitro ubiquitylation reactions. Synthesis was performed at the Max Planck Institute of Biochemistry Core Facility. High-performance liquid chromatography (HPLC) was employed to accomplish a purity of greater than 95%.

In vitro ubiquitylation assays

The transfer of *UB transfer to the substrate was monitored using a pulse-chase format. The first step of the reaction, the pulse, was started by charging UBE2L3 with *UB, forming a thioester bond between the two. The reaction conditions were chosen to the point where all visible detectable UBE2L3 was converted to thioester-bonded UBE2L3~*UB and were examined by Coomassie-stained SDS-PAGE. The pulse reaction was performed at a final concentration of 15 µM *UB, 15 µM UBE2L3 and 0.3 µM UBA1, in ubiquitylation buffer for 30 minutes at room temperature. Adding a final concentration of 2 U/mL apyrase stopped the reaction. The quenched solution was diluted to a final concentration of 5 µM UBE2L3~*UB with dilution buffer.

For the chase reaction, another reaction setup was made. The E3 Ligases were mixed with their respective adaptor-SR-substrate complex mixed together and incubated on ice for 10 min before the actual chase reaction.

The chase reaction was initiated by adding the pulse reaction-mix to the pre-mixed components resulting in a final concentration of 0.4 µM UBE2L3~*UB. For testing the

84

activities of various CRL5 and ARIH2 mutants, in their abilities to ubiquitylate the substrates (either CKB, A3C or A3G) the following concentrations were used: 0.1 µM ARIH2, 0.4 µM NEDD8–CUL5-RBX2/RBX1, 0.4 µM ELOBC-Vif-CBFβ or ELOBC-ASB9 and 4 µM A3G/C or CKB.

To test autoubiquitylation of ARIH2, the concentration of ARIH2 was increased to 0.4 µM, 0.4 µM NEDD8–CUL5-RBX2 or CRL5 and no substrate was added. For CRL1 pulse-chase assays, pCycE was used as substrate. Reaction conditions are described in ref. [90].

Chase reactions were performed at room temperature. Aliquots were quenched in non-reducing SDS-PAGE sample buffer at the indicated time points. The samples were loaded onto pre-made gradient gels (SERVA*Gel*™ TG PRiME™ 4-12 %) and were run with no reducing reagent present. An Amersham Typhoon imager (GE Healthcare) was used to scan all gels. ImageQuant TL v8.2.0.0 was used to quantify the band intensities of UB* labelled substrates (A3G or CKB). The intensities were normalized to the amount of ubiquitylated substrates generated by WT CUL5 and ARIH2. The obtained raw intensities were processed in Microsoft Excel v16.16.25 graphically visualized in GraphPad Prism v8.4.1 (GraphPad Software). The 10 min timepoint was used to generate all graphs. All reactions were performed as technical duplicates. The identity of *UB, A3G~*UB, CKB~*UB, UBE2L3~*UB, and ARIH2~*UB was determined by staining the SDS PAGE gel with Coomassie after fluorescence scanning. These proteins served as markers of molecular weights 8 kDa, 56 kDa, 54 kDa, 26 kDa, and 66 kDa, respectively.

In vitro neddylation assay

CUL5 WT and variants were neddylated using fluorescently labelled NEDD8 to verify their proper folding. The reaction was set up previously described[192]. The final UBE2F~*NEDD8 concentration in the final reaction set-up was 0.2 µM, and 0.5 µM of all CUL5-RBX2 versions. Reactions were carried out at room temperature in dilution buffer. Aliquots were quenched with non-reducing SDS-PAGE sample buffer at the displayed time-points and run on on SDS-PAGE gels to verify the neddylation status, They were scanned on a Amersham Typhoon imager (GE Healthcare).

Set-up of crystallization condition for ARIH2 truncation

Crystals of the truncated ARIH2 version (residues 51-C) were grown at 4°C at a concentration of 10 mg/ml by the sitting drop vapor diffusion method. Two Phoenix nanodispenser robots from Art Robbins Instruments which are capable of setting hanging drops at the rate of 96 conditions every 2 minutes were used. For mixing individual buffer conditions during the optimization step, a Scorpion robot was used. The final condition consisted of 20% PEG 3350, 0.1 M Bis-Tris propane pH 8.5 and 0.2 M Sodium nitrate and was added in a 1:1 ratio to the sample. The plates were set up at 4°C. Pictures of the individual droplets were taken every 48h by a Imaging Station based on a Leica microscope and a Thermo Scientific cabinet. The crystals took approximately 10 days to grow and had a rod-like shape. 35% ethylene glycol was added to the reservoir solution as cryoprotection. The crystals were fished, dipped into the cryoprotection solution and then flash-frozen in liquid nitrogen.

Data collection at the SLS

The crystals were sent to the Swiss Light Source (SLS, Switzerland). The PXIII beamline at a wavelength of 1.2783 Å was used to collect the diffraction data. A dataset of one full rotation (360°) across one crystal as well as three different translations was collected. XSCALE was used to merge three independent datasets into a single reflection file. For indexing, integrating and scaling of the data XDS[282] was used.

Determining the crystal structure

Using single anomalous diffraction from the zinc atoms bound by the RING1, IBR and Rcat domain, their location and structure was determined with SHELXC/D/E[280]. PHENIX Autosol was used in the next step for phase extension. Buccaneer[284] was used afterwards for chain tracing with the novel map and building the initial model. The resulting structures were repeatedly improved by rounds of manual building and refinement in COOT[278] and PHENIX[279]. Due to higher flexibility and missing densities, N-terminal residues 51-57 and 128-138 could not be modelled. The exact refinement statistics (Clash score, Ramachandran statistics, etc.) of the published structure can be found in Table 4.

Preparation of cryo-EM samples and grids

For the formation of a stable NEDD8–CRL5-ARIH2-A3C/G complexes, 10 μM ARIH2* (L381A E382A E455A), 12 μM Vif-CBFβ-ELOBC, 10 μM neddylated CUL5-RBX2 and 14 μM A3C or A3G were mixed and placed on ice for at least 30 minutes. Afterwards, they were loaded onto a Superose^{TM} 6 Increase size-exclusion chromatography column into cryo-EM SEC buffer. The fractions of the sizing peak (judged by 280 nm absorbance) were subsequently concentrated to 0.5 mg/ml. To reduce surface hydrophobicity, the Quantifoil holey carbon grids (R1.2/1.3 200 mesh) were glow discharged (30 sec at medium intensity). A vitrobot (Mark IV; Thermo Fisher Scientific) was used for plunging the grids. Plunging conditions consisted of a 100 % humidity and 4°C chamber temperature. A sample volume of 3 μL was applied to the grids.

Data collection

For high resolution structural models of the complexes, we collected datasets on a Titan Krios (FEI) electron microscope (K3 detector in counting mode) at 300 kV. We used SerialEM v3.8.0-b5[285] to set up the collection. For the A3C complex, 9,271 images were collected at a pixel size of 0.8512 Å and for A3G, 7,830 images at a pixel size of 1.094 Å. The datasets were recorded at a dosage of 75 to 90 e$^-$/ Å^2 and -0.7 to -2.5 μm defocus. Exact parameters of the data collection and processing can be found in Table 5.

Processing workflow

Micrographs were imported into RELION 3.1[273]. Dose weighing and motion correction was performed with MotionCorr2[275], followed by CTF estimation with Gctf v.1.06[274].

Gautomatch v.056 (K. Zhang, MRC Laboratory of Molecular Biology) was used to pick the initial 5,030,529 particles of A3C-bound neddylated CRL5$^{Vif-CBFβ}$-ARIH2*. 2D and 3D classification helped to separate promising high-resolution classes from unyielding classes. Iterative rounds of 2D and 3D classifications were performed to get rid of poorly resolved classes (Fig. 8). Due to the high similarity between the A3C- and the A3G-bound neddylated CRL5$^{Vif-CBFβ}$-ARIH2* complexes, 3D classification of both complexes yielded several similar but also unique classes. The initial processing revealed a lack of high-resolution classes which contained the bound substrates,

87

presumably due to high flexibility and heterogeneous orientation of SR-substrate subunits. Interestingly, during 3D classification one class featured the entire complex including A3C. This class was processed until it reached a resolution of 6.8 Å, and "was low-pass filtered to 7.5 Å"[198] (Fig. 8). For the initial consensus refinement, a very narrow mask covering the entire CRL5[Vif-CBFβ]-A3C-ARIH2* density was used and allowed us to reconstruct a density map with a global resolution of 3.7 Å (Fig. 8).

Unfortunately, density for the Vif-CBFβ-A3C subunits still lacked clear structural features. On the opposite end, the neddylated CUL5-RBX2-ARIH2* part of the map displayed clear density with distinct features. This led us to focus on the neddylated CUL5 (C-terminal region)-RBX2-ARIH2 part, using a mask covering just this region for further 3D classification. The final resolution reached 3.4 Å where the interfaces between ARIH2* and neddylated CUL5-RBX2 are clearly visible. All major steps during processing are shown in the flowchart in Fig.8. The gold-standard Fourier Shell Correlation (FSC) at 0.143 was used to determine the final and reported resolution (Fig. 8). Final maps were sharpened using RELION[273] postprocessing or DeepEMhancer[281]. To improve the map quality two half maps from the final refinement were used as an input for DeepEMhancer which led to local sharpening and noise reduction, thereby facilitating model building. The processing flowchart of the NEDD8– CRL5[Vif-CBFβ]-ARIH2*-A3G assembly is shown in Fig. 9.

Model building and refinement

To build and refine the model, a number of maps were used to guide the progress. Initially, the coordinates from already published structures were docked into the 7.5 Å map (initial resolution was 6.8 Å; Electron microscopy data bank (EMDB)-12998). The following PDB files were fit into the corresponding densities of the subunits: A3C (PDB ID: 3VOW[255]); CUL5 NTD and ELOBC-Vif-CBFβ (PDB ID: 4N9F[251]), our crystal structure of ARIH2, the CUL5 CR3 (PDB ID: 6V9I[254]), 4HB, C/R domain with RBX1 and WHB domain (PDB ID: 3DQV).

For building the model of the NEDD8–CUL5-RBX2-ARIH2* E3-E3 superassembly (Fig. 8, EMDB-12995), the 3.4 Å A3C E3-E3catalytic focused map was used to fit all coordinates from the CRL5[Vif-CBFβ]-ARIH2*-A3C dataset. First, crystal structures of CUL5, RBX2, ARIH2 and NEDD8 were fit into the focus refined map using Chimera v1.14[276]. Next, PHENIX[279] was used for rigid body refinements to allow all components to move independently of each. Parts of ARIH2* (UBA-L, RING1, and RTI-helix region)

88

showed only poorly visible density in all cryo-EM maps, most likely due to higher flexibility requiring further rigid body refinements. The rest of the E3-E3 structure was built manually using COOT[278]. The structure of RBX1 (from PDB ID: 3DQV) was converted to RBX2 by exchanging the relevant amino acids. Phenix.refine[279] was subsequently used for real space refinements to iteratively improve the fit. Some regions in ARIH2* could not be resolved including its Rcat domain (residues 283-351) and residues 1-34, 51-53, 128-133 and 492-493. The following regions could not be modeled: RBX2 regions 6-27, CUL5 1-151, 170-173, 189-193, 386-400 and 675-679. The side chains of ARIH2* UBA-L, RING1 and RTI-helix are oriented the same way as in the crystal structure of autoinhibited ARIH2 (from this study), as these parts are less well-resolved in the cryo-EM maps and had to be restrained during the refinement process. The side-chain of CUL5 Glu717 was also modeled based on the crystal structure of neddylated CUL5 (PDB ID: 3DQV)[132] as it was not visible in the density. PyMOL or ChimeraX v1.0 were used for figure-making. The exact refinement statistics can be found in Table 5.

Table 4. Crystal structure data collection and refinement statistics (adapted from ref. [198])

	Autoinhibited ARIH2
Data collection	
Space group	P 1 21 1
Cell dimensions	
a, b, c (Å)	77.57 80.54 92.09
α, β, γ (°)	90 105.76 90
Resolution (Å)	66.7 - 2.45 (2.54 - 2.45)*
R_{sym} or R_{merge}	0.13 (2.4)
I / σI	19.5 (1.0)
Completeness (%)	95.9 (75.0)
Redundancy	18.6 (11.2)
Refinement	
Resolution (Å)	2.45
No. reflections	38685 (2975)
R_{work} / R_{free}	22.1 / 26.1
No. atoms	6972
Protein	6940
Ligand/ion	12
Water	20
B-factors	
Protein	76.9
Ligand/ion	81.4
Water	60.9
R.m.s. deviations	
Bond lengths (Å)	0.003
Bond angles (°)	0.56

*Values in parentheses are for highest-resolution shell.

Table 5. Cryo-EM data collection, refinement and validation statistics (adapted from ref. [198])

	Neddylated CRL5$^{Vif-CBF\beta}$-ARIH2*-APOBEC3C A3C consensus (EMDB-13000)	Neddylated CRL5$^{Vif-CBF\beta}$-ARIH2*-APOBEC3C A3C fullcomplex consensus (EMDB-12998)	Neddylated CUL5 C-terminal region-RBX2-ARIH2* A3C E3-E3 catalytic focused (EMDB-12995) (PDB 7ONI)	Neddylated CRL5$^{Vif-CBF\beta}$-ARIH2*-APOBEC3G A3G consensus (EMDB-13001)	Neddylated CUL5 C-terminal region-RBX2-ARIH2* A3G E3-E3 catalytic focused (EMDB-12999)
Data collection and processing					
Microscope/detector	Krios/K3	Krios/K3	Krios/K3	Krios/K3	Krios/K3
Magnification	105,000	105,000	105,000	81,000	81,000
Voltage (kV)	300	300	300	300	300
Electron exposure (e^{-}/Å^2)	14.9	14.9	14.9	15	15
Defocus range (µm)	0.7 ~ 2.5	0.7 ~ 2.5	0.7 ~ 2.5	0.7 ~ 2.5	0.7 ~ 2.5
Pixel size (Å)	0.8512	0.8512	0.8512	1.094	1.094
Symmetry imposed	n/a	n/a	n/a	n/a	n/a
Initial particle images (no.)	5,030,529	5,030,529	5,030,529	1,200,719	1,200,719
Final particle images (no.)	191,538	7,689	191,792	194,585	194,585
Map resolution (Å) FSC threshold	3.68	6.81	3.40	3.83	3.48
Map resolution range (Å)	3.3 – 8.2	-	3.2 – 6.2	3.4 – 8.0	3.3 – 6.3
Refinement					
Initial model used (PDB code)			3DQV 7OD1		
Model resolution (Å) FSC threshold			3.40 0.143		
Map sharpening *B* factor (Å^2)			-70		
Model composition					
Non-hydrogen atoms			8840		
Protein residues			1141		
Ligands			7		
B factors (Å^2)					
Protein			99		
Ligand			155		
R.m.s. deviations					
Bond lengths (Å)			0.003		
Bond angles (°)			0.529		
Validation					
MolProbity score			1.7		
Clashscore			7.5		
Poor rotamers (%)			0		
Ramachandran plot					
Favored (%)			96		
Allowed (%)			4		
Disallowed (%)			0		

SPECIAL RIGHTS AND PERMISSIONS

Fig. 1c Informations regarding this article can be viewed under <https://pubs.acs.org/doi/10.1021/acs.chemrev.6b00737>. For further permission related to the material excerpted please contact ACS directly.

Fig 2a Informations regarding this article can be viewed under <https://pubs.acs.org/doi/10.1021/acs.chemrev.6b00737>. For further permission related to the material excerpted please contact ACS directly.

Fig 3a Reprinted by permission from EMBO Press: John Wiley and Sons; "RBR E3 Ligases at work", Judith J Smit, Titia K Sixma, (2014). © 2014 The Authors

b Reprinted by permission from Springer Nature, *Nat Rev Mol Cell Biol* **10**, 659-671 "Ubiquitin-binding domains - from structures to functions". Dikic, I., Wakatsuki, S. & Walters, K. J., (2009). © 2009 The Authors

e, f Reprinted by permission from Annual Reviews, *Annu Rev Biochem* **90**, 403-429, "Cullin-RING Ubiquitin Ligase Regulatory Circuits: A Quarter Century Beyond the F-Box Hypothesis" (2021). Harper, J. W. & Schulman, B. A. © 2021 The Authors

Fig 4a Reprinted from "RING-Between-RING E3s ligases: Emerging themes amid the variations" Volume 429, Issue 22, Dove, K. K. & Klevit, R. E., (2017) Pages 3363-3375, with permission from Elsevier

Fig 5a Reprinted by permission from Springer Nature, *Nat Struct Mol Biol* **25,** 623-630, "Mechanism of parkin activation by phosphorylation", Sauve, V. *et al.,* (2018) © *2018, The Author(s)*

All other figures are publicly available and open acess.

REFERENCES

1   Huttenhain, R. *et al.* ARIH2 Is a Vif-Dependent Regulator of CUL5-Mediated APOBEC3G Degradation in HIV Infection. *Cell Host Microbe* **26**, 86-99 e87, doi:10.1016/j.chom.2019.05.008 (2019).

2   Yu, X. *et al.* Induction of APOBEC3G ubiquitination and degradation by an HIV-1 Vif-Cul5-SCF complex. *Science* **302**, 1056-1060, doi:10.1126/science.1089591 (2003).

3   Andersson, A. K. *et al.* IDH1 and IDH2 mutations in pediatric acute leukemia. *Leukemia* **25**, 1570-1577, doi:10.1038/leu.2011.133 (2011).

4   Jager, S. *et al.* Global landscape of HIV-human protein complexes. *Nature* **481**, 365-370, doi:10.1038/nature10719 (2011).

5   Kelsall, I. R. *et al.* TRIAD1 and HHARI bind to and are activated by distinct neddylated Cullin-RING ligase complexes. *EMBO J* **32**, 2848-2860, doi:10.1038/emboj.2013.209 (2013).

6   Scott, D. C. *et al.* Two Distinct Types of E3 Ligases Work in Unison to Regulate Substrate Ubiquitylation. *Cell* **166**, 1198-1214 e1124, doi:10.1016/j.cell.2016.07.027 (2016).

7   Bhattacharyya, R. P., Remenyi, A., Yeh, B. J. & Lim, W. A. Domains, motifs, and scaffolds: the role of modular interactions in the evolution and wiring of cell signaling circuits. *Annu Rev Biochem* **75**, 655-680, doi:10.1146/annurev.biochem.75.103004.142710 (2006).

8   Jin, J. & Pawson, T. Modular evolution of phosphorylation-based signalling systems. *Philos Trans R Soc Lond B Biol Sci* **367**, 2540-2555, doi:10.1098/rstb.2012.0106 (2012).

9   Marmorstein, R. & Zhou, M. M. Writers and readers of histone acetylation: structure, mechanism, and inhibition. *Cold Spring Harb Perspect Biol* **6**, a018762, doi:10.1101/cshperspect.a018762 (2014).

10   Husnjak, K. & Dikic, I. Ubiquitin-binding proteins: decoders of ubiquitin-mediated cellular functions. *Annu Rev Biochem* **81**, 291-322, doi:10.1146/annurev-biochem-051810-094654 (2012).

11   Swatek, K. N. & Komander, D. Ubiquitin modifications. *Cell Res* **26**, 399-422, doi:10.1038/cr.2016.39 (2016).

12   Afonine, P. V. *et al.* New tools for the analysis and validation of cryo-EM maps and atomic models. *Acta Crystallogr D Struct Biol* **74**, 814-840, doi:10.1107/S2059798318009324 (2018).

13   Kirkin, V. & Dikic, I. Role of ubiquitin- and Ubl-binding proteins in cell signaling. *Curr Opin Cell Biol* **19**, 199-205, doi:10.1016/j.ceb.2007.02.002 (2007).

14   Dantuma, N. P. & Bott, L. C. The ubiquitin-proteasome system in neurodegenerative diseases: precipitating factor, yet part of the solution. *Front Mol Neurosci* **7**, 70, doi:10.3389/fnmol.2014.00070 (2014).

15   Fhu, C. W. & Ali, A. Dysregulation of the Ubiquitin Proteasome System in Human Malignancies: A Window for Therapeutic Intervention. *Cancers (Basel)* **13**, doi:10.3390/cancers13071513 (2021).

16   Choudhary, C. *et al.* Lysine acetylation targets protein complexes and co-regulates major cellular functions. *Science* **325**, 834-840, doi:1175371 [pii] 10.1126/science.1175371 (2009).

17   Lundby, A. *et al.* Proteomic analysis of lysine acetylation sites in rat tissues reveals organ specificity and subcellular patterns. *Cell Rep* **2**, 419-431, doi:10.1016/j.celrep.2012.07.006 (2012).

18   Ohtake, F. *et al.* Ubiquitin acetylation inhibits polyubiquitin chain elongation. *EMBO Rep* **16**, 192-201, doi:10.15252/embr.201439152 (2015).

19   Weinert, B. T. *et al.* Lysine succinylation is a frequently occurring modification in prokaryotes and eukaryotes and extensively overlaps with acetylation. *Cell Rep* **4**, 842-851, doi:10.1016/j.celrep.2013.07.024 (2013).

20   Kane, L. A. *et al.* PINK1 phosphorylates ubiquitin to activate Parkin E3 ubiquitin ligase activity. *J Cell Biol* **205**, 143-153, doi:10.1083/jcb.201402104 (2014).

21   Peng, J. *et al.* A proteomics approach to understanding protein ubiquitination. *Nat Biotechnol* **21**, 921-926 (2003).

22   Lee, J. R. *et al.* The HECT domain of the ubiquitin ligase Rsp5 contributes to substrate recognition. *J Biol Chem* **284**, 32126-32137, doi:10.1074/jbc.M109.048629 (2009).

23   Zhou, L. *et al.* The role of RING box protein 1 in mouse oocyte meiotic maturation. *PLoS ONE* **8**, e68964, doi:10.1371/journal.pone.0068964 (2013).

24   Lundby, A. *et al.* Quantitative maps of protein phosphorylation sites across 14 different rat organs and tissues. *Nat Commun* **3**, 876, doi:10.1038/ncomms1871 (2012).

25   Swaney, D. L. *et al.* Global analysis of phosphorylation and ubiquitylation cross-talk in protein degradation. *Nat Methods* **10**, 676-682, doi:10.1038/nmeth.2519 (2013).

26   Rikova, K. *et al.* Global survey of phosphotyrosine signaling identifies oncogenic kinases in lung cancer. *Cell* **131**, 1190-1203, doi:10.1016/j.cell.2007.11.025 (2007).

27   Olsen, S. K. *et al.* Structural basis by which alternative splicing modulates the organizer activity of FGF8 in the brain. *Genes Dev* **20**, 185-198, doi:10.1101/gad.1365406 (2006).

28   Vijay-Kumar, S., Bugg, C. E. & Cook, W. J. Structure of ubiquitin refined at 1.8 A resolution. *J Mol Biol* **194**, 531-544 (1987).

29   Walden, H. *et al.* The structure of the APPBP1-UBA3-NEDD8-ATP complex reveals the basis for selective ubiquitin-like protein activation by an E1. *Mol Cell* **12**, 1427-1437, doi:10.1016/s1097-2765(03)00452-0 (2003).

30   Metzger, M. B., Pruneda, J. N., Klevit, R. E. & Weissman, A. M. RING-type E3 ligases: Master manipulators of E2 ubiquitin-conjugating enzymes and ubiquitination. *Biochim Biophys Acta* **1843**, 47-60, doi:10.1016/j.bbamcr.2013.05.026 (2014).

31   Dove, K. K. & Klevit, R. E. RING-Between-RING E3s ligases: Emerging themes amid the variations. *J Mol Biol*, doi:10.1016/j.jmb.2017.08.008 (2017).

32   Zheng, N. & Shabek, N. Ubiquitin Ligases: Structure, Function, and Regulation. *Annu Rev Biochem* **86**, 129-157, doi:10.1146/annurev-biochem-060815-014922 (2017).

33   Cappadocia, L. & Lima, C. D. Ubiquitin-like Protein Conjugation: Structures, Chemistry, and Mechanism. *Chem Rev* **118**, 889-918, doi:10.1021/acs.chemrev.6b00737 (2018).

34   Walden, H. & Rittinger, K. RBR ligase-mediated ubiquitin transfer: a tale with many twists and turns. *Nat Struct Mol Biol* **25**, 440-445, doi:10.1038/s41594-018-0063-3 (2018).

35   McDowell, G. S. & Philpott, A. New Insights Into the Role of Ubiquitylation of Proteins. *Int Rev Cell Mol Biol* **325**, 35-88, doi:10.1016/bs.ircmb.2016.02.002 (2016).

36   Kliza, K. & Husnjak, K. Resolving the Complexity of Ubiquitin Networks. *Front Mol Biosci* **7**, 21, doi:10.3389/fmolb.2020.00021 (2020).

37   Yau, R. & Rape, M. The increasing complexity of the ubiquitin code. *Nat Cell Biol* **18**, 579-586, doi:10.1038/ncb3358 (2016).

38   Komander, D. The emerging complexity of protein ubiquitination. *Biochem Soc Trans* **37**, 937-953, doi:10.1042/BST0370937 (2009).

39   Haglund, K. *et al.* Multiple monoubiquitination of RTKs is sufficient for their endocytosis and degradation. *Nat Cell Biol* **5**, 461-466, doi:10.1038/ncb983 (2003).

40   Jura, N., Scotto-Lavino, E., Sobczyk, A. & Bar-Sagi, D. Differential modification of Ras proteins by ubiquitination. *Mol Cell* **21**, 679-687, doi:10.1016/j.molcel.2006.02.011 (2006).

41   Di Fiore, P. P., Polo, S. & Hofmann, K. When ubiquitin meets ubiquitin receptors: a signalling connection. *Nat Rev Mol Cell Biol* **4**, 491-497, doi:10.1038/nrm1124 (2003).

42   Hoege, C., Pfander, B., Moldovan, G. L., Pyrowolakis, G. & Jentsch, S. RAD6-dependent DNA repair is linked to modification of PCNA by ubiquitin and SUMO. *Nature* **419**, 135-141 (2002).

43   Pavri, R. *et al.* Histone H2B monoubiquitination functions cooperatively with FACT to regulate elongation by RNA polymerase II. *Cell* **125**, 703-717, doi:10.1016/j.cell.2006.04.029 (2006).

44   Zhou, W. *et al.* Histone H2A monoubiquitination represses transcription by inhibiting RNA polymerase II transcriptional elongation. *Mol Cell* **29**, 69-80, doi:10.1016/j.molcel.2007.11.002 (2008).

45   Mevissen, T. E. T. *et al.* Molecular basis of Lys11-polyubiquitin specificity in the deubiquitinase Cezanne. *Nature* **538**, 402-405, doi:10.1038/nature19836 (2016).

46   Husnjak, K. *et al.* Proteasome subunit Rpn13 is a novel ubiquitin receptor. *Nature* **453**, 481-488, doi:10.1038/nature06926 (2008).

47   Chau, V. *et al.* A multiubiquitin chain is confined to specific lysine in a targeted short-lived protein. *Science* **243**, 1576-1583 (1989).

48   Pickart, C. M. & Fushman, D. Polyubiquitin chains: polymeric protein signals. *Curr Opin Chem Biol* **8**, 610-616, doi:10.1016/j.cbpa.2004.09.009 (2004).

49   Yang, Z. & Klionsky, D. J. An overview of the molecular mechanism of autophagy. *Curr Top Microbiol Immunol* **335**, 1-32, doi:10.1007/978-3-642-00302-8_1 (2009).

50   Lim, J. & Yue, Z. Neuronal aggregates: formation, clearance, and spreading. *Dev Cell* **32**, 491-501, doi:10.1016/j.devcel.2015.02.002 (2015).

51   Sugeno, N. *et al.* Lys-63-linked ubiquitination by E3 ubiquitin ligase Nedd4-1 facilitates endosomal sequestration of internalized alpha-synuclein. *J Biol Chem* **289**, 18137-18151, doi:10.1074/jbc.M113.529461 (2014).

52   Kirisako, T. *et al.* A ubiquitin ligase complex assembles linear polyubiquitin chains. *The EMBO journal* **25**, 4877-4887, doi:10.1038/sj.emboj.7601360 (2006).

53   Ikeda, F. *et al.* SHARPIN forms a linear ubiquitin ligase complex regulating NF-kappaB activity and apoptosis. *Nature* **471**, 637-641, doi:10.1038/nature09814 (2011).

54   Rahighi, S. *et al.* Specific recognition of linear ubiquitin chains by NEMO is important for NF-kappaB activation. *Cell* **136**, 1098-1109, doi:10.1016/j.cell.2009.03.007 (2009).

55   Perrin, A. J., Jiang, X., Birmingham, C. L., So, N. S. & Brumell, J. H. Recognition of bacteria in the cytosol of Mammalian cells by the ubiquitin system. *Curr Biol* **14**, 806-811, doi:10.1016/j.cub.2004.04.033 (2004).

56   van Well, E. M. *et al.* A protein quality control pathway regulated by linear ubiquitination. *The EMBO journal* **38**, doi:10.15252/embj.2018100730 (2019).

57   Wu, G. *et al.* Structure of a beta-TrCP1-Skp1-beta-catenin complex: destruction motif binding and lysine specificity of the SCF(beta-TrCP1) ubiquitin ligase. *Mol Cell* **11**, 1445-1456, doi:10.1016/s1097-2765(03)00234-x (2003).

58   Elia, A. E. *et al.* Quantitative Proteomic Atlas of Ubiquitination and Acetylation in the DNA Damage Response. *Mol Cell* **59**, 867-881, doi:10.1016/j.molcel.2015.05.006 (2015).

59   Morris, J. R. & Solomon, E. BRCA1 : BARD1 induces the formation of conjugated ubiquitin structures, dependent on K6 of ubiquitin, in cells during DNA replication and repair. *Hum Mol Genet* **13**, 807-817, doi:10.1093/hmg/ddh095 (2004).

60   Lu, C. S. *et al.* The RING finger protein RNF8 ubiquitinates Nbs1 to promote DNA double-strand break repair by homologous recombination. *J Biol Chem* **287**, 43984-43994, doi:10.1074/jbc.M112.421545 (2012).

61   Heidelberger, J. B. *et al.* Proteomic profiling of VCP substrates links VCP to K6-linked ubiquitylation and c-Myc function. *EMBO Rep* **19**, doi:10.15252/embr.201744754 (2018).

62   Michel, M. A., Swatek, K. N., Hospenthal, M. K. & Komander, D. Ubiquitin Linkage-Specific Affimers Reveal Insights into K6-Linked Ubiquitin Signaling. *Mol Cell* **68**, 233-246 e235, doi:10.1016/j.molcel.2017.08.020 (2017).

63   Xu, Y., Anderson, D. E. & Ye, Y. The HECT domain ubiquitin ligase HUWE1 targets unassembled soluble proteins for degradation. *Cell Discov* **2**, 16040, doi:10.1038/celldisc.2016.40 (2016).

64   Locke, M., Toth, J. I. & Petroski, M. D. Lys11- and Lys48-linked ubiquitin chains interact with p97 during endoplasmic-reticulum-associated degradation. *Biochem J* **459**, 205-216, doi:10.1042/BJ20120662 (2014).

65   Boughton, A. J., Krueger, S. & Fushman, D. Branching via K11 and K48 Bestows Ubiquitin Chains with a Unique Interdomain Interface and Enhanced Affinity for Proteasomal Subunit Rpn1. *Structure* **28**, 29-43 e26, doi:10.1016/j.str.2019.10.008 (2020).

66   Yau, R. G. *et al.* Assembly and Function of Heterotypic Ubiquitin Chains in Cell-Cycle and Protein Quality Control. *Cell* **171**, 918-933 e920, doi:10.1016/j.cell.2017.09.040 (2017).

67   Liu, J. *et al.* Structural Insights into SHARPIN-Mediated Activation of HOIP for the Linear Ubiquitin Chain Assembly. *Cell Rep* **21**, 27-36, doi:10.1016/j.celrep.2017.09.031 (2017).

68   Kuang, P., Tan, M., Zhou, W., Zhang, Q. & Sun, Y. SAG/RBX2 E3 ligase complexes with UBCH10 and UBE2S E2s to ubiquitylate beta-TrCP1 via K11-linkage for degradation. *Sci Rep* **6**, 37441, doi:10.1038/srep37441 (2016).

69   Wang, H. *et al.* RNF216 contributes to proliferation and migration of colorectal cancer via suppressing BECN1-dependent autophagy. *Oncotarget* **7**, 51174-51183, doi:10.18632/oncotarget.9433 (2016).

70   Dynek, J. N. *et al.* c-IAP1 and UbcH5 promote K11-linked polyubiquitination of RIP1 in TNF signalling. *The EMBO journal* **29**, 4198-4209, doi:10.1038/emboj.2010.300 (2010).

71   Li, Z. *et al.* Ube2s stabilizes beta-Catenin through K11-linked polyubiquitination to promote mesendoderm specification and colorectal cancer development. *Cell Death Dis* **9**, 456, doi:10.1038/s41419-018-0451-y (2018).

72   Gu, H. & Jan Fada, B. Specificity in Ubiquitination Triggered by Virus Infection. *Int J Mol Sci* **21**, doi:10.3390/ijms21114088 (2020).

96

73   Zeng, W., Xu, M., Liu, S., Sun, L. & Chen, Z. J. Key role of Ubc5 and lysine-63 polyubiquitination in viral activation of IRF3. *Mol Cell* **36**, 315-325, doi:10.1016/j.molcel.2009.09.037 (2009).

74   Yu, Y. & Hayward, G. S. The ubiquitin E3 ligase RAUL negatively regulates type i interferon through ubiquitination of the transcription factors IRF7 and IRF3. *Immunity* **33**, 863-877, doi:10.1016/j.immuni.2010.11.027 (2010).

75   Swami, N. *et al.* Novel genomic signature predictive of response to immune checkpoint blockade: A pan-cancer analysis from project Genomics Evidence Neoplasia Information Exchange (GENIE). *Cancer Genet* **258-259**, 61-68, doi:10.1016/j.cancergen.2021.08.004 (2021).

76   Doil, C. *et al.* RNF168 binds and amplifies ubiquitin conjugates on damaged chromosomes to allow accumulation of repair proteins. *Cell* **136**, 435-446, doi:10.1016/j.cell.2008.12.041 (2009).

77   Gatti, M. *et al.* RNF168 promotes noncanonical K27 ubiquitination to signal DNA damage. *Cell Rep* **10**, 226-238, doi:10.1016/j.celrep.2014.12.021 (2015).

78   Zucchelli, S. *et al.* TRAF6 promotes atypical ubiquitination of mutant DJ-1 and alpha-synuclein and is localized to Lewy bodies in sporadic Parkinson's disease brains. *Hum Mol Genet* **19**, 3759-3770, doi:10.1093/hmg/ddq290 (2010).

79   Tauriello, D. V. & Maurice, M. M. The various roles of ubiquitin in Wnt pathway regulation. *Cell Cycle* **9**, 3700-3709, doi:10.4161/cc.9.18.13204 (2010).

80   Fei, C. *et al.* Smurf1-mediated Lys29-linked nonproteolytic polyubiquitination of axin negatively regulates Wnt/beta-catenin signaling. *Mol Cell Biol* **33**, 4095-4105, doi:10.1128/MCB.00418-13 (2013).

81   Yuan, W. C. *et al.* K33-Linked Polyubiquitination of Coronin 7 by Cul3-KLHL20 Ubiquitin E3 Ligase Regulates Protein Trafficking. *Mol Cell* **54**, 586-600, doi:10.1016/j.molcel.2014.03.035 (2014).

82   Haakonsen, D. L. & Rape, M. Branching Out: Improved Signaling by Heterotypic Ubiquitin Chains. *Trends Cell Biol* **29**, 704-716, doi:10.1016/j.tcb.2019.06.003 (2019).

83   Meyer, H. J. & Rape, M. Enhanced protein degradation by branched ubiquitin chains. *Cell* **157**, 910-921, doi:10.1016/j.cell.2014.03.037 (2014).

84   Oh, E. *et al.* Gene expression and cell identity controlled by anaphase-promoting complex. *Nature* **579**, 136-140, doi:10.1038/s41586-020-2034-1 (2020).

85   Ohtake, F., Saeki, Y., Ishido, S., Kanno, J. & Tanaka, K. The K48-K63 Branched Ubiquitin Chain Regulates NF-kappaB Signaling. *Mol Cell* **64**, 251-266, doi:10.1016/j.molcel.2016.09.014 (2016).

86   Ohtake, F., Tsuchiya, H., Saeki, Y. & Tanaka, K. K63 ubiquitylation triggers proteasomal degradation by seeding branched ubiquitin chains. *Proc Natl Acad Sci U S A* **115**, E1401-E1408, doi:10.1073/pnas.1716673115 (2018).

87   Schimmel, J. *et al.* The ubiquitin-proteasome system is a key component of the SUMO-2/3 cycle. *Mol Cell Proteomics* **7**, 2107-2122, doi:10.1074/mcp.M800025-MCP200 (2008).

88   Hjerpe, R., Thomas, Y. & Kurz, T. NEDD8 overexpression results in neddylation of ubiquitin substrates by the ubiquitin pathway. *J Mol Biol* **421**, 27-29, doi:10.1016/j.jmb.2012.05.013 (2012).

89   Geoffroy, M. C. & Hay, R. T. An additional role for SUMO in ubiquitin-mediated proteolysis. *Nat Rev Mol Cell Biol* **10**, 564-568, doi:10.1038/nrm2707 (2009).

90   Horn-Ghetko, D. *et al.* Ubiquitin ligation to F-box protein targets by SCF-RBR E3-E3 super-assembly. *Nature* **590**, 671-676, doi:10.1038/s41586-021-03197-9 (2021).

97

91   Jumper, J. *et al.* Highly accurate protein structure prediction with AlphaFold. *Nature* **596**, 583-589, doi:10.1038/s41586-021-03819-2 (2021).

92   Ronau, J. A., Beckmann, J. F. & Hochstrasser, M. Substrate specificity of the ubiquitin and Ubl proteases. *Cell Res* **26**, 441-456, doi:10.1038/cr.2016.38 (2016).

93   Bloom, J., Amador, V., Bartolini, F., DeMartino, G. & Pagano, M. Proteasome-mediated degradation of p21 via N-terminal ubiquitinylation. *Cell* **115**, 71-82, doi:10.1016/s0092-8674(03)00755-4 (2003).

94   Ritchie, K. J. & Zhang, D. E. ISG15: the immunological kin of ubiquitin. *Semin Cell Dev Biol* **15**, 237-246, doi:10.1016/j.semcdb.2003.12.005 (2004).

95   Ichimura, Y. *et al.* A ubiquitin-like system mediates protein lipidation. *Nature* **408**, 488-492 (2000).

96   Suzuki, N. N., Yoshimoto, K., Fujioka, Y., Ohsumi, Y. & Inagaki, F. The crystal structure of plant ATG12 and its biological implication in autophagy. *Autophagy* **1**, 119-126, doi:1859 [pii] (2005).

97   Bayer, P. *et al.* Structure determination of the small ubiquitin-related modifier SUMO-1. *J Mol Biol* **280**, 275-286, doi:10.1006/jmbi.1998.1839 (1998).

98   Gill, G. SUMO and ubiquitin in the nucleus: different functions, similar mechanisms? *Genes Dev* **18**, 2046-2059, doi:10.1101/gad.1214604 (2004).

99   Seeler, J. S. & Dejean, A. Nuclear and unclear functions of SUMO. *Nat Rev Mol Cell Biol* **4**, 690-699, doi:10.1038/nrm1200 (2003).

100   Melchior, F., Schergaut, M. & Pichler, A. SUMO: ligases, isopeptidases and nuclear pores. *Trends Biochem Sci* **28**, 612-618, doi:10.1016/j.tibs.2003.09.002 (2003).

101   Eifler, K. & Vertegaal, A. C. Mapping the SUMOylated landscape. *FEBS J* **282**, 3669-3680, doi:10.1111/febs.13378 (2015).

102   Choi, S. G. *et al.* SUMO-Modified FADD Recruits Cytosolic Drp1 and Caspase-10 to Mitochondria for Regulated Necrosis. *Mol Cell Biol* **37**, doi:10.1128/MCB.00254-16 (2017).

103   Liu, Y. C. *et al.* A MHC-encoded ubiquitin-like protein (FAT10) binds noncovalently to the spindle assembly checkpoint protein MAD2. *Proc Natl Acad Sci U S A* **96**, 4313-4318, doi:10.1073/pnas.96.8.4313 (1999).

104   Lukasiak, S. *et al.* Proinflammatory cytokines cause FAT10 upregulation in cancers of liver and colon. *Oncogene* **27**, 6068-6074, doi:10.1038/onc.2008.201 (2008).

105   Hipp, M. S., Kalveram, B., Raasi, S., Groettrup, M. & Schmidtke, G. FAT10, a ubiquitin-independent signal for proteasomal degradation. *Mol Cell Biol* **25**, 3483-3491, doi:10.1128/MCB.25.9.3483-3491.2005 (2005).

106   Aichem, A. *et al.* USE1 is a bispecific conjugating enzyme for ubiquitin and FAT10, which FAT10ylates itself in cis. *Nat Commun* **1**, 13, doi:10.1038/ncomms1012 (2010).

107   Ebstein, F., Lehmann, A. & Kloetzel, P. M. The FAT10- and ubiquitin-dependent degradation machineries exhibit common and distinct requirements for MHC class I antigen presentation. *Cellular and molecular life sciences : CMLS* **69**, 2443-2454, doi:10.1007/s00018-012-0933-5 (2012).

108   Aichem, A. *et al.* The proteomic analysis of endogenous FAT10 substrates identifies p62/SQSTM1 as a substrate of FAT10ylation. *J Cell Sci* **125**, 4576-4585, doi:10.1242/jcs.107789 (2012).

109   Aichem, A., Catone, N. & Groettrup, M. Investigations into the auto-FAT10ylation of the bispecific E2 conjugating enzyme UBA6-specific E2 enzyme 1. *FEBS J* **281**, 1848-1859, doi:10.1111/febs.12745 (2014).

98

110   Krug, R. M., Zhao, C. & Beaudenon, S. Properties of the ISG15 E1 enzyme UbE1L. *Methods Enzymol* **398**, 32-40, doi:10.1016/S0076-6879(05)98004-X (2005).

111   Zhao, C. *et al.* The UbcH8 ubiquitin E2 enzyme is also the E2 enzyme for ISG15, an IFN-alpha/beta-induced ubiquitin-like protein. *Proc Natl Acad Sci U S A* **101**, 7578-7582, doi:10.1073/pnas.0402528101 (2004).

112   Liu, M., Li, X. L. & Hassel, B. A. Proteasomes modulate conjugation to the ubiquitin-like protein, ISG15. *J Biol Chem* **278**, 1594-1602, doi:10.1074/jbc.M208123200 (2003).

113   Knight, E., Jr. & Cordova, B. IFN-induced 15-kDa protein is released from human lymphocytes and monocytes. *J Immunol* **146**, 2280-2284 (1991).

114   Malakhova, O. A. *et al.* UBP43 is a novel regulator of interferon signaling independent of its ISG15 isopeptidase activity. *The EMBO journal* **25**, 2358-2367, doi:10.1038/sj.emboj.7601149 (2006).

115   Kim, M. J., Hwang, S. Y., Imaizumi, T. & Yoo, J. Y. Negative feedback regulation of RIG-I-mediated antiviral signaling by interferon-induced ISG15 conjugation. *J Virol* **82**, 1474-1483, doi:10.1128/JVI.01650-07 (2008).

116   Li, Y. J. *et al.* Allosteric Inhibition of Ubiquitin-like Modifications by a Class of Inhibitor of SUMO-Activating Enzyme. *Cell Chem Biol* **26**, 278-288 e276, doi:10.1016/j.chembiol.2018.10.026 (2019).

117   Recht, M., Borden, E. C. & Knight, E., Jr. A human 15-kDa IFN-induced protein induces the secretion of IFN-gamma. *J Immunol* **147**, 2617-2623 (1991).

118   D'Cunha, J., Knight, E., Jr., Haas, A. L., Truitt, R. L. & Borden, E. C. Immunoregulatory properties of ISG15, an interferon-induced cytokine. *Proc Natl Acad Sci U S A* **93**, 211-215, doi:10.1073/pnas.93.1.211 (1996).

119   Schoenborn, J. R. & Wilson, C. B. Regulation of interferon-gamma during innate and adaptive immune responses. *Adv Immunol* **96**, 41-101, doi:10.1016/S0065-2776(07)96002-2 (2007).

120   Bogunovic, D. *et al.* Mycobacterial disease and impaired IFN-gamma immunity in humans with inherited ISG15 deficiency. *Science* **337**, 1684-1688, doi:10.1126/science.1224026 (2012).

121   den Besten, W., Verma, R., Kleiger, G., Oania, R. S. & Deshaies, R. J. NEDD8 links cullin-RING ubiquitin ligase function to the p97 pathway. *Nat Struct Mol Biol* **19**, 511-516, S511, doi:10.1038/nsmb.2269 (2012).

122   Walden, H., Podgorski, M. S. & Schulman, B. A. Insights into the ubiquitin transfer cascade from the structure of the activating enzyme for NEDD8. *Nature* **422**, 330-334, doi:10.1038/nature01456 (2003).

123   Hjerpe, R. *et al.* Changes in the ratio of free NEDD8 to ubiquitin triggers NEDDylation by ubiquitin enzymes. *Biochem J* **441**, 927-936, doi:10.1042/BJ20111671 (2012).

124   Singh, R. K. *et al.* Recognition and cleavage of related to ubiquitin 1 (Rub1) and Rub1-ubiquitin chains by components of the ubiquitin-proteasome system. *Mol Cell Proteomics* **11**, 1595-1611, doi:10.1074/mcp.M112.022467 (2012).

125   Amir, R. E., Iwai, K. & Ciechanover, A. The NEDD8 pathway is essential for SCF(beta - TrCP)-mediated ubiquitination and processing of the NF-kappa B precursor p105. *J Biol Chem* **277**, 23253-23259 (2002).

126   Schulman, B. A. & Harper, J. W. Ubiquitin-like protein activation by E1 enzymes: the apex for downstream signalling pathways. *Nat Rev Mol Cell Biol* **10**, 319-331, doi:10.1038/nrm2673 (2009).

99

127   Kawakami, T. *et al.* NEDD8 recruits E2-ubiquitin to SCF E3 ligase. *Embo J* **20**, 4003-4012 (2001).

128   Liakopoulos, D., Doenges, G., Matuschewski, K. & Jentsch, S. A novel protein modification pathway related to the ubiquitin system. *Embo J* **17**, 2208-2214 (1998).

129   Kamitani, T., Kito, K., Nguyen, H. P. & Yeh, E. T. Characterization of NEDD8, a developmentally down-regulated ubiquitin-like protein. *J Biol Chem* **272**, 28557-28562, doi:10.1074/jbc.272.45.28557 (1997).

130   Pan, Z. Q., Kentsis, A., Dias, D. C., Yamoah, K. & Wu, K. Nedd8 on cullin: building an expressway to protein destruction. *Oncogene* **23**, 1985-1997 (2004).

131   Lydeard, J. R., Schulman, B. A. & Harper, J. W. Building and remodelling Cullin-RING E3 ubiquitin ligases. *EMBO Rep* **14**, 1050-1061, doi:10.1038/embor.2013.173 (2013).

132   Duda, D. M. *et al.* Structural insights into NEDD8 activation of cullin-RING ligases: conformational control of conjugation. *Cell* **134**, 995-1006 (2008).

133   Xirodimas, D. P., Saville, M. K., Bourdon, J. C., Hay, R. T. & Lane, D. P. Mdm2-mediated NEDD8 conjugation of p53 inhibits its transcriptional activity. *Cell* **118**, 83-97, doi:10.1016/j.cell.2004.06.016 (2004).

134   Liu, N. *et al.* HDM2 Promotes NEDDylation of Hepatitis B Virus HBx To Enhance Its Stability and Function. *J Virol* **91**, doi:10.1128/JVI.00340-17 (2017).

135   Maghames, C. M. *et al.* NEDDylation promotes nuclear protein aggregation and protects the Ubiquitin Proteasome System upon proteotoxic stress. *Nat Commun* **9**, 4376, doi:10.1038/s41467-018-06365-0 (2018).

136   Ma, T. *et al.* RNF111-dependent neddylation activates DNA damage-induced ubiquitination. *Mol Cell* **49**, 897-907, doi:10.1016/j.molcel.2013.01.006 (2013).

137   Choo, Y. S. *et al.* Regulation of parkin and PINK1 by neddylation. *Hum Mol Genet* **21**, 2514-2523, doi:10.1093/hmg/dds070 (2012).

138   Xie, P. *et al.* The covalent modifier Nedd8 is critical for the activation of Smurf1 ubiquitin ligase in tumorigenesis. *Nat Commun* **5**, 3733, doi:10.1038/ncomms4733 (2014).

139   Smit, J. J. & Sixma, T. K. RBR E3-ligases at work. *EMBO Rep* **15**, 142-154, doi:10.1002/embr.201338166 (2014).

140   Dikic, I., Wakatsuki, S. & Walters, K. J. Ubiquitin-binding domains - from structures to functions. *Nat Rev Mol Cell Biol* **10**, 659-671, doi:10.1038/nrm2767 (2009).

141   French, M. E., Koehler, C. F. & Hunter, T. Emerging functions of branched ubiquitin chains. *Cell Discov* **7**, 6, doi:10.1038/s41421-020-00237-y (2021).

142   Harper, J. W. & Schulman, B. A. Cullin-RING Ubiquitin Ligase Regulatory Circuits: A Quarter Century Beyond the F-Box Hypothesis. *Annu Rev Biochem* **90**, 403-429, doi:10.1146/annurev-biochem-090120-013613 (2021).

143   Gao, F. *et al.* The functions and properties of cullin-5, a potential therapeutic target for cancers. *Am J Transl Res* **12**, 618-632 (2020).

144   Buetow, L. & Huang, D. T. Structural insights into the catalysis and regulation of E3 ubiquitin ligases. *Nat Rev Mol Cell Biol* **17**, 626-642, doi:10.1038/nrm.2016.91 (2016).

145   Deshaies, R. J. & Joazeiro, C. A. RING domain E3 ubiquitin ligases. *Annu Rev Biochem* **78**, 399-434, doi:10.1146/annurev.biochem.78.101807.093809 (2009).

146   Riley, B. E. *et al.* Structure and function of Parkin E3 ubiquitin ligase reveals aspects of RING and HECT ligases. *Nat Commun* **4**, 1982, doi:10.1038/ncomms2982 (2013).

147   Bernassola, F., Karin, M., Ciechanover, A. & Melino, G. The HECT family of E3 ubiquitin ligases: multiple players in cancer development. *Cancer Cell* **14**, 10-21 (2008).

100

148   Metzger, M. B., Hristova, V. A. & Weissman, A. M. HECT and RING finger families of E3 ubiquitin ligases at a glance. *J Cell Sci* **125**, 531-537, doi:10.1242/jcs.091777 (2012).

149   Dove, K. K., Stieglitz, B., Duncan, E. D., Rittinger, K. & Klevit, R. E. Molecular insights into RBR E3 ligase ubiquitin transfer mechanisms. *EMBO Rep* **17**, 1221-1235, doi:10.15252/embr.201642641 (2016).

150   Wenzel, D. M., Lissounov, A., Brzovic, P. S. & Klevit, R. E. UBCH7 reactivity profile reveals parkin and HHARI to be RING/HECT hybrids. *Nature* **474**, 105-108, doi:10.1038/nature09966 (2011).

151   Pao, K. C. *et al.* Activity-based E3 ligase profiling uncovers an E3 ligase with esterification activity. *Nature* **556**, 381-385, doi:10.1038/s41586-018-0026-1 (2018).

152   Mabbitt, P. D. *et al.* Structural basis for RING-Cys-Relay E3 ligase activity and its role in axon integrity. *Nat Chem Biol* **16**, 1227-1236, doi:10.1038/s41589-020-0598-6 (2020).

153   Sato, Y. *et al.* Specific recognition of linear ubiquitin chains by the Npl4 zinc finger (NZF) domain of the HOIL-1L subunit of the linear ubiquitin chain assembly complex. *Proc Natl Acad Sci U S A* **108**, 20520-20525, doi:10.1073/pnas.1109088108 (2011).

154   Sekiyama, N. *et al.* NMR analysis of Lys63-linked polyubiquitin recognition by the tandem ubiquitin-interacting motifs of Rap80. *J Biomol NMR* **52**, 339-350, doi:10.1007/s10858-012-9614-9 (2012).

155   Michel, M. A. *et al.* Assembly and specific recognition of k29- and k33-linked polyubiquitin. *Mol Cell* **58**, 95-109, doi:10.1016/j.molcel.2015.01.042 (2015).

156   Kristariyanto, Y. A. *et al.* K29-selective ubiquitin binding domain reveals structural basis of specificity and heterotypic nature of k29 polyubiquitin. *Mol Cell* **58**, 83-94, doi:10.1016/j.molcel.2015.01.041 (2015).

157   He, J., Zhu, Q., Wani, G., Sharma, N. & Wani, A. A. Valosin-containing Protein (VCP)/p97 Segregase Mediates Proteolytic Processing of Cockayne Syndrome Group B (CSB) in Damaged Chromatin. *J Biol Chem* **291**, 7396-7408, doi:10.1074/jbc.M115.705350 (2016).

158   Kristariyanto, Y. A., Abdul Rehman, S. A., Weidlich, S., Knebel, A. & Kulathu, Y. A single MIU motif of MINDY-1 recognizes K48-linked polyubiquitin chains. *EMBO Rep* **18**, 392-402, doi:10.15252/embr.201643205 (2017).

159   Sato, Y. *et al.* Structural insights into ubiquitin recognition and Ufd1 interaction of Npl4. *Nat Commun* **10**, 5708, doi:10.1038/s41467-019-13697-y (2019).

160   Lu, X., Ebelle, D. L., Matsuo, H. & Walters, K. J. An Extended Conformation for K48 Ubiquitin Chains Revealed by the hRpn2:Rpn13:K48-Diubiquitin Structure. *Structure* **28**, 495-506 e493, doi:10.1016/j.str.2020.02.007 (2020).

161   van Wijk, S. J. *et al.* Fluorescence-based sensors to monitor localization and functions of linear and K63-linked ubiquitin chains in cells. *Mol Cell* **47**, 797-809, doi:10.1016/j.molcel.2012.06.017 (2012).

162   Wu, T. *et al.* Targeted protein degradation as a powerful research tool in basic biology and drug target discovery. *Nat Struct Mol Biol* **27**, 605-614, doi:10.1038/s41594-020-0438-0 (2020).

163   Armstrong, A. A., Mohideen, F. & Lima, C. D. Recognition of SUMO-modified PCNA requires tandem receptor motifs in Srs2. *Nature* **483**, 59-63, doi:10.1038/nature10883 (2012).

101

164   Valencia-Sanchez, M. I. *et al.* Structural Basis of Dot1L Stimulation by Histone H2B Lysine 120 Ubiquitination. *Mol Cell* **74**, 1010-1019 e1016, doi:10.1016/j.molcel.2019.03.029 (2019).

165   Anderson, C. J. *et al.* Structural Basis for Recognition of Ubiquitylated Nucleosome by Dot1L Methyltransferase. *Cell Rep* **26**, 1681-1690 e1685, doi:10.1016/j.celrep.2019.01.058 (2019).

166   Xue, H. *et al.* Structural basis of nucleosome recognition and modification by MLL methyltransferases. *Nature* **573**, 445-449, doi:10.1038/s41586-019-1528-1 (2019).

167   Worden, E. J., Zhang, X. & Wolberger, C. Structural basis for COMPASS recognition of an H2B-ubiquitinated nucleosome. *Elife* **9**, doi:10.7554/eLife.53199 (2020).

168   Hsu, P. L. *et al.* Structural Basis of H2B Ubiquitination-Dependent H3K4 Methylation by COMPASS. *Mol Cell* **76**, 712-723 e714, doi:10.1016/j.molcel.2019.10.013 (2019).

169   Worden, E. J., Hoffmann, N. A., Hicks, C. W. & Wolberger, C. Mechanism of Cross-talk between H2B Ubiquitination and H3 Methylation by Dot1. *Cell* **176**, 1490-1501 e1412, doi:10.1016/j.cell.2019.02.002 (2019).

170   Bilokapic, S. & Halic, M. Nucleosome and ubiquitin position Set2 to methylate H3K36. *Nat Commun* **10**, 3795, doi:10.1038/s41467-019-11726-4 (2019).

171   Lange, O. F. *et al.* Recognition dynamics up to microseconds revealed from an RDC-derived ubiquitin ensemble in solution. *Science* **320**, 1471-1475, doi:10.1126/science.1157092 (2008).

172   Sloper-Mould, K. E., Jemc, J. C., Pickart, C. M. & Hicke, L. Distinct functional surface regions on ubiquitin. *J Biol Chem* **276**, 30483-30489 (2001).

173   Winget, J. M. & Mayor, T. The diversity of ubiquitin recognition: hot spots and varied specificity. *Mol Cell* **38**, 627-635, doi:10.1016/j.molcel.2010.05.003 (2010).

174   Bienko, M. *et al.* Ubiquitin-binding domains in Y-family polymerases regulate translesion synthesis. *Science* **310**, 1821-1824, doi:10.1126/science.1120615 (2005).

175   Reyes-Turcu, F. E. *et al.* The ubiquitin binding domain ZnF UBP recognizes the C-terminal diglycine motif of unanchored ubiquitin. *Cell* **124**, 1197-1208, doi:10.1016/j.cell.2006.02.038 (2006).

176   Lee, S. *et al.* Structural basis for ubiquitin recognition and autoubiquitination by Rabex-5. *Nat Struct Mol Biol* **13**, 264-271, doi:10.1038/nsmb1064 (2006).

177   Scott, D., Oldham, N. J., Strachan, J., Searle, M. S. & Layfield, R. Ubiquitin-binding domains: mechanisms of ubiquitin recognition and use as tools to investigate ubiquitin-modified proteomes. *Proteomics* **15**, 844-861, doi:10.1002/pmic.201400341 (2015).

178   Searle, M. S. *et al.* Structural insights into specificity and diversity in mechanisms of ubiquitin recognition by ubiquitin-binding domains. *Biochem Soc Trans* **40**, 404-408, doi:10.1042/BST20110729 (2012).

179   Fushman, D. & Walker, O. Exploring the linkage dependence of polyubiquitin conformations using molecular modeling. *J Mol Biol* **395**, 803-814, doi:10.1016/j.jmb.2009.10.039 (2010).

180   Fisher, R. D. *et al.* Structure and ubiquitin binding of the ubiquitin-interacting motif. *J Biol Chem* **278**, 28976-28984, doi:10.1074/jbc.M302596200 (2003).

181   Hofmann, K. & Falquet, L. A ubiquitin-interacting motif conserved in components of the proteasomal and lysosomal protein degradation systems. *Trends Biochem Sci* **26**, 347-350, doi:10.1016/s0968-0004(01)01835-7 (2001).

182   Clague, M. J., Urbe, S. & Komander, D. Breaking the chains: deubiquitylating enzyme specificity begets function. *Nat Rev Mol Cell Biol* **20**, 338-352, doi:10.1038/s41580-019-0099-1 (2019).

183   Leznicki, P. & Kulathu, Y. Mechanisms of regulation and diversification of deubiquitylating enzyme function. *J Cell Sci* **130**, 1997-2006, doi:10.1242/jcs.201855 (2017).

184   Ye, Y. *et al.* Polyubiquitin binding and cross-reactivity in the USP domain deubiquitinase USP21. *EMBO Rep* **12**, 350-357, doi:10.1038/embor.2011.17 (2011).

185   Hospenthal, M. K., Mevissen, T. E. T. & Komander, D. Deubiquitinase-based analysis of ubiquitin chain architecture using Ubiquitin Chain Restriction (UbiCRest). *Nat Protoc* **10**, 349-361, doi:10.1038/nprot.2015.018 (2015).

186   Renatus, M. *et al.* Structural basis of ubiquitin recognition by the deubiquitinating protease USP2. *Structure* **14**, 1293-1302, doi:10.1016/j.str.2006.06.012 (2006).

187   Soucy, T. A. *et al.* An inhibitor of NEDD8-activating enzyme as a new approach to treat cancer. *Nature* **458**, 732-736, doi:10.1038/nature07884 (2009).

188   Goldenberg, S. J. *et al.* Structure of the Cand1-Cul1-Roc1 complex reveals regulatory mechanisms for the assembly of the multisubunit cullin-dependent ubiquitin ligases. *Cell* **119**, 517-528, doi:10.1016/j.cell.2004.10.019 (2004).

189   Zheng, N. *et al.* Structure of the Cul1-Rbx1-Skp1-F boxSkp2 SCF ubiquitin ligase complex. *Nature* **416**, 703-709 (2002).

190   Enchev, R. I. *et al.* Structural basis for a reciprocal regulation between SCF and CSN. *Cell Rep* **2**, 616-627, doi:10.1016/j.celrep.2012.08.019 (2012).

191   Mosadeghi, R. *et al.* Structural and kinetic analysis of the COP9-Signalosome activation and the cullin-RING ubiquitin ligase deneddylation cycle. *Elife* **5**, doi:10.7554/eLife.12102 (2016).

192   Scott, D. C. *et al.* Structure of a RING E3 trapped in action reveals ligation mechanism for the ubiquitin-like protein NEDD8. *Cell* **157**, 1671-1684, doi:10.1016/j.cell.2014.04.037 (2014).

193   Bennett, E. J., Rush, J., Gygi, S. P. & Harper, J. W. Dynamics of cullin-RING ubiquitin ligase network revealed by systematic quantitative proteomics. *Cell* **143**, 951-965, doi:10.1016/j.cell.2010.11.017 (2010).

194   Rusnac, D. V. & Zheng, N. Structural Biology of CRL Ubiquitin Ligases. *Adv Exp Med Biol* **1217**, 9-31, doi:10.1007/978-981-15-1025-0_2 (2020).

195   Xu, L. *et al.* BTB proteins are substrate-specific adaptors in an SCF-like modular ubiquitin ligase containing CUL-3. *Nature* **425**, 316-321, doi:10.1038/nature01985 (2003).

196   Angers, S. *et al.* Molecular architecture and assembly of the DDB1-CUL4A ubiquitin ligase machinery. *Nature* **443**, 590-593, doi:10.1038/nature05175 (2006).

197   Ohta, T., Michel, J. J., Schottelius, A. J. & Xiong, Y. ROC1, a homolog of APC11, represents a family of cullin partners with an associated ubiquitin ligase activity. *Mol Cell* **3**, 535-541, doi:10.1016/s1097-2765(00)80482-7 (1999).

198   Kostrhon, S. *et al.* CUL5-ARIH2 E3-E3 ubiquitin ligase structure reveals cullin-specific NEDD8 activation. *Nat Chem Biol* **17**, 1075-1083, doi:10.1038/s41589-021-00858-8 (2021).

199   Baek, K. *et al.* NEDD8 nucleates a multivalent cullin-RING-UBE2D ubiquitin ligation assembly. *Nature* **578**, 461-466, doi:10.1038/s41586-020-2000-y (2020).

200   Wang, K., Deshaies, R. J. & Liu, X. Assembly and Regulation of CRL Ubiquitin Ligases. *Adv Exp Med Biol* **1217**, 33-46, doi:10.1007/978-981-15-1025-0_3 (2020).

201   Zhao, Y., Xiong, X. & Sun, Y. Cullin-RING Ligase 5: Functional characterization and its role in human cancers. *Semin Cancer Biol* **67**, 61-79, doi:10.1016/j.semcancer.2020.04.003 (2020).

202   Kunkler, B. *et al.* CUL5 is required for thalidomide-dependent inhibition of cellular proliferation. *PLoS ONE* **13**, e0196760, doi:10.1371/journal.pone.0196760 (2018).

203   Johnson, A. E. *et al.* VACM-1/cul5 expression in vascular tissue in vivo is induced by water deprivation and its expression in vitro regulates aquaporin-1 concentrations. *Cell Tissue Res* **349**, 527-539, doi:10.1007/s00441-012-1419-3 (2012).

204   Antonioli, M. *et al.* AMBRA1 interplay with cullin E3 ubiquitin ligases regulates autophagy dynamics. *Dev Cell* **31**, 734-746, doi:10.1016/j.devcel.2014.11.013 (2014).

205   Zhao, Y. & Sun, Y. Targeting the mTOR-DEPTOR pathway by CRL E3 ubiquitin ligases: therapeutic application. *Neoplasia* **14**, 360-367, doi:10.1593/neo.12532 (2012).

206   Duda, D. M. *et al.* Structure of HHARI, a RING-IBR-RING ubiquitin ligase: autoinhibition of an Ariadne-family E3 and insights into ligation mechanism. *Structure* **21**, 1030-1041, doi:10.1016/j.str.2013.04.019 (2013).

207   Lechtenberg, B. C. *et al.* Structure of a HOIP/E2~ubiquitin complex reveals RBR E3 ligase mechanism and regulation. *Nature* **529**, 546-550, doi:10.1038/nature16511 (2016).

208   Wauer, T. & Komander, D. Structure of the human Parkin ligase domain in an autoinhibited state. *The EMBO journal* **32**, 2099-2112, doi:10.1038/emboj.2013.125 (2013).

209   Kumar, A. *et al.* Parkin-phosphoubiquitin complex reveals cryptic ubiquitin-binding site required for RBR ligase activity. *Nat Struct Mol Biol* **24**, 475-483, doi:10.1038/nsmb.3400 (2017).

210   Dove, K. K. *et al.* Structural Studies of HHARI/UbcH7 approximately Ub Reveal Unique E2 approximately Ub Conformational Restriction by RBR RING1. *Structure* **25**, 890-900 e895, doi:10.1016/j.str.2017.04.013 (2017).

211   Yuan, L., Lv, Z., Atkison, J. H. & Olsen, S. K. Structural insights into the mechanism and E2 specificity of the RBR E3 ubiquitin ligase HHARI. *Nat Commun* **8**, 211, doi:10.1038/s41467-017-00272-6 (2017).

212   Spratt, D. E., Walden, H. & Shaw, G. S. RBR E3 ubiquitin ligases: new structures, new insights, new questions. *Biochem J* **458**, 421-437, doi:10.1042/BJ20140006 (2014).

213   Gladkova, C., Maslen, S. L., Skehel, J. M. & Komander, D. Mechanism of parkin activation by PINK1. *Nature* **559**, 410-414, doi:10.1038/s41586-018-0224-x (2018).

214   Sauve, V. *et al.* Publisher Correction: Mechanism of parkin activation by phosphorylation. *Nat Struct Mol Biol* **25**, 744, doi:10.1038/s41594-018-0105-x (2018).

215   Sauve, V. *et al.* Mechanism of parkin activation by phosphorylation. *Nat Struct Mol Biol* **25**, 623-630, doi:10.1038/s41594-018-0088-7 (2018).

216   Pruneda, J. N., Stoll, K. E., Bolton, L. J., Brzovic, P. S. & Klevit, R. E. Ubiquitin in motion: structural studies of the ubiquitin-conjugating enzyme approximately ubiquitin conjugate. *Biochemistry* **50**, 1624-1633, doi:10.1021/bi101913m (2011).

217   Pruneda, J. N. *et al.* Structure of an E3:E2 approximately Ub Complex Reveals an Allosteric Mechanism Shared among RING/U-box Ligases. *Mol Cell* **47**, 933-942, doi:10.1016/j.molcel.2012.07.001 (2012).

218   Plechanovova, A., Jaffray, E. G., Tatham, M. H., Naismith, J. H. & Hay, R. T. Structure of a RING E3 ligase and ubiquitin-loaded E2 primed for catalysis. *Nature* **489**, 115-120, doi:10.1038/nature11376 (2012).

219   Dou, H., Buetow, L., Sibbet, G. J., Cameron, K. & Huang, D. T. BIRC7-E2 ubiquitin conjugate structure reveals the mechanism of ubiquitin transfer by a RING dimer. *Nat Struct Mol Biol* **19**, 876-883, doi:10.1038/nsmb.2379 (2012).

220   Martino, L., Brown, N. R., Masino, L., Esposito, D. & Rittinger, K. Determinants of E2-ubiquitin conjugate recognition by RBR E3 ligases. *Sci Rep* **8**, 68, doi:10.1038/s41598-017-18513-5 (2018).

221   Trempe, J. F. *et al.* Structure of Parkin Reveals Mechanisms for Ubiquitin Ligase Activation. *Science* **340**, 1451-1455, doi:10.1126/science.1237908 (2013).

222   Wauer, T. & Komander, D. Structure of the human Parkin ligase domain in an autoinhibited state. *The EMBO journal*, doi:10.1038/emboj.2013.125 (2013).

223   Koyano, F. *et al.* Ubiquitin is phosphorylated by PINK1 to activate parkin. *Nature* **510**, 162-166, doi:10.1038/nature13392 (2014).

224   Kondapalli, C. *et al.* PINK1 is activated by mitochondrial membrane potential depolarization and stimulates Parkin E3 ligase activity by phosphorylating Serine 65. *Open biology* **2**, 120080, doi:10.1098/rsob.120080 (2012).

225   Wauer, T., Simicek, M., Schubert, A. & Komander, D. Mechanism of phospho-ubiquitin-induced PARKIN activation. *Nature* **524**, 370-374, doi:10.1038/nature14879 (2015).

226   Lin, A. E. *et al.* ARIH2 is essential for embryogenesis, and its hematopoietic deficiency causes lethal activation of the immune system. *Nat Immunol* **14**, 27-33, doi:10.1038/ni.2478 (2013).

227   Kawashima, A. *et al.* ARIH2 Ubiquitinates NLRP3 and Negatively Regulates NLRP3 Inflammasome Activation in Macrophages. *J Immunol* **199**, 3614-3622, doi:10.4049/jimmunol.1700184 (2017).

228   Martinon, F. Detection of immune danger signals by NALP3. *J Leukoc Biol* **83**, 507-511, doi:10.1189/jlb.0607362 (2008).

229   Marteijn, J. A. *et al.* The ubiquitin ligase Triad1 inhibits myelopoiesis through UbcH7 and Ubc13 interacting domains. *Leukemia* **23**, 1480-1489, doi:10.1038/leu.2009.57 (2009).

230   Lauwers, E., Jacob, C. & Andre, B. K63-linked ubiquitin chains as a specific signal for protein sorting into the multivesicular body pathway. *J Cell Biol* **185**, 493-502, doi:10.1083/jcb.200810114 (2009).

231   Hassink, G. *et al.* Identification of the ubiquitin ligase Triad1 as a regulator of endosomal transport. *Biol Open* **1**, 607-614, doi:10.1242/bio.2012778 (2012).

232   Lecker, S. H., Goldberg, A. L. & Mitch, W. E. Protein degradation by the ubiquitin-proteasome pathway in normal and disease states. *J Am Soc Nephrol* **17**, 1807-1819, doi:10.1681/ASN.2006010083 (2006).

233   Sandri, M. Signaling in muscle atrophy and hypertrophy. *Physiology (Bethesda)* **23**, 160-170, doi:10.1152/physiol.00041.2007 (2008).

234   Lindner, A. B. & Demarez, A. Protein aggregation as a paradigm of aging. *Biochim Biophys Acta* **1790**, 980-996, doi:10.1016/j.bbagen.2009.06.005 (2009).

235   Bingol, B. & Sheng, M. Deconstruction for reconstruction: the role of proteolysis in neural plasticity and disease. *Neuron* **69**, 22-32, doi:10.1016/j.neuron.2010.11.006 (2011).

236   Brais, B. *et al.* Short GCG expansions in the PABP2 gene cause oculopharyngeal muscular dystrophy. *Nat Genet* **18**, 164-167, doi:10.1038/ng0298-164 (1998).

237   Raz, V. *et al.* A novel feed-forward loop between ARIH2 E3-ligase and PABPN1 regulates aging-associated muscle degeneration. *Am J Pathol* **184**, 1119-1131, doi:10.1016/j.ajpath.2013.12.011 (2014).

238   Wang, H. *et al.* The E3 ubiquitin ligase Triad1 influences development of Mll-Ell-induced acute myeloid leukemia. *Oncogene* **37**, 2532-2544, doi:10.1038/s41388-018-0131-5 (2018).

239   Dove, K. K. *et al.* Two functionally distinct E2/E3 pairs coordinate sequential ubiquitination of a common substrate in Caenorhabditis elegans development. *Proc Natl Acad Sci U S A* **114**, E6576-E6584, doi:10.1073/pnas.1705060114 (2017).

240   Huang, D. T. *et al.* E2-RING expansion of the NEDD8 cascade confers specificity to cullin modification. *Mol Cell* **33**, 483-495, doi:10.1016/j.molcel.2009.01.011 (2009).

241   Chaudhuri, J. *et al.* Transcription-targeted DNA deamination by the AID antibody diversification enzyme. *Nature* **422**, 726-730, doi:10.1038/nature01574 (2003).

242   Conticello, S. G., Thomas, C. J., Petersen-Mahrt, S. K. & Neuberger, M. S. Evolution of the AID/APOBEC family of polynucleotide (deoxy)cytidine deaminases. *Mol Biol Evol* **22**, 367-377, doi:10.1093/molbev/msi026 (2005).

243   Strebel, K. & Khan, M. A. APOBEC3G encapsidation into HIV-1 virions: which RNA is it? *Retrovirology* **5**, 55, doi:10.1186/1742-4690-5-55 (2008).

244   Hu, Y. *et al.* Structural basis of antagonism of human APOBEC3F by HIV-1 Vif. *Nat Struct Mol Biol* **26**, 1176-1183, doi:10.1038/s41594-019-0343-6 (2019).

245   Stanley, D. J. *et al.* Inhibition of a NEDD8 Cascade Restores Restriction of HIV by APOBEC3G. *PLoS Pathog* **8**, e1003085, doi:10.1371/journal.ppat.1003085 (2012).

246   Stieglitz, B. *et al.* Structural basis for ligase-specific conjugation of linear ubiquitin chains by HOIP. *Nature* **503**, 422-426, doi:10.1038/nature12638 (2013).

247   Chaugule, V. K. *et al.* Autoregulation of Parkin activity through its ubiquitin-like domain. *The EMBO journal* **30**, 2853-2867, doi:10.1038/emboj.2011.204 (2011).

248   Wauer, T. *et al.* Ubiquitin Ser65 phosphorylation affects ubiquitin structure, chain assembly and hydrolysis. *EMBO J* **34**, 307-325, doi:10.15252/embj.201489847 (2015).

249   Condos, T. E. *et al.* Synergistic recruitment of UbcH7~Ub and phosphorylated Ubl domain triggers parkin activation. *EMBO J* **37**, doi:10.15252/embj.2018100014 (2018).

250   Marin, I. Diversification of the cullin family. *BMC Evol Biol* **9**, 267, doi:10.1186/1471-2148-9-267 (2009).

251   Guo, Y. *et al.* Structural basis for hijacking CBF-beta and CUL5 E3 ligase complex by HIV-1 Vif. *Nature* **505**, 229-233, doi:10.1038/nature12884 (2014).

252   Binning, J. M., Chesarino, N. M., Emerman, M. & Gross, J. D. Structural Basis for a Species-Specific Determinant of an SIV Vif Protein toward Hominid APOBEC3G Antagonism. *Cell Host Microbe* **26**, 739-747 e734, doi:10.1016/j.chom.2019.10.014 (2019).

253   Lumpkin, R. J., Ahmad, A. S., Blake, R., Condon, C. J. & Komives, E. A. The Mechanism of NEDD8 Activation of CUL5 Ubiquitin E3 Ligases. *Mol Cell Proteomics*, doi:10.1074/mcp.RA120.002414 (2020).

254   Lumpkin, R. J., Baker, R. W., Leschziner, A. E. & Komives, E. A. Structure and dynamics of the ASB9 CUL-RING E3 Ligase. *Nat Commun* **11**, 2866, doi:10.1038/s41467-020-16499-9 (2020).

255   Kitamura, S. *et al.* The APOBEC3C crystal structure and the interface for HIV-1 Vif binding. *Nat Struct Mol Biol* **19**, 1005-1010, doi:10.1038/nsmb.2378 (2012).

256   Mittag, T. *et al.* Structure/function implications in a dynamic complex of the intrinsically disordered Sic1 with the Cdc4 subunit of an SCF ubiquitin ligase. *Structure* **18**, 494-506, doi:10.1016/j.str.2010.01.020 (2010).

257   van der Lee, R. *et al.* Intrinsically disordered segments affect protein half-life in the cell and during evolution. *Cell Rep* **8**, 1832-1844, doi:10.1016/j.celrep.2014.07.055 (2014).

258   Fuxreiter, M. & Tompa, P. Fuzzy complexes: a more stochastic view of protein function. *Adv Exp Med Biol* **725**, 1-14, doi:10.1007/978-1-4614-0659-4_1 (2012).

259   Baek, K., Scott, D. C. & Schulman, B. A. NEDD8 and ubiquitin ligation by cullin-RING E3 ligases. *Curr Opin Struct Biol* **67**, 101-109, doi:10.1016/j.sbi.2020.10.007 (2021).

260   Sato, Y. *et al.* Degradation of phosphorylated p53 by viral protein-ECS E3 ligase complex. *PLoS Pathog* **5**, e1000530, doi:10.1371/journal.ppat.1000530 (2009).

261   Blanchette, P. *et al.* Both BC-box motifs of adenovirus protein E4orf6 are required to efficiently assemble an E3 ligase complex that degrades p53. *Mol Cell Biol* **24**, 9619-9629, doi:10.1128/MCB.24.21.9619-9629.2004 (2004).

262   Castilla, L. H. *et al.* Failure of embryonic hematopoiesis and lethal hemorrhages in mouse embryos heterozygous for a knocked-in leukemia gene CBFB-MYH11. *Cell* **87**, 687-696, doi:10.1016/s0092-8674(00)81388-4 (1996).

263   Kundu, M. & Liu, P. P. Function of the inv(16) fusion gene CBFB-MYH11. *Curr Opin Hematol* **8**, 201-205, doi:10.1097/00062752-200107000-00004 (2001).

264   Marcotte, E. M. *et al.* Detecting protein function and protein-protein interactions from genome sequences. *Science* **285**, 751-753, doi:10.1126/science.285.5428.751 (1999).

265   Skaar, J. R. *et al.* PARC and CUL7 form atypical cullin RING ligase complexes. *Cancer Res* **67**, 2006-2014, doi:10.1158/0008-5472.CAN-06-3241 (2007).

266   Smit, J. J. *et al.* The E3 ligase HOIP specifies linear ubiquitin chain assembly through its RING-IBR-RING domain and the unique LDD extension. *The EMBO journal* **31**, 3833-3844, doi:10.1038/emboj.2012.217 (2012).

267   Stieglitz, B., Morris-Davies, A. C., Koliopoulos, M. G., Christodoulou, E. & Rittinger, K. LUBAC synthesizes linear ubiquitin chains via a thioester intermediate. *EMBO Rep* **13**, 840-846, doi:10.1038/embor.2012.105 (2012).

268   Hardeland, U., Steinacher, R., Jiricny, J. & Schar, P. Modification of the human thymine-DNA glycosylase by ubiquitin-like proteins facilitates enzymatic turnover. *The EMBO journal* **21**, 1456-1464, doi:10.1093/emboj/21.6.1456 (2002).

269   Baba, D. *et al.* Crystal structure of thymine DNA glycosylase conjugated to SUMO-1. *Nature* **435**, 979-982 (2005).

270   Flick, K. *et al.* Proteolysis-independent regulation of the transcription factor Met4 by a single Lys 48-linked ubiquitin chain. *Nat Cell Biol* **6**, 634-641, doi:10.1038/ncb1143 (2004).

271   Asaad, M. *et al.* Mycobacterium tuberculosis PPE10 (Rv0442c) alters host cell apoptosis and cytokine profile via linear ubiquitin chain assembly complex HOIP-NF-kappaB signaling axis. *Int Immunopharmacol* **94**, 107363, doi:10.1016/j.intimp.2020.107363 (2021).

272   Liu, Y. & Tan, X. Viral Manipulations of the Cullin-RING Ubiquitin Ligases. *Adv Exp Med Biol* **1217**, 99-110, doi:10.1007/978-981-15-1025-0_7 (2020).

273   Scheres, S. H. Processing of Structurally Heterogeneous Cryo-EM Data in RELION. *Methods in enzymology* **579**, 125-157, doi:10.1016/bs.mie.2016.04.012 (2016).

274   Zhang, K. Gctf: Real-time CTF determination and correction. *J Struct Biol* **193**, 1-12, doi:10.1016/j.jsb.2015.11.003 (2016).

275   Zheng, S. Q. *et al.* MotionCor2: anisotropic correction of beam-induced motion for improved cryo-electron microscopy. *Nat Methods* **14**, 331-332, doi:10.1038/nmeth.4193 (2017).

276   Pettersen, E. F. *et al.* UCSF Chimera--a visualization system for exploratory research and analysis. *J Comput Chem* **25**, 1605-1612, doi:10.1002/jcc.20084 (2004).

277   Pettersen, E. F. *et al.* UCSF ChimeraX: Structure visualization for researchers, educators, and developers. *Protein Sci* **30**, 70-82, doi:10.1002/pro.3943 (2021).

278   Emsley, P. & Cowtan, K. Coot: model-building tools for molecular graphics. *Acta crystallographica* **60**, 2126-2132 (2004).

279   Adams, P. D. *et al.* PHENIX: a comprehensive Python-based system for macromolecular structure solution. *Acta crystallographica* **66**, 213-221, doi:S0907444909052925 [pii]

10.1107/S0907444909052925 (2010).

280   Sheldrick, G. M. Experimental phasing with SHELXC/D/E: combining chain tracing with density modification. *Acta crystallographica* **66**, 479-485, doi:10.1107/S0907444909038360 (2010).

281   Sanchez-Garcia, R. *et al.* DeepEMhancer: a deep learning solution for cryo-EM volume post-processing. *bioRxiv* (2020).

282   Kabsch, W. Xds. *Acta crystallographica* **66**, 125-132, doi:10.1107/S0907444909047337 (2010).

283   Gibson, D. G. *et al.* Enzymatic assembly of DNA molecules up to several hundred kilobases. *Nat Methods* **6**, 343-345, doi:10.1038/nmeth.1318 (2009).

284   Cowtan, K. The Buccaneer software for automated model building. 1. Tracing protein chains. *Acta crystallographica* **62**, 1002-1011, doi:10.1107/S0907444906022116 (2006).

285   Mastronarde, D. N. Automated electron microscope tomography using robust prediction of specimen movements. *J Struct Biol* **152**, 36-51, doi:10.1016/j.jsb.2005.07.007 (2005).